Stony Brook University

Studies of Entanglement Entropy, and Relativistic Fluids for Thermal Field Theories

A Dissertation presented

by

Michael Spillane

to

The Graduate School

in Partial Fulfillment of the

Requirements

for the Degree of

Doctor of Philosophy

in

Department of Physics and Astronomy

Stony Brook University

August 2016

Stony Brook University

The Graduate School

Michael Spillane

We, the dissertation committee for the above candidate for the Doctor of Philosophy degree, hereby recommend acceptance of this dissertation

Christopher Herzog - Dissertation Advisor
Associate Professor, Department of Physics and Astronomy

Martin Roček - Chairperson of Defense
Professor, Department of Physics and Astronomy

Matthew Dawber - Committee Member
Professor, Department of Physics and Astronomy

Michael Anderson - Outside Member
Professor, Department of Mathematics

This dissertation is accepted by the Graduate School

Charles Taber
Dean of the Graduate School

Abstract of the Dissertation

Studies of Entanglement Entropy, and Relativistic Fluids for Thermal Field Theories

by

Michael Spillane

Doctor of Philosophy

in

Physics and Astronomy Department

Stony Brook University

2016

In this dissertation we consider physical consequences of adding a finite temperature to quantum field theories. At small length scales entanglement is a critically important feature. It is therefore unsurprising that entanglement entropy and Rényi entropy are useful tools in studying quantum phase transition, and quantum information. In this thesis we consider the corrections to entanglement and Rényi entropies due to addition of a finite temperature.

More specifically, we investigate the entanglement entropy of a massive scalar field in 1+1 dimensions at nonzero temperature. In the small mass (m) and temperature (T) limit, we put upper and lower bounds on the two largest eigenvalues of the covariance matrix used to compute the entanglement entropy. We argue that the entanglement entropy has $e^{-m/T}$ scaling in the limit $T \ll m$.

Additionally, we calculate thermal corrections to Rényi entropies for free massless fermions on $\mathbb{R} \times \mathbb{S}^{d-1}$. By expanding the density matrix in a Boltzmann sum, the problem of finding the Rényi entropies can be mapped to the problem of calculating a two point function on an n-sheeted cover of the sphere. We map the problem on the sphere to a conical region in Euclidean space. By using the method of images, we calculate the two point function and recover the Rényi entropies.

At large length scales hydrodynamics is a useful way to study quantum field theories. We review recent interest in the Riemann problem as a method for generating a non-equilibrium steady state. The initial conditions consist of a planar interface between two halves of a system held at different temperatures in a hydrodynamic regime. The resulting fluid flow contains a fixed temperature region with a nonzero flux. We briefly discuss the effects of a conserved charge. Next we discuss deforming the relativistic equations with a nonlinear term and how that deformation affects the temperature and velocity in the region connecting the asymptotic fluids.

Finally, we study properties of a non-equilibrium steady state generated when two heat baths are initially in contact with one another. The dynamics of the system in question are governed by holographic duality to a blackhole. We discuss the "phase diagram" associated with the steady state of the dual, dynamical black hole and its relation to the fluid/gravity correspondence.

To my family.

Contents

Acknowledgements

There are enough people to thank to fill pages, with out whom some part of this would not have been possible. From primary school teachers who encouraged me to ask questions, too sports coaches who taught me about team work. Also extremely important to this process have been my friends, both inside school and out. Through interactions with these people, whose names are too plentiful to list, they have shaped my life and contributed to parts of this work. However, there are some people without whom none of this would be possible who's names do need to be written down.

While this is mostly about my academic pursuits I would be remise if I did thank my doctors Edward Libby and Fengshuo Lan who treated me when I was sick and provided me the opportunity to finish my thesis. For their hard work I am eternally grateful. I would also like to thank the countless other doctors, nurses and administrators at Stony Brook Hospital and SCCA in Seattle for their contributions.

I would like to thank Professor Karch at the University of Washington and Professor Zahed at Stony Brook. They separately introduced me to the practice of science. In my senior year of undergrad I worked with Professor Karch on a project analyzing minimal surfaces. A year later Professor Zahed collaborated with me on a paper analyzing energy lose of quarks. They helped me take what I had learned in the classroom and apply it to modern problems in physics.

Thank you to all of my committee members both for my oral exam (Dr. Abanov, Dr. Weinacht, Dr. Rocek, and Dr. Herzog) and PhD defense (Dr. Rocek, Dr. Dawber, Dr. Anderson and Dr. Herzog). They provided guidance and constructive criticism both for my work at Stony Brook and for my work as I continue my adventures in physics.

The primary contributor for the content and direction of this thesis came from my advisor Chris Herzog. While others had provided a foundation, Chris built upon it. He listened to my ideas and showed me how to transform questions into a research topic. He was always available to answer questions when I was confused, provided guidance when I was lost and provide encouragement when I was struggling. I also need to thank him for his understanding and support while I was sick.

Finally, I would like to thank all my family. Since I was young my parents, Mick and Phyllis, encouraged me to learn about math and science. Around the dinner table I learned about their lives as scientists and that made me want to pursue that path as well. My brother Brian has been a constant

source of support, a true friend and an amazing brother. Lastly, my wife Li Sha has been my companion for the last 6 years, comforting me in my struggles and sharing in my triumphs. When the rest of the world seemed crazy I could always find comfort in her presence. I am excited for our life together.

This thesis is based on the following publications:

- C. P. Herzog, M. Spillane and A. Yarom, "The holographic dual of a Riemann problem in a large number of dimensions," arXiv:1605.01404 [hep-th].
- M. Spillane and C. P. Herzog, "Relativistic Hydrodynamics and Non-Equilibrium Steady States," arXiv:1512.09071 [hep-th].
- C. P. Herzog and M. Spillane, "Thermal corrections to Rnyi entropies for free fermions," JHEP **1604**, 124 (2016) doi:10.1007/JHEP04(2016)124 [arXiv:1506.06757 [hep-th]].
- C. P. Herzog and M. Spillane, "Tracing Through Scalar Entanglement," Phys. Rev. D **87**, no. 2, 025012 (2013) doi:10.1103/PhysRevD.87.025012 [arXiv:1209.6368 [hep-th]].

Additional work completed by the author:

- M. Spillane, "Constructing Space From Entanglement Entropy," arXiv:1311.4516 [hep-th].
- M. Spillane, A. Stoffers and I. Zahed, "Jet quenching in shock waves," JHEP **1202**, 023 (2012) doi:10.1007/JHEP02(2012)023 [arXiv:1110.5069 [hep-th]].

1 Introduction

The 20th century was a tumultuous time for physics. Old ideas were discarded as new experiments disproved them and new theories superseded them. It took decades for these new theories to be solidified out and for their implications to be discovered. In some cases, it took just as long for the new consequences to be accepted. In this chapter we will discuss some of the discovery and acceptance of these new ideas.

1.1 General Relativity

In the late 19th century the theory of aether was under attack. Experiments by Arago, Airy and Michelson-Morley cast doubt on the existence of the aether and why its effects remained undetected. Einstein resolved this problem by discarding aether entirely as well as Galilean addition of velocity and the rigid notion of time. Special relativity also allowed for a covariant Lagrangian of Maxwell's electromagnetic field [1]. Using the mostly positive metric (–,+,+,+), the electromagnetic Lagrangian

$$\begin{aligned} F_{\mu\nu} &= \partial_\mu A_\nu - \partial_\nu A_\mu, \\ \mathcal{L} &= -\frac{1}{4} F^{\mu\nu} F_{\mu\nu}, \end{aligned} \tag{1.1}$$

was invariant under transformations of the new space-time.

The next step in the restructuring was a covariant theory of gravity, which Einstein understood to be indistinguishable from acceleration. Within two years all the conceptual pieces for this theory and some consequences were in place including gravitational redshift and light bending. However, the correct mathematical framework would be another 8 years in the making. In November of 1915 Einstein and Hilbert identified the field equations

$$G_{\mu\nu} \equiv R_{\mu\nu} - \frac{1}{2} R g_{\mu\nu} = T_{\mu\nu}. \tag{1.2}$$

It is worth noting that the Bianchi identities imply that

$$\nabla^\mu G_{\mu\nu} = 0. \tag{1.3}$$

The Einstein field equations arise from the minimization of the Einstein-Hilbert action

$$S = \frac{1}{2\kappa} \int d\vec{x} \sqrt{-g} R. \tag{1.4}$$

In both cosmological and theoretical analysis it is common to add an additional term to the metric $2\Lambda\sqrt{-g}$. Known as the cosmological constant, Λ, the measured value in our universe is 1.7×10^{-121}[2] as measured in Planck units.

1.1.1 Black Holes

One of the first solutions found was the spherically symmetric solution equivalent to a point mass at the origin. The metric corresponding to this in four space time dimensions is given by

$$ds^2 = -(1 - r_s/r)dt^2 + (1 - r_s/r)^{-1}dr^2 + r^2 d\Omega^2, \tag{1.5}$$

where r_s is the radius of the blackhole and $d\Omega$ is the metric on $\mathbf{S}^2$. In 1923 it was proved, by Birkoff, that this is the unique spherically symmetric solution in 4-spacetime dimensions[1]. This has the immediate implication that just like electromagnetism, monopoles cannot radiate. That is not to say, however, that gravity cannot produce radiation; Einstein had already predicted the existence of a quadrupole wave which was finally experimentally observed in 2016 [3].

We can also look at black holes when there is a cosmological constant. In doing so an interesting result occurs, a 3d black hole. There is no allowed 3-dimensional black hole that is asymptotically flat. In general the black hole metric is given by

$$ds^2 = -\left(1 + \frac{r^2}{L^2} - \frac{C}{r^{d-3}}\right) dt^2 + \left(1 + \frac{r^2}{L^2} - \frac{C}{r^{d-3}}\right)^{-1} dr^2 + r^2 d\Omega^2, \tag{1.6}$$

where L is the radius of curvature.

If we take the massless limit ($C \to 0$) we obtain the metric for global anti de Sitter space(AdS). AdS is a maximally symmetric Lorentzian manifold

[1]This theorem applies to spacetimes in 4-dimensions with cosmological constants as well.

with symmetry group $SO(d-1,2)$. Shockingly, this is the same symmetry group as a conformal field theory (CFT) in $d-1$ dimensions. This observation in part lead to the conjecture that string theories in AdS space are equivalent to conformal field theories in one smaller spacetime dimension, known as the AdS/CFT correspondence. This is a rich and wide ranging field of study, of which this dissertation will only touch the edges. As we will see below the study of asymptotically AdS manifolds yields insight into both entanglement entropy and fluid dynamics.

1.1.2 Outlook

General relativity is classical theory of gravity and has long resisted efforts of quantization. Adding supersymmetry has offered some insights into a possible quantum nature of gravity. String theory provides a possible complete description of quantum gravity, however there are many complications which are being actively investigated. In an interesting twist the discovery of AdS/CFT correspondence allowed for classical gravity solutions to be applied to solutions of quantum mechanical problems. Solutions in classical gravity now provide insight into quantum systems from low energy condensed matter systems, to high energy quark gluon plasmas.

1.2 Hydrodynamics

Hydrodynamics is the study of macroscopic features of liquids and gases. As such it can be obtained as the continuum limit of the Boltzmann equation or from an analysis Newton's second law applied to fluid elements, (see Appendix A). These simple equations then govern physical systems ranging in size from small collisions of heavy ions to red giant stars.

Early attempts did not include the modern view of considering forces on infinitesimal elements of the fluids, but instead made analogies between fluids and the better understood dynamics of rigid bodies. The first attempt at a dynamical model of fluids was carried out by Bernoulli in 1738 [4].

The result was the one-dimensional Euler equation, relating to the fluid flow in a vessel known as Bernoulli's law. By 1749 D'Alembert had found a special case of the two dimensional Euler equation, in his explanation of winds as caused by the tidal forces of the moon. This is now known to be false. Nevertheless his analysis pushed forward the study of fluid flows. Finally in 1752, considering internal pressures as well as external forces acting

on a infinitesimal element of a fluid Euler derived

$$\partial_t \mathbf{u} + (\mathbf{u} \cdot \nabla)\mathbf{u} = \mathbf{F} - \nabla P, \tag{1.7}$$

$$\nabla \cdot \mathbf{u} = 0, \tag{1.8}$$

where $\mathbf{u}$ is the velocity, $\mathbf{F}$ is the force and P is the pressure. Three years later Euler would extend this to compressible fluids

$$\partial_t \mathbf{u} + (\mathbf{u} \cdot \nabla)\mathbf{u} = \frac{1}{\rho}(\mathbf{F} - \nabla P), \tag{1.9}$$

$$\partial_t \rho + \nabla \cdot (\rho \mathbf{u}) = 0, \tag{1.10}$$

where ρ is the density.

While this model of perfect fluids was mathematically sound it did little to help with the real world problems of the drag on ships or flow through pipes. This was remedied by Navier in 1821 who translated his work on elastic bodies into hydrodynamics thereby adding viscous corrections to Euler's perfect fluid equations. His result would be rediscovered by Cauchy, Poisson, Saint–Venant and Stokes.

From this point on a plethora of new subfields sprung out. Helmholtz embarked on a study of vortices, dovetailed into an analysis of instabilities of surface discontinuities, the Kelvin–Helmholtz instability. A half century later in 1880 Reynolds would explore the instability of laminar flows and their transition to a turbulent flow. These phenomena are made possible by the nonlinear terms in the equations governing fluids. The complications imposed by these terms ensure that it will continue to be a vibrant area of research going into the future. This interest is exemplified by the inclusion of fluids in the Millennium Prize Problems.

After the discovery of relativity a covariant description of fluids was necessary. From the Einstein equation and the Bianchi identity it is clear that the fluid should be described by a conserved stress tensor

$$\nabla_\mu T^{\mu\nu} = 0. \tag{1.11}$$

A perfect fluid should be described by a vector u^μ. In the rest frame the T^{00} component should be the energy and the other diagonal elements should be the pressure. The unique symmetric stress tensor is then given by

$$T^{\mu\nu} = (\epsilon + P)u^\mu u^\nu + P g^{\mu\nu}, \tag{1.12}$$

where ϵ is the energy density and p is the pressure. The conservation equations associated with this stress tensor are equivalent to Euler's equations in the non-relativistic limit.[2]

To add viscosity an expansion in derivatives is formed. At first order in derivatives there are many possible combinations and the appropriate combination needs to be found for the application in mind. One example is a conformal fluid. This case forces the stress tensor to be traceless and the gradient corrections to be orthogonal to the velocity

$$\sigma^{\mu\nu} = 2\nabla^{\langle\mu}u^{\nu\rangle}, \tag{1.13}$$

where

$$A^{\langle\mu\nu\rangle} \equiv \frac{1}{2}\Delta^{\mu\alpha}\Delta^{\nu\beta}(A_{\alpha\beta} + A_{\beta\alpha}) - \frac{1}{d}\Delta^{\mu\nu}\Delta^{\alpha\beta}A_{\alpha\beta}, \tag{1.14}$$

$$\Delta^{\mu\nu} \equiv g^{\mu\nu} + u^{\mu}u^{\nu}. \tag{1.15}$$

At next order in the derivative expansion a plethora of new terms appear including terms coupling to the curvature.

As mentioned before there is a relationship between gravity and CFTs and this relationship is true for fluids as well. If we consider an extended object, black brane, producing a black hole instead of a point like object considered above, we obtain a metric of the form

$$ds^2 = -2u_\mu dx^\mu dr - r^2 f(br)u_\mu u_\nu dx^\mu dx^\nu + r^2\Delta_{\mu\nu}dx^\mu dx^\nu, \tag{1.16}$$

where the suggestively written u_μ is the uniform velocity of the brane and r is the new holographic direction measured from the boundary. This metric is a solution to the vacuum Einstein equations provided that b and u^μ are constants. However, if we allow b and u^μ to vary as a function of the boundary coordinates then provided that they satisfy the perfect fluid equations the metric is still an approximate solution to vacuum Einstein equations. Perturbative corrections to the metric are matched by the derivative expansion in the relativistic fluid.

1.2.1 Outlook

Research in hydrodynamics has receive interest in phenomenological communities since the discovery that the result of high energy collisions of large

[2]The ideal fluid also has a conserved entropy current $\nabla_\mu s u^\mu = 0$.

atomic nuclei creates a near perfect fluid. Another recent avenue of research involves Hall viscosity which is a term added to the gradient expansion in 2+1 dimensions which violates parity. This term does not lead to dissipation as normal viscosity does. This thesis follows along the path of field theories out of equilibrium.

1.3 Entanglement

In the early 20th century classical physics dating back to Newton was in trouble. A new particle, the electron, had been found in cathode rays and emitted in the photoelectric effect. They were 2000 times lighter than the lightest known atom and were negatively charged. The electrons however emitted in the photoelectric effect had curious correlation with the light causing the emission. Rather than their energy increasing as the intensity of the light was increased the number of electrons increased. Even more curious was the observation that their energy increased as the frequency of light increased. Einstein solved this mystery by proposing that the electrons were excited by discrete packets of light, later called photons [3]. The photoelectric effect, along with Bohr's model of the hydrogen atom, sparked the quantum revolution.

The next two decades sharpened the understanding of the effects of this new quantum theory of physics. However, by the 30's some of the giants of the field, particularly Einstein, were concerned by the implications of the field they had helped start. In 1935 Einstein, Podolsky and Rosen published a paper questioning whether quantum mechanics was complete. In response Schrodinger coined the term entanglement in his paper as well as his famous cat. The Einstein-Podolsky-Rosen (EPR) paradox remained largely ignored until the 1950s when it was resurrected by David Bohm who formulated the problem in terms of a finite dimensional system, the electron spin. Bohm's work was followed by John Bell's investigations which lead to experimental verification[5] .

Simultaneous to the conversation about whether entanglement was real, von Neumann was laying down the mathematical framework underlying quantum mechanics. He proposed that physical states were vectors in a Hilbert space and measurable quantities were Hermitian operators on the Hilbert

[3]This was immediately tied with Planck's explanation of the spectrum of blackbody radiation.

space. As part of his work he defined the density matrix, ρ of a pure state $|\psi\rangle$, as

$$\rho = |\psi\rangle\langle\psi|. \tag{1.17}$$

More generally, given a system with probabilities p_i of being in a state $|\psi_i\rangle$ the density matrix is

$$\rho = \sum_i |\psi_i\rangle\langle\psi_i|. \tag{1.18}$$

Pure states are defined as those states for which $\rho^2 = \rho$. The density matrix formalism implies the expectation value of an operator is then

$$\langle\mathcal{O}\rangle = \mathrm{tr}(\rho\mathcal{O}). \tag{1.19}$$

Von Neumann then turned his interest to quantum thermodynamics and determined the quantum analogue, for thermal states with Hamiltonian $\mathbf{H}$, of entropy to be

$$S = -k_B \,\mathrm{tr}(\rho \log \rho), \tag{1.20}$$

$$\rho = \exp(-\mathbf{H}/kT). \tag{1.21}$$

This von Neumann entropy is also used in determining the entanglement of a quantum state. If we can split the Hilbert space of a quantum system into two parts (A, B) such that the Hilbert space of the whole system is a tensor product of the Hilbert spaces of the separate parts, $H = H_A \otimes H_B$, the reduced density matrix on A is defined as

$$\rho_A = \mathrm{tr}_B\, \rho. \tag{1.22}$$

For pure states the entanglement entropy,

$$S_A = -\,\mathrm{tr}(\rho_A \log \rho_A), \tag{1.23}$$

is a good measure of the entanglement between subsystems A and B.[4]

[4]In fact, Shannon proved that $S(p_1, ..p_n) = -K\sum_i p_i \log p_i$ is the unique function satisfying the the following assumptions

1. Continous in all variables
2. Symmetric in all variables
3. Satisfies the recursion relation
   $S(p_1, ..., \lambda p_n, (1-\lambda)p_n) = S(p_1, ..., p_n) + p_n S(\lambda, (1-\lambda))$

Schmidt decomposition tells us that for any pure state

$$|\psi\rangle = \sum_i \lambda_i |i_A\rangle |i_B\rangle. \tag{1.24}$$

It is clear the eigenvalues of ρ_A and ρ_B are equal and therefore $S_A = S_B$. A more involved derivation [6] shows that entanglement entropy obeys the triangle inequality and subadditivity

$$|S_A - S_B| \leq S_{AB} \leq S_A + S_B. \tag{1.25}$$

In fact, entanglement entropy satisfies the strong-subadditivity condition

$$S_A + S_B \leq S_{AC} + S_{BC}, \tag{1.26}$$

$$S_{ABC} + S_B \leq S_{AB} + S_{BC}. \tag{1.27}$$

While entanglement entropy has many nice qualities, it is difficult to calculate. For this reason a different measure of entanglement is often calculated, the Rényi entropy

$$S_n(A) = \frac{1}{1-n} \log \operatorname{tr} \rho_A^n. \tag{1.28}$$

The pre-factor is specially chosen so that the entanglement entropy is the $n \to 1$ limit of the Rényi entropy. Therefore if we are able to find a general form for the Rényi entropies it is often possible to analytically continue in n and obtain the entanglement entropy. This is often easier because the partition function and the density matrix are related as

$$\operatorname{tr} \rho_A^n = \frac{Z_n(A)}{Z_1^n}, \tag{1.29}$$

where Z_n is the partition function on an n-sheeted cover stitched together along A.

1.3.1 Entanglement entropy in QFTs

For a randomly selected state in the Hilbert space the corresponding entanglement entropy for a subsystem will be proportional to the volume of the subsystem. However, when it comes to more physically relevant states the entanglement entropy is no longer extensive. This is obvious for pure

states because for pure states $S_A = S_B$. Even for non pure states this seems reasonable as the majority of entanglement is local and so the majority of the entanglement occurs at the boundary separating the two regions. For gapped systems, the lowest energy state has a finite difference in energy from the ground state and this scaling is known as the area law[7, 8]. For gapless systems the falloff of the two point function is no longer exponential, but rather is a power law. It is therefore unsurprising that for gapless systems the area law does not necessarily apply.

In 1+1 dimensions there are two simple systems we can study, a massive scalar and a CFT[9]. The simplest subsystem A is a single interval of length ℓ. First consider the massive scalar

$$\mathcal{L} = \frac{1}{2}\left(\partial_\mu \phi \partial^\mu \phi + m^2 \phi^2\right). \tag{1.30}$$

For non-interacting QFTs the following identity holds

$$\partial_{m^2} \log Z_n = -\frac{1}{2}\int d^2 r G_n(\vec{r}, \vec{r}). \tag{1.31}$$

The Greens function G_n of the Helmholtz equation can be found by the use of an expansion in Bessel functions. The result is

$$G_n(\vec{r}, \vec{r}) = I_0(mr)K_0(mr) + 2\sum_{k=1}^{\infty} I_{k/n}(mr)K_{k/n}(mr). \tag{1.32}$$

The integral over the plane can be done simply and the result is

$$\partial_{m^2} \log Z_n = -\frac{1}{2nm^2}\sum_k k. \tag{1.33}$$

If we interpret the sum[5] as $\zeta(-1) = -1/12$ and integrate we obtain the entanglement entropy

$$S_A = -\frac{1}{12}\log(ma) \tag{1.34}$$

where a is the UV cutoff. This result is independent of the area of A, and proportional to its boundary.

[5] A more careful analysis in which the sum is done first using the Euler-MacLaurin formula yields the same result.

An analogous derivation yields the entanglement entropy for a 2d CFT

$$S_A = \frac{c}{3}\log(\ell/a). \tag{1.35}$$

This result is not independent of the area of A, but neither is it proportional as we would expect of thermal entropy. Rather because of the power law decay of the two point function it is a mix of the two.

1.3.2 Holographic Entanglement Entropy

As one with passing familiarity with AdS_3 might recognize, $\log(\ell/a)$ is the length of a geodesic attached to the conformal boundary. Noting our previous observation of a relationship between CFTs in two dimensions and gravity in AdS_3 along with the relationship between thermal entropy of a blackhole and its area, one may be left to wonder if there is some relationship. This lead to the conjecture that for holographic duals of QFTs, the entanglement entropy in the CFT could be calculated as

$$S_A = \frac{\text{Area}(\gamma_A)}{4G_N}, \tag{1.36}$$

where γ_A is the minimal surface deformable to the region A on the boundary and G_N is the Newton constant[10]. This conjecture passes many important tests including $S_A = S_B$ for pure states and strong-subaddativity. It also naturally leads to an area law. This conjecture has since been proved for 2 dimensional theories.

The simplest case to consider is a single interval of length ℓ in AdS_3/CFT_2. We can use the Poincaré upper half plane for our calculation. The metric for a constant time slice is

$$ds^2 = R^2\frac{dz^2 + dx^2}{z^2}, \tag{1.37}$$

where R is the AdS radius of curvature. Geodesics for this metric are given by circles in the xz-plane. To find the length of the geodesic we need to do the integral

$$\text{Area}(\gamma_A) = 2R\int_\epsilon^{z_*}\frac{dz}{z}\frac{1}{\sqrt{z_*^2 - z^2}}\,, \tag{1.38}$$

$$= \log(2z_*/\epsilon)\,, \tag{1.39}$$

where ϵ is the UV cutoff of the theory and z_* is the radius of the circle. Writing every thing in terms of CFT variable using the relation between the central charge c and Newton's constant $c = 3R/2G$

$$S_A = \frac{c}{3} \log(\ell/\epsilon). \tag{1.40}$$

1.3.3 Outlook

Modern scholarship has spread in a variety of directions from the initial works. The Ryu-Takayanagi opened the door to a wide range of calculations for known holographic duals as well as renewing interest in entropy of black-holes. Other research investigates the effects of boundaries on entanglement. The path that this thesis follows is the addition of temperature to field theories. This dovetails with research in entanglement negativity which is an alternate measure of entanglement for bipartite subsystems.

1.4 Outline

This dissertation is organized into two parts. The first part analyzes the effects of temperature on gapped QFTs. Specifically it focuses on the corrections to the entanglement and Rényi entropies at finite temperature. Chapter 1 lays out the first evidence of the scaling at small temperatures of corrections to the zero temperature result for a scalar field. This result arises from a Boltzmann expansion of the density matrix. Chapter 2 presents studies fermions on an n-sphere. Corrections to Rényi entropies are calculated analytically for even dimensions and the entanglement entropy is calculated in all dimensions.

The second part looks at various versions of the Riemann problem. Recently, the Riemann problem has received recent interest because at late times a non-equilibrium steady state appears (NESS) in fluids. The first chapter considers a relativistic charged fluid. Various features are observed including contact discontinuities. We also consider corrections to the pressure and current in the NESS region as a result of nonlinear deformations. The second chapter considers the Riemann problem for AdS blackholes. Specifically, by taking the number of spacetime dimensions to be large we arrive at simple equations governing the dynamics of the blackhole.

Part I
Entanglement at Finite Temperature

2 Scalar Entanglement on a Circle

2.1 Background

The notion of entanglement entropy (and more generally quantum entanglement) looms large in theoretical physics today. Entanglement entropy may be a good order parameter for topological phase transitions in condensed matter systems. For conformal field theories in 1+1 dimensions, numerical computation of the entanglement entropy provides a rapid way to calculate the central charge c. In relativistic field theories more generally, certain special kinds of entanglement entropy show monotonicity properties under renormalization group flow [11, 12]. See [13] and [14] for reviews.

To compute the entanglement entropy for a quantum mechanical system, we must first divide the associated Hilbert space up into two pieces. Usually, the division is made with respect to spatial regions A and complement $\bar{A} = B$. We find the reduced density matrix $\rho_A \equiv \mathrm{tr}_B\, \rho$ by tracing over the degrees of freedom in B. Finally, the entanglement entropy is defined to be

$$S \equiv -\,\mathrm{tr}\, \rho_A \log \rho_A \ . \tag{2.1}$$

It is surprising that even for what many consider to be the simplest field theoretic system – a massive scalar field in 1+1 dimensions – the entanglement entropy has thus far been computed analytically only in certain limits. In the limit $m = 0$, one can use results from conformal field theory [15, 16]. In particular, for the massless scalar field on the cylinder $\mathbb{R} \times S^1$ where $\mathbb{R}$ is interpreted as the time direction, one has

$$S = \frac{1}{3} \log \left(\frac{L}{\pi\epsilon} \sin \frac{\pi \ell}{L} \right) + c_0 \ , \tag{2.2}$$

where L is the circumference of the S^1, ℓ is the length of the interval, ϵ is a UV regulator and c_0 is a constant that depends on the regulation scheme. (In fact, for the massless scalar, there is an additional IR divergence, and

c_0 depends also on an IR cutoff.) Reinterpreting S^1 as a Euclidean time direction, one obtains a result at nonzero temperature $T = 1/\beta$ for the scalar on $\mathbb{R}$.

$$S = \frac{1}{3} \log \left(\frac{\beta}{\pi\epsilon} \sinh \frac{\pi\ell}{\beta} \right) + c_0 \ . \tag{2.3}$$

When $m \neq 0$ for the scalar field on $\mathbb{R}^2$, Huerta and Casini [9] have shown that the entanglement entropy can be computed from the solution to a certain Painlevé equation. Their work allows analytic access to the small and large mass limits. For $m\ell \ll 1$, one obtains

$$S \sim \frac{1}{3} \log \frac{\ell}{\epsilon} + \frac{1}{2} \log \left(\frac{\log(m\epsilon)}{\log(m\ell)} \right) \ , \tag{2.4}$$

while for $m\ell \gg 1$, one finds instead exponential suppression[6]

$$S \sim \frac{1}{16} \sqrt{\frac{\pi}{m\ell}} \, e^{-2m\ell} \ . \tag{2.5}$$

Ideally, one would like to understand the case where m, T, and $1/L$ are all nonzero. Numerically, the entanglement entropy can be computed with ease using a generalization [17] of the procedure introduced by Srednicki [7]. One realizes the scalar field as the continuum limit of an N-site harmonic chain. For such a chain, one introduces two point functions $\langle \phi_i \phi_j \rangle$ and $\langle \pi_i \pi_j \rangle$ of the oscillator positions and conjugate momenta respectively. Restricting now to an interval $n\epsilon = \ell < L$ where $1 \leq i, j, k \leq n$, one constructs the $n \times n$ matrix

$$(C^2)_{ij} \equiv \sum_{k=1}^{n} \langle \phi_i \phi_k \rangle \langle \pi_k \pi_j \rangle \ . \tag{2.6}$$

The entanglement entropy is then

$$S = \mathrm{tr} \left[(C + 1/2) \ln(C + 1/2) - (C - 1/2) \ln(C - 1/2) \right] \ . \tag{2.7}$$

To our knowledge, this quantity has not been computed analytically for the real scalar field with two or more of the quantities m, T, and $1/L$ nonzero. Happily, with today's desktop computers, it is relatively quick to diagonalize C numerically for $N \sim 10^3$. Ref. [20] provides a numerical analysis of the harmonic chain using this approach.

[6] A generalization was obtained by Doyon and collaborators [18] and [19] allowing for multiple masses.

In this chapter, we take some steps toward an analytic understanding of the eigenvalues of C. As noted in [20], the parity operator P commutes with C where parity here is a reflection of the circle S^1 with respect to the midpoint of the interval. Thus, one may divide C into even and odd parity blocks C_e and C_o. We compute the two partial traces $\operatorname{tr} C_e^2$ and $\operatorname{tr} C_o^2$ in the limit $m, T \ll 1/L$. As the spectrum of C^2 is bounded below by $1/4$, these traces give us upper bounds on the two largest eigenvalues of C. A variational approach gives a lower bound to the largest (parity even) eigenvalue. These bounds in turn give us some intuition for the m, T, and L dependence of the entanglement entropy in the limit $m, T \ll 1/L$.

The original motivation for this project came from our interest in the Ryu-Takayanagi proposal [10] for computing the entanglement entropy of field theories with dual holographic classical gravity descriptions. Given two complementary regions A and B in the field theory, the Ryu-Takayanagi proposal associates a nonzero $S_A - S_B$ to gravity descriptions with black holes, while in the absence of such defects $S_A = S_B$. In the dual field theory, the existence of a black hole typically implies deconfined gauge theory degrees of freedom [21, 22].

We may contrast this result with the quantum mechanical point of view where at $T = 0$, the density matrix is constructed from a pure state. (We are assuming the existence of a unique ground state.) It follows from a Schmidt decomposition of the Hilbert space that for pure states $S_A = S_B$ (see for example [14]). However, at any nonzero temperature, regardless of the presence of deconfined degrees of freedom, the density matrix is not constructed from a pure state and one would generically expect $S_A \neq S_B$. As gauge theories are more difficult to study than the free scalar field and as the entanglement entropy of the free scalar field has not yet been completely understood, our toy model of confinement in this chapter is a 1+1 dimensional massive scalar field on a circle at $T > 0$. Morally, the regime $T \ll m$ can be thought of as "confining".[7] One of our results is that in this regime, the entanglement entropy difference does not vanish but rather scales as[8]

$$S_A - S_B \sim e^{-m/T} \ .$$

[7] Klebanov et. al. [23] were the first to consider the entanglement entropy of confining theories from a holographic perspective. Their work at zero temperature was later followed up by lattice computations [24, 25, 26].

[8] After finishing this work, we became aware of ref. [27] where the same exponential behavior was found for a "renormalized thermal entropy" similar in some respects to the entanglement entropy we study here.

2.2 From the Harmonic Chain to the Scalar Field

Consider the Hamiltonian for a real free massive scalar field on a circle of circumference L at $T > 0$:

$$H = \frac{1}{2}\int dx \left[\pi(x)^2 + (\partial_x \phi(x))^2 + m^2\phi(x)^2\right] \ . \tag{2.8}$$

We discretize the circle into N points where $L = N\epsilon$:

$$H = \frac{1}{2\epsilon}\sum_{j=1}^{N}\left[\pi_j^2 + (\phi_{j+1} - \phi_j)^2 + m^2\epsilon^2\phi_j^2\right] \ , \tag{2.9}$$

where $\pi(j\epsilon) = \pi_j/\epsilon$ but $\phi(j\epsilon) = \phi_j$. The thermal density matrix can be written in terms of H in the standard way:

$$\rho = \frac{e^{-H/T}}{\mathrm{tr}(e^{-H/T})} \ , \tag{2.10}$$

and expectation values are defined via $\langle X\rangle \equiv \mathrm{tr}(\rho X)$. A short calculation yields the two point functions of the oscillator positions ϕ_j and their conjugate momenta π_j:

$$\langle\phi_j\phi_k\rangle = \frac{1}{2N}\sum_{a=0}^{N-1}\frac{1}{\epsilon\omega_a}\coth\left(\frac{\omega_a}{2T}\right)\cos\left(\frac{2\pi(j-k)a}{N}\right) \ , \tag{2.11}$$

$$\langle\pi_j\pi_k\rangle = \frac{1}{2N}\sum_{a=0}^{N-1}\epsilon\omega_a\coth\left(\frac{\omega_a}{2T}\right)\cos\left(\frac{2\pi(j-k)a}{N}\right) \ , \tag{2.12}$$

where

$$\omega_a^2 = m^2 + \frac{4}{\epsilon^2}\sin^2\frac{\pi a}{N} \ .$$

From eqs. (2.6) and (2.7), we may compute the entanglement entropy from the matrix $C^2 = \langle\pi\pi\rangle\cdot\langle\phi\phi\rangle$ where the two point functions are now restricted to the interval A: $-s \le j,k \le s$. In terms of n, we have $2s+1 = n$. For simplicity, we choose n to be an odd number. Any dependence on the parity of n should disappear in the large N limit.

The Hamiltonian H is a set of N coupled harmonic oscillators. Diagonalizing the Hamiltonian, one finds $H = \sum_a \omega_a b_a^\dagger b_a$ where $[b_a, b_b^\dagger] = \delta_{ab}$. Surprisingly for a free scalar field, the reduced density matrix $\rho_A \sim e^{-H_A}$ can

be written in terms of a similar entanglement Hamiltonian $H_A = \sum_k \epsilon_k b_k^\dagger b_k$ (see for example [14]). Moreover, there is a one-to-one correspondence between eigenvalues λ_k of C^2 and the energies ϵ_k:

$$\lambda_k = \frac{1}{4} \coth^2 \frac{\epsilon_k}{2} \ . \tag{2.13}$$

As the ϵ_k are real, we conclude that $\lambda_k \geq 1/4$.

2.3 Taking Traces

For a region $-s \leq k \leq s$, the matrix C^2 commutes with the parity operator[9] which sends $k \to -k$. Thus, we can decompose C^2 into even and odd parity pieces, $C^2 = C_e^2 + C_o^2$. The matrices C_o^2 and C_e^2 are then given by

$$C_e^2 = \frac{1}{4N^2} \sum_{a,b} \frac{\omega_a}{\omega_b} \coth\left(\frac{\omega_a}{2T}\right) \coth\left(\frac{\omega_b}{2T}\right) \frac{\sin\frac{\pi n(a-b)}{N}}{\sin\frac{\pi(a-b)}{N}} \cos\frac{2\pi ja}{N} \cos\frac{2\pi kb}{N} \tag{2.14}$$

$$C_o^2 = \frac{1}{4N^2} \sum_{a,b} \frac{\omega_a}{\omega_b} \coth\left(\frac{\omega_a}{2T}\right) \coth\left(\frac{\omega_b}{2T}\right) \frac{\sin\frac{\pi n(a-b)}{N}}{\sin\frac{\pi(a-b)}{N}} \sin\frac{2\pi ja}{N} \sin\frac{2\pi kb}{N} \tag{2.15}$$

While our main interest is a circle with periodic boundary conditions, the eigenvalues of C_e and C_o also allow us to compute the entanglement entropy for an interval of length s sitting at one end of a strip of length $N/2$. The matrix C_o gives the two point function of a strip with Dirichlet boundary conditions, while C_e corresponds to Neumann boundary conditions.

The numerics suggest that for small masses ($mL \ll 1$) and low temperatures ($TL \ll 1$), the matrix C^2 has only a handful of eigenvalues which are significantly different from $1/4$. The largest of these eigenvalues corresponds to an eigenvector with even parity, while the second largest has odd parity. We approximate these eigenvalues by computing $\operatorname{tr} C_e^2$ and $\operatorname{tr} C_o^2$. We find in

[9]Note that C^2 commutes with the parity operator for both odd and even n. For example, if we indexed C^2 from $1 \leq k \leq n$, parity would send $k \to n - k + 1$.

the even sector that

$$\begin{aligned}\operatorname{tr} C_e^2 &= \frac{1}{2\pi mL}\coth\left(\frac{m}{2T}\right)\left[\gamma+\ln\left(\frac{4N\sin(\pi r)}{\pi}\right)\right]+\frac{r^2}{4}\operatorname{csch}^2\left(\frac{m}{2T}\right)\\ &\quad+\frac{1}{4}\Bigg[s+\frac{11}{12}-\frac{1}{\pi^2}\\ &\quad+\frac{1}{2\pi^2}\left(-2+\gamma+4\ln\frac{2N}{\pi}-3\ln\frac{4N\sin(\pi r)}{\pi}\right)\left(\gamma+\ln\frac{4N\sin(\pi r)}{\pi}\right)\Bigg]\\ &\quad-\frac{3mL}{32\pi^3}\coth\left(\frac{m}{2T}\right)\left[\mathrm{Li}_3(e^{2\pi ir})+\mathrm{Li}_3(e^{-2\pi ir})-2\zeta(3)\right]\\ &\quad+O((mL)^2,e^{-2\pi/TL},\log N/N)\ , \end{aligned}\tag{2.16}$$

and that in the odd sector

$$\begin{aligned}\operatorname{tr} C_o^2 &= \frac{1}{4}\Big[s+\frac{1}{12}-\frac{3}{2\pi^2}+\frac{1}{2\pi^2}\left(\gamma-1+\ln\frac{4N\sin(\pi r)}{\pi}\right)^2\Big]\\ &\quad+O((mL)^2,e^{-2\pi/TL},\log N/N)\ , \end{aligned}\tag{2.17}$$

where $r=\ell/L$ and $2s+1$ is the number of lattice sites. We make some brief remarks about how these traces were computed below.

Because of the relation $\lambda_k=\frac{1}{4}\coth^2(\epsilon_k/2)$ between the entanglement spectrum and the eigenvalues of C^2, we know that the eigenvalues of C^2 are bounded below by $1/4$. The largest even eigenvalue λ_e and odd eigenvalue λ_o are thus bounded above by

$$\lambda_e \le \operatorname{tr} C_e^2-\frac{s}{4}\ , \tag{2.18}$$

$$\lambda_o \le \operatorname{tr} C_o^2-\frac{s-1}{4}\ . \tag{2.19}$$

We can also put a lower bound on λ_e by using the variational principle and a "trial wave function". In this case, we use a constant trial wave function,

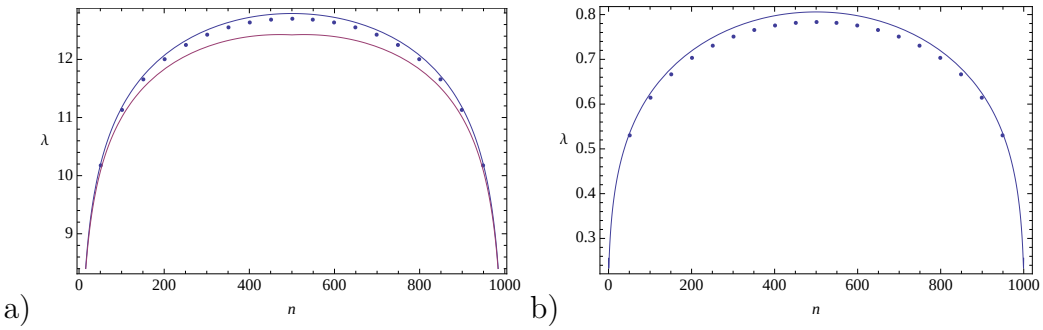

Figure 1: The largest (a) and second largest (b) eigenvalue of C^2 plotted against the interval length for $mL = 1/10$, $T = 0$, and $N = 1000$. The points are numerically computed. The curves above the points are the analytic upper bounds (2.18) and (2.19) computed from the traces. The solid curve below the points on the left is the lower bound (2.20) computed from the variational principle.

$\psi_e = (1, 1, \ldots, 1)/\sqrt{n}$. The expectation value then provides a lower bound:

$$\begin{aligned} \lambda_e &\geq \langle \psi_e | C_e^2 | \psi_e \rangle \qquad (2.20) \\ &= \frac{1}{2\pi mL} \coth\left(\frac{m}{2T}\right) \left[\gamma + \ln\left(\frac{4N\sin(\pi r)}{\pi}\right)\right] + \frac{1}{12} \\ &\quad -\frac{i}{8\pi^3 r}\left[\gamma + \ln\left(\frac{4N\sin(\pi r)}{\pi}\right)\right]\left[\mathrm{Li}_2(e^{2\pi i r}) - \mathrm{Li}_2(e^{-2\pi i r})\right] \\ &\quad -\frac{r^2}{4}\left[\frac{1}{3} - \coth^2\left(\frac{m}{2T}\right)\right] + O(mL, e^{-2\pi/TL}, \log N/N) \ . \end{aligned}$$

Figure 1 demonstrates that our upper and lower bounds provide relatively good estimates of the two largest eigenvalues at $T = 0$. We could try to produce an analytic lower bound on λ_o by similar methods. However, simple trial wave functions such as $(\psi_o)_j \sim \sin(\pi j/N)$ or $(\psi_o)_j \sim j$ do not seem to give strong lower bounds numerically and are harder to work with analytically than the constant trial wave function used above in the even case.

The zero mode $a = 0$ terms in $\langle\phi\phi\rangle$ and $\langle\pi\pi\rangle$ have a large influence on the structure of these traces in our $m, T \ll 1/L$ limit. As these zero modes have even parity, they do not contribute to C_o^2. For example, note that $\mathrm{tr}\, C_e^2 = O(1/mL)$ is much larger than $\mathrm{tr}\, C_o^2 = O(1)$ because the zero mode $a = 0$ term in $\langle\phi\phi\rangle$ is $O(1/mL)$ but only contributes to the even sector of C^2.

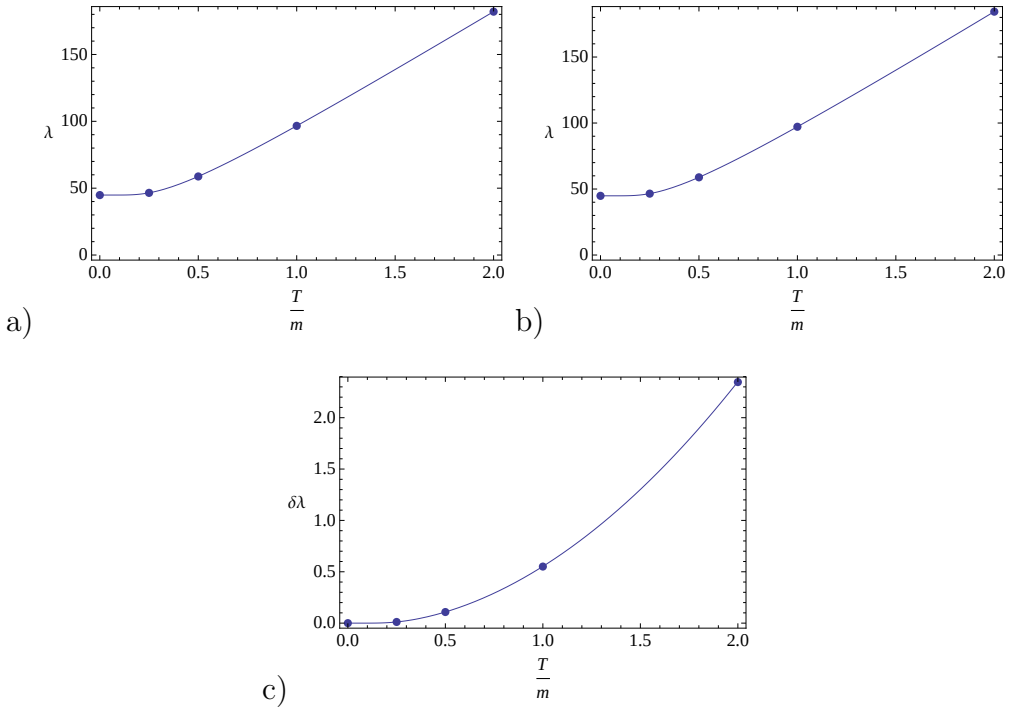

Figure 2: The largest eigenvalue of C^2 as a function of temperature for $mL = 1/50$: a) $\ell/L = 1/5$; b) $\ell/L = 4/5$; c) the difference between the two for a lattice with $N = 200$. The points are numerical while the curve is the upper bound computed from $\mathrm{tr}\, C_e^2$.

Also note that only $\mathrm{tr}\, C_e^2$ depends on T. The reason is that $\coth(\omega_a/2T) \approx 1$ up to exponentially suppressed terms except when $a = 0$.

Another interesting feature of these traces is their behavior under the exchange of the interval A with its complement B. By translation invariance, this exchange can be implemented by sending $r \to 1 - r$. At $T = 0$, both $\mathrm{tr}\, C_o^2$ and $\mathrm{tr}\, C_e^2$ are invariant under this transformation. This invariance is expected in order to guarantee that $S_A = S_B$. For $T \neq 0$, the breaking of this symmetry is due entirely to the $r^2\, \mathrm{csch}^2(m/2T)$ term in $\mathrm{tr}\, C_e^2$. This symmetry breaking term comes from multiplying the $a = 0$ zero modes in $\langle\phi\phi\rangle$ and $\langle\pi\pi\rangle$ together. Figure 2 demonstrates that $\mathrm{tr}\, C_e^2$ gives a remarkably good estimate of the temperature dependence of the largest eigenvalues for regions A and B, and also for their difference.

We should say a few words about the lengthy computation performed to obtain (2.16), (2.17), and (2.20). Consider first the $O(1/mL)$ contribution to $\mathrm{tr}\, C_e^2$:

$$\mathrm{tr}\, C_e^2 = \frac{1}{2mL} \coth\left(\frac{m}{2T}\right) f(n,N) + O(mL)^0 + O(e^{-2\pi/TL}) \ , \tag{2.21}$$

where

$$f(n,N) \equiv \frac{1}{N}\sum_{a=1}^{N} \frac{\sin^2(\pi a n/N)}{\sin(\pi a/N)} = \frac{1}{N}\sum_{j=1}^{n} \cot\frac{\pi}{N}(j-1/2) \ . \tag{2.22}$$

We want to evaluate this sum in the continuum limit where n and N are both large but $r = n/N$ is held fixed between zero and one. Replacing the sum over j by an integral introduces unacceptably large errors because of the divergence at $j = 1/2$. Instead, we compute a related integral that does not have this divergence:

$$\begin{aligned} f(n,N) &\approx \int_{1/N}^{r} \left(\cot\pi(x-1/2N) - \frac{1}{\pi(x-1/2N)}\right) dx \\ &\qquad + \frac{1}{N}\sum_{j=1}^{n} \frac{N}{\pi(j-1/2)} \qquad (2.23) \\ &= \frac{1}{\pi}\left[\ln\left(\frac{4N\sin(\pi r)}{\pi}\right) + \gamma\right] + O(1/N^2) \ . \qquad (2.24) \end{aligned}$$

Calculating the $O(mL)^0$ and $O(mL)$ terms is a more complicated enterprise. As mentioned already above, one contribution to C_e^2 comes from multiplying the zero modes in $\langle\phi\phi\rangle$ and $\langle\pi\pi\rangle$ together and yields $r^2\,\mathrm{csch}^2(m/2T)$. The remaining order one pieces can be computed from the matrix C_e^2 with the zero modes removed in the limit $m = 0 = T$:

$$(\tilde{C}_e^2)_{jk} = \frac{1}{4N^2}\sum_{a,b=1}^{N-1}\sum_{l=-s}^{s} \frac{\sin\frac{\pi a}{N}}{\sin\frac{\pi b}{N}} \cos\frac{2\pi la}{N}\cos\frac{2\pi lb}{N}\cos\frac{2\pi ja}{N}\cos\frac{2\pi kb}{N} \tag{2.25}$$

Similarly, the $O(mL)^0$ contribution to $\mathrm{tr}\, C_o^2$ can be calculated from the $m = T = 0$ limit of the matrix C_o:

$$(\tilde{C}_o^2)_{jk} = \frac{1}{N^2}\sum_{a,b=1}^{N-1}\sum_{l=1}^{s} \frac{\sin\frac{\pi a}{N}}{\sin\frac{\pi b}{N}} \sin\frac{2\pi la}{N}\sin\frac{2\pi lb}{N}\sin\frac{2\pi ja}{N}\sin\frac{2\pi kb}{N} \tag{2.26}$$

The $O(mL)$ term of $(C_e^2)_{jk}$ comes from zero modes pieces of C^2 where either $a = 0$ in the $\langle\phi\phi\rangle$ sum or $a = 0$ in the $\langle\pi\pi\rangle$ sum:

$$\frac{3mL}{16N^3}\coth\left(\frac{m}{2T}\right)\sum_{b=1}^{N-1}\sum_{l=-s}^{s}\frac{\cos\frac{2\pi lb}{N}\cos\frac{2\pi kb}{N}}{\sin\frac{\pi b}{N}}\ . \tag{2.27}$$

(For $(C_e)_{jk}$, the indices have the range $-s \le j,k \le s$, while for $(C_o)_{jk}$, we restrict to $1 \le j,k \le s$.) In the appendix B, we describe how to perform the sums (2.25), (2.26), and (2.27) along with (2.20) in the the large N limit with s/N held fixed.

2.4 Raising the Temperature

We present three arguments that the entanglement entropy depends exponentially on the ratio m/T in the limit $T \ll m$. The first argument is heuristic and relies on the structure of the matrix C^2. The second argument is based on our earlier calculation of $\mathrm{tr}\, C_e^2$. The third argument is based on numerical evidence. We would like to show two things. The first is that for a fixed interval A,

$$S(T) - S(0) \sim e^{-m/T}\ . \tag{2.28}$$

The second is that for two complementary intervals A and $\bar{A} = B$,

$$S_A - S_B \sim e^{-m/T}\ . \tag{2.29}$$

The first argument relies on the fact that the temperature dependence of C^2 comes entirely from the factors of $\coth(\omega_a/2T)$ in $\langle\phi\phi\rangle$ and $\langle\pi\pi\rangle$. The frequency ω_a is bounded below by m. Thus we conclude that

$$\coth\left(\frac{\omega_a}{2T}\right) \le \coth\left(\frac{m}{2T}\right) = 1 + 2e^{-m/T} + O(e^{-2m/T})\ . \tag{2.30}$$

In other words, the matrix C has a low temperature expansion of the form

$$C(T) = C(0) + e^{-m/T}\delta C + \ldots \tag{2.31}$$

where the ellipsis denotes terms that are more exponentially suppressed. Now if $C(T)$ has such an expansion, then the eigenvalues $\nu_k(T) = \nu_k(0) + e^{-m/T}\delta\nu_k + \ldots$ will as well. Assuming $\nu_k(0) - 1/2 \gg e^{-m/T}$, expanding eq.

(2.7) in the small T limit, one concludes that the entanglement entropy for a single interval shifts by an amount

$$\delta S = 2\sum_k [\ln(\nu_k(0)+1/2) - \ln(\nu_k(0)-1/2)]\delta\nu_k e^{-m/T} + \dots \ , \tag{2.32}$$

implying the scaling (2.28). Assuming δS is different for an interval and its complement, one also concludes the scaling (2.29).

While, the numerical evidence we present below suggests both scalings (2.28) and (2.29) are correct, there are some loop holes in our argument. An obvious problem is that the $e^{-m/T}$ term in the small T expansion may vanish; the temperature dependence may be of the form $e^{M/T}$ for some $M > m$. A more subtle loop hole involves the fact that many of the $\nu_k(0)$ are close to $1/2$. In this case, the correction to the entanglement entropy δS can scale as $(m/T)e^{-m/T}$ instead of just $e^{-m/T}$. Numerically, we see no evidence for this behavior. Instead, in these cases we find that the logarithmic enhancement is not enough to make up for the smallness of $\delta\nu_k$; these eigenvalues contribute negligibly to the entanglement entropy.

The second argument for the scalings (2.28) and (2.29) is based on using $\operatorname{tr} C_e^2$ as an estimate of the largest eigenvalue λ_e. Using $\operatorname{tr} C_e^2$, we estimate the contribution of λ_e to S and infer the scalings from this contribution. The temperature dependence of a single interval comes principally from the leading $\coth(m/2T)/mL$ term in (2.16). One finds agreement with (2.28):

$$[S(T) - S(0)]|_{\lambda_e} \sim e^{-m/T} \ . \tag{2.33}$$

Next we consider the entanglement difference $S_B - S_A$. This type of temperature dependence comes from the $r^2\,\mathrm{csch}^2(m/2T)$ piece of (2.16). One finds agreement with (2.29):

$$[S_B(T) - S_A(T)]|_{\lambda_{e,A},\lambda_{e,B}} \sim \frac{\pi}{2}\frac{mL}{\log N}(1-2r)\, e^{-m/T} \ . \tag{2.34}$$

We should emphasize that using $\operatorname{tr} C_e^2$ and the largest eigenvalue λ_e to estimate the temperature scalings is flawed. An obvious limitation is that we only have a result for $\operatorname{tr} C_e^2$ in the limit $mL \ll 1$ while we expect the temperature scalings to hold more generally. A less obvious limitation is that despite the fact that λ_e is much larger than the other eigenvalues in the small mass limit, the logarithms in (2.7) play a democratizing role and let smaller eigenvalues contribute substantially to the entanglement entropy. For

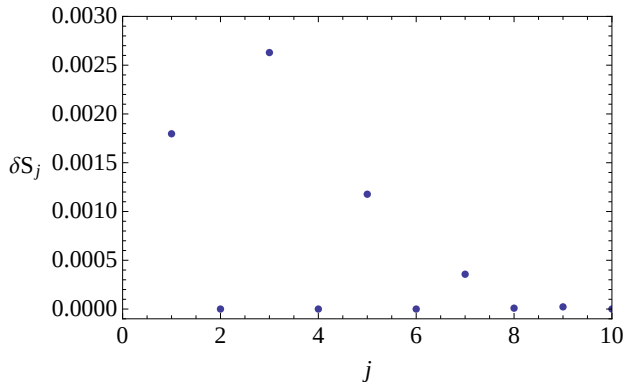

Figure 3: The contribution to $\delta S = S_A - S_B$ for the ten largest pairs of eigenvalues $\lambda_{j,A}$ and $\lambda_{j,B}$, arranged from largest to smallest. In this plot $mL = 0.02$, $m/T = 1$ and $\ell/L = 1/5$ for region B. Note that the odd parity eigenvalues do not contribute. ($N = 200$ was used for this plot.)

example, in this small mass limit numerical analysis shows that the dominant contribution to $S_A - S_B$ comes from the second largest even eigenvalue (see figure 3).

Our most convincing evidence for the scalings (2.28) and (2.29) is numerical and is presented in figures 4 and 5. Figure 4 demonstrates unambiguous evidence for (2.28), not only for $mL \ll 1$ but also for $mL > 1$. Figure 5a displays unambiguous evidence for (2.29), again both for small and large values of mL. More ambitiously, we can try to investigate numerically whether the $mL(1-2r)/\log N$ behavior of eq. (2.34) is correct as well. Figure 5a provides evidence for the mL scaling. Figure 5b provides some limited evidence for the $1-2r$ behavior for large values of mL and for intervals with $r \sim 1/2$. However, we find no evidence for the $\log N$ behavior of (2.34).

2.5 Discussion

As mentioned in the introduction, the original motivation for this chapter came from the Ryu-Takayanagi proposal [10] for computing the entanglement entropy of field theories with holographic dual classical gravity descriptions. In their proposal, the field theory lives on the boundary of the space-time in the dual description. Let C be the curve that separates region A from region B in the field theory. Let C also be the boundary of a minimal surface M

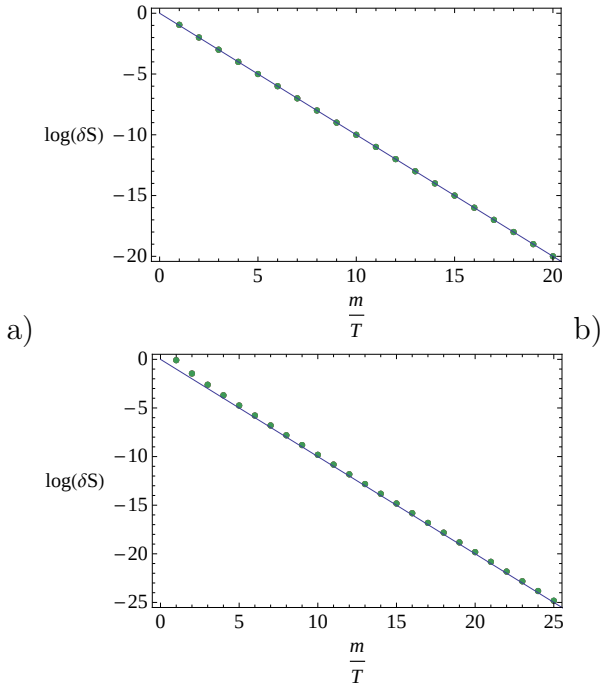

Figure 4: A log plot of the entanglement entropy $\delta S = S(T) - S(0)$ vs. m/T with an interval size $\ell/L = 3/10$. The points are numerically computed, and the line $\log(\delta S) = -m/T$ is a guide to the eye: a) $mL = 5 \times 10^{-3}$; b) $mL = 5$. (For both plots, the points were computed with $N = 50$, 100, 200, and 400. The data points for different values of N all lie roughly on top of each other.)

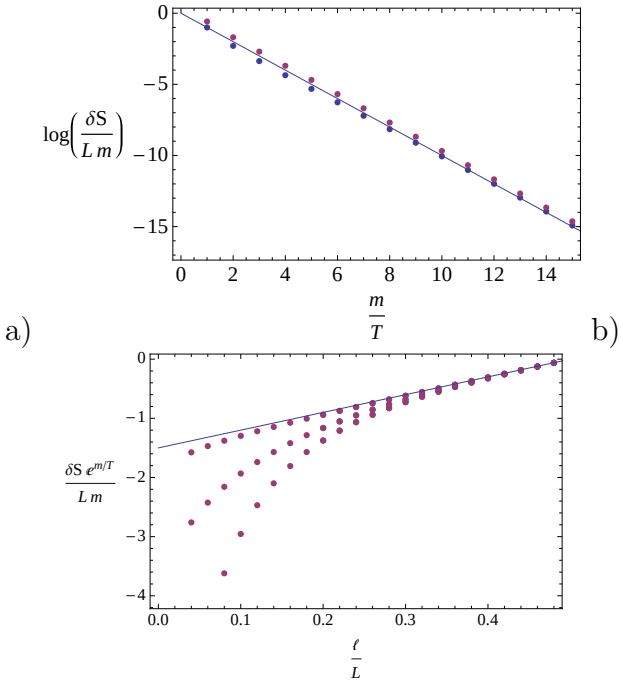

Figure 5: a) A log plot of the entanglement entropy difference $\delta S = S_A - S_B$ vs. m/T for $mL = 5$ and 5×10^{-3}, and an interval B of size $\ell/L = 1/5$. At fixed m/T, the larger mass points lie below the smaller ones. The line $\log(\delta S/mL) = -m/T$ is a guide to the eye. (The lattice was taken to have size $N = 200$, but there is no noticeable difference between this graph and a graph with $N = 100$.) b) The entanglement entropy difference δS vs. ℓ/L for (from bottom to top) $mL = 5 \times 10^{-3}$, 2, and 5. The mass to temperature ratio is $m/T = 10$. The line $e^{m/T}\delta S/mL = 3m/T - 3/2$ is a guide to the eye. (The lattice was taken to have $N = 400$, but there is no difference between this graph and a graph with $N = 200$.)

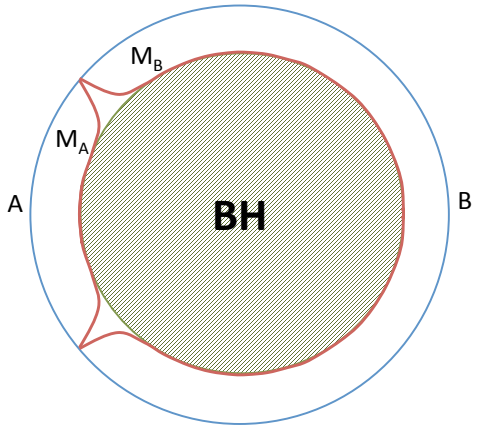

Figure 6: The two minimal surfaces M_A and M_B corresponding to a region A and its complement B when the dual space time contains a black hole (BH).

that falls into the space-time. The proposal is that the entanglement entropy is proportional to the area of M:

$$S_A = \frac{\text{Area}(M)}{4G_N} \ , \tag{2.35}$$

where G_N is Newton's constant. Assuming a unique such M, the entanglement entropy of a region and its complement are always equal, $S_A = S_B$.

When the space-time contains a black hole, Ryu-Takayanagi modified their proposal to account for the existence of two minimal surfaces M_A and M_B. The entanglement entropy for A must be computed from the surface M_A that is deformable into A. Correspondingly, for region B, we must use M_B. For large black holes, $\text{Area}(M_A) - \text{Area}(M_B)$ will come mostly from the differing amount of black hole horizon area that the two surfaces wrap (see figure 6). The Hawking temperature of the black hole corresponds to the temperature of the field theory, and thus this modification of the proposal provides a way for $S_A - S_B$ to be nonzero for certain thermal field theories.

However, there are instances where field theories at $T > 0$ have dual gravity descriptions without a black hole. A classic example is the large N, strong coupling limit of maximally supersymmetric $SU(N)$ Yang-Mills theory on $S^3 \times S^1$ [21]. At temperatures small compared to the inverse radius of the S^3, the dual description is thermal $AdS_5 \times S^5$. At a critical temperature T_c, the gravity description undergoes a first order Hawking-Page phase transition to a state with a large black hole. For the field theory, this transition is understood as a deconfinement phase transition.

On the one hand, their proposal implies that the entanglement entropy will serve as an order parameter for the phase transition: for $T < T_c$, $S_A - S_B = 0$, while for $T > T_c$, $S_A - S_B \neq 0$. On the other, at any finite N, we have a system at finite volume for which there can be no phase transitions. The transition from $S_A = S_B$ at $T = 0$ to $S_A \neq S_B$ at $T > T_c$ must be smooth. We conclude that the Ryu-Takayanagi formula is only valid in the strict large N limit, but it would be nice to understand the form of the $1/N$ corrections. In principle, one should be able to compute the entanglement entropy for maximally supersymmetric Yang-Mills at weak coupling. In practice, such a computation is substantially more difficult, and we instead considered a 1+1 dimensional massive scalar field on a circle at $T > 0$. Morally, the regime $T < m$ should correspond to the confining regime of the Yang-Mills theory where the fields get a mass through their coupling to the curvature of the S^3. For our scalar field, we argued that in the regime $T \ll m$, the entanglement entropy difference scales as

$$S_B - S_A \sim e^{-m/T} \ .$$

We conjecture that this type of scaling should be a generic feature of all gapped systems.

3 Thermal Corrections to Rényi entropies for Free Fermions

3.1 Background

In this chapter, we use the conventional definition of entanglement entropy. We assume that the Hilbert space factors nicely with respect to two complementary spatial regions, A and $\bar{A}$. The reduced density matrix and Rényi

entropies are then defined as

$$\rho_A \equiv \mathrm{tr}_{\bar{A}}\, \rho, \tag{3.1}$$

$$S_n \equiv \frac{1}{1-n} \log\, \mathrm{tr}(\rho_A)^n. \tag{3.2}$$

The factor of $1/(1-n)$ in the the definition of the Rényi entropy is convenient for taking a $n \to 1$ limit and recovering the entanglement entropy:

$$S_{EE} \equiv -\,\mathrm{tr}\,[\rho_A \log(\rho_A)] = \lim_{n\to 1} S_n\ . \tag{3.3}$$

It was argued in the previous chapter that for gapped systems at small temperature, thermal corrections to the entanglement entropy are Boltzmann suppressed. Further evidence in $d = 1 + 1$ can be found in Refs. [30, 31, 32, 33, 34]. For general conformal field theories with temperature $1/\beta$ on a circle of perimeter L, the coefficient of the Boltzman factor was calculated [35]:

$$\delta S_n \equiv S_n(T) - S_n(0) = \frac{g}{1-n}\left[\frac{1}{n^{2\Delta-1}}\frac{\sin^{2\Delta}\left(\frac{\pi\ell}{L}\right)}{\sin^{2\Delta}\left(\frac{\pi\ell}{nL}\right)} - n\right] e^{-2\pi\beta\Delta/L} + o(e^{-2\pi\beta\Delta/L}), \tag{3.4}$$

$$\delta S_{EE} \equiv S_{EE}(T) - S_{EE}(0) = 2g\Delta\left[1 - \frac{\pi\ell}{L}\cot\left(\frac{\pi\ell}{L}\right)\right] e^{-2\pi\beta\Delta/L} + o(e^{-2\pi\beta\Delta/L}), \tag{3.5}$$

where g is the degeneracy of the first excited state, Δ is the smallest scaling dimension among the operators, and ℓ is the interval length. (In order for these formulae to hold, the conformal field theory on the circle has to have a unique ground state and a mass gap.)

For higher dimensional conformal field theories on $\mathbb{S}^1 \times \mathbb{S}^{d-1}$, an analogous thermal correction to entanglement entropy is also known [36]. The result for the entanglement entropy for a cap on a sphere with polar angle θ and radius R is given in general by the following integral:

$$\delta S_{EE} = g\Delta I_d(\theta) e^{-\beta\Delta/R} + o\left(e^{-\beta\Delta/R}\right), \tag{3.6}$$

$$I_d(\theta) = 2\pi \frac{\mathrm{Vol}(S^{d-2})}{\mathrm{Vol}(S^{d-1})} \int_0^\theta d\theta' \frac{\cos(\theta') - \cos(\theta)}{\sin(\theta)} \sin^{d-2}(\theta')\ . \tag{3.7}$$

The derivation of this result relies on a conformal transformation from the sphere to hyperbolic space. The conformal transformation allows one to

identify the reduced density matrix for the ground state as a unitary transformation of the thermal density matrix on hyperbolic space. There is a corresponding identification between the logarithm of the reduced density matrix (or modular Hamiltonian) and the Hamiltonian for the conformal field theory on hyperbolic space. Unfortunately, there can be subtleties associated with boundary terms for the modular Hamiltonian when this transformation is invoked. In the case of conformally coupled scalars [36, 37], these boundary terms mean the result (3.6) should be corrected; one replaces I_d in the result above with I_{d-2}. The issue is that the conformal coupling requires a Gibbons-Hawking like term on the boundary. The natural constant θ boundary is different from the boundary of hyperbolic space, and this difference contaminates the entanglement entropy. In this chapter we study free fermions which have no such Gibbons-Hawking like term and consequently no subtleties associated with the boundary. Thus we expect and indeed find that the result (3.6) holds for massless free fermions. As an added benefit, we also compute thermal corrections to Rényi entropies for fermions.

This chapter is organized as follows. First we briefly review the mapping used in Ref. [37] that maps from the multi-sheeted cover of the sphere to a wedge in flat space. We then calculate the two point function using the method of images, from which we can read off the thermal corrections to Rényi entropies. Finally, we compare these calculations of entanglement and Rényi entropies with numerical results for fermions in $d = 2+1$ and $d = 3+1$.

3.2 Rényi's for a General CFT

A main result from Ref. [37] was a general equation for the thermal correction to the Rényi entropy for a conformal field theory. We assume that when the conformal field theory is placed on a $\mathbb{S}^{d-1} \times \mathbb{R}$, there is a unique ground state $|0\rangle$ and a set of degenerate first excited states $|\psi_i\rangle$ with energy E_ψ. We divide the $\mathbb{S}^{d-1}$ into a spatial region A and complement $\bar{A}$ and consider instead of $\mathbb{S}^{d-1} \times \mathbb{R}$, an n-sheeted branched cover of this spacetime where the branching is over the region A. The result from Ref. [37] is

$$\delta S_n = \frac{n}{1-n} \sum_i \left(\frac{\langle \psi_i(z) \psi_i(z') \rangle_n}{\langle \psi_i(z) \psi_i(z') \rangle_1} - 1 \right) e^{-\beta E_\psi} + o(e^{-\beta E_\psi}) \tag{3.8}$$

where ψ_i is an operator that creates one of the first excited states. The point z is in the far Euclidean future and the point z' in the far Euclidean

past. The subscript n indicates the two-point function is to be evaluated on this n-sheeted branched cover. (Note that the result (3.8) could have been anticipated from a very similar result in 1+1 dimensional conformal field theories [35].)

In general, it is not clear how to evaluate $\langle\psi_i(z)\psi_i(z')\rangle_n$. However, if we restrict to the case where A is a cap on a sphere of opening angle 2θ, then we can take advantage of a conformal transformation that maps the n-sheeted branched cover of $\mathbb{S}^{d-1}\times\mathbb{R}$ to $C_n\times\mathbb{R}^{d-2}$ where C_n is an n-sheeted cover of the complex plane, branched over the negative real axis. It is convenient to make the transformation in a couple of steps, as was outlined in Ref. [37]. The first step takes the cap on $\mathbb{S}^{d-1}$ to a ball in $\mathbb{R}^{d-1}$ (see the appendix of Ref. [38]):

$$ds^2 = -dt^2 + dr^2 + r^2 d\Omega^2 \tag{3.9}$$

$$= \Omega^2\left(-d\tau^2 + d\theta^2 + \sin^2(\theta)d\Omega^2\right), \tag{3.10}$$

where

$$t \pm r = \tan\left(\frac{t\pm\theta}{2}\right), \tag{3.11}$$

$$\Omega = \frac{1}{2}\sec\left(\frac{\tau+\theta}{2}\right)\sec\left(\frac{\tau-\theta}{2}\right), \tag{3.12}$$

and $d\Omega^2$ is the line element on $\mathbb{S}^{d-2}$. If the cap has opening angle $2\theta_0$, then the ball has radius $r_0 = \tan(\theta_0/2)$. A further special conformal transformation maps the ball to a half space:

$$y^\mu = \frac{x^\mu - b^\mu x^2}{1 - 2b\cdot x + b^2x^2}, \tag{3.13}$$

$$ds^2 = dy^\mu dy^\nu \delta_{\mu\nu} = (1 - 2b\cdot x + b^2x^2)^{-2} dx^\mu dx^\nu \delta_{\mu\nu}. \tag{3.14}$$

We let x^0 and y^0 correspond to Euclidean times, and take $b^1 = 1/r_0$ to be the only non-vanishing value of the vector b. After further rescaling and rotations, the inserted operators can be placed at $y' = (1,2\theta_0,\vec{0})$ and $y = (1,0,\vec{0})$, where we are using polar coordinates (r,θ) on the C_n. (For further details, see Ref. [37].)

We will employ a method of images strategy for computing $\langle\psi_i(y)\psi_i(y')\rangle_n$ on $C_n\times\mathbb{R}^{d-2}$. This strategy was already used successfully for the scalar in Refs. [37, 39]. The idea is to compute the two-point function using the

method of images on the orbifold $\mathbb{C}/\mathbb{Z}_m$ for general m and then to obtain $\langle\psi_i(y)\psi_i(y')\rangle_n$ by analytic continuation, setting $n = 1/m$. As the method of images relies on the fact that the underlying equations of motion are linear, we do not expect this method will be useful for interacting field theories.

In the fermionic case, there are issues associated with nontrivial phases, signs and a choice of spin structure which we must address. One issue, which we now review, is that rotations act nontrivially on spinor wave functions.

3.2.1 Rotation on Fermions

For a Dirac fermion we know the effect of a rotation on the components of the spinor [40]. A general Lorentz transformation in Euclidean signature, Λ, is given by

$$\psi(x) \to \Lambda_{1/2}\psi(\Lambda^{-1}x), \tag{3.15}$$

$$\Lambda_{1/2} = \exp\left(\frac{1}{8}\omega_{\mu\nu}[\gamma^\mu, \gamma^\nu]\right), \tag{3.16}$$

$$\{\gamma^\mu, \gamma^\nu\} = 2\delta^{\mu\nu}, \tag{3.17}$$

where $\omega_{\mu\nu}$ parameterizes the rotations and Lorentz boosts. For the case of interest we are only interested in rotations in (0,1) plane, for which the only non-vanishing components are $\omega_{01} = -\omega_{10} = \phi$. The matrix exponential can be done simply and is given by

$$\Lambda_{1/2}(\phi) = \cos(\phi/2) + \sin(\phi/2)\gamma^0\gamma^1. \tag{3.18}$$

If we then define

$$\gamma^z = \gamma^0 + i\gamma^1 \text{ and } \gamma^{\bar{z}} = \gamma^0 - i\gamma^1, \tag{3.19}$$

then equation (3.18) simplifies to

$$\Lambda_{1/2}(\phi) = \frac{1}{2}\gamma^0(e^{-i\phi/2}\gamma^z + e^{i\phi/2}\gamma^{\bar{z}}). \tag{3.20}$$

A fact that we will rely on heavily moving forward is that $\gamma^0\gamma^z$ and $\gamma^0\gamma^{\bar{z}}$ are projectors:

$$(\gamma^0\gamma^z)^2 = 2(\gamma^0\gamma^z)\ , \quad (\gamma^0\gamma^{\bar{z}})^2 = 2(\gamma^0\gamma^{\bar{z}})\ , \tag{3.21}$$

$$(\gamma^0\gamma^z)(\gamma^0\gamma^{\bar{z}}) = 0\ , \quad (\gamma^0\gamma^{\bar{z}})(\gamma^0\gamma^z) = 0\ . \tag{3.22}$$

3.3 Analytic calculation of Rényi Entropies

In flat space the fermion 2-point function is, up to normalization,

$$\langle\bar{\psi}(y')\psi(y)\rangle = \frac{\gamma^0\gamma^\mu(y-y')_\mu}{|y-y'|^d} \tag{3.23}$$

$$= -\frac{1}{d-2}\gamma^0\gamma^\mu\frac{\partial}{\partial x^\mu}\frac{1}{|y-y'|^{d-2}} \ . \tag{3.24}$$

Following Ref. [37], the Green's function on a wedge $\mathbb{C}/\mathbb{Z}_m \times \mathbb{R}^{d-2}$ can be calculated via the method of images. The Green's function via the method of images is given by rotating one of the fermions by $2\pi k/m$ where k indexes the wedges and m is the number of wedges. In going between adjacent wedges an extra factor of (-1) is added due to the spin structure (for example see Ref. [41]). The result is then

$$\langle\bar{\psi}(y')\psi(y)\rangle_{1/m} = -\frac{\gamma^0\gamma^\mu\partial_\mu}{d-2}\sum_{k=0}^{m-1}\frac{(-1)^k\Lambda_{1/2}(2\pi k/m)}{[|z-e^{2\pi ik/m}z'|^2+(\mathbf{y}-\mathbf{y}')^2]^{(d-2)/2}} \ . \tag{3.25}$$

(Curiously, this expression only makes sense for m an odd integer. Nevertheless, we find that knowing the two-point function for odd integers is in general sufficient to make the analytic continuation to $n = 1/m$.) In the case of interest $\mathbf{y} = \mathbf{y}' = 0$, $z' = e^{2i\theta}$ and $z \to 1$, the two-point function can be rewritten

$$G^F_{(1/m,d)}(2\theta) = -\frac{\gamma^0}{d-2}\lim_{z\to 1}\sum_{k=0}^{m-1}\left(e^{\frac{-\pi ik(m-1)}{m}}\gamma^z\partial_z + e^{\frac{\pi ik(m-1)}{m}}\gamma^{\bar{z}}\partial_{\bar{z}}\right)\frac{1}{|z-e^{2i(\pi k/m+\theta)}|^{d-2}} \tag{3.26}$$

$$= \frac{\gamma^0}{4(d-2)}\left[\gamma^z\left((d-2)-i\partial_\theta\right)\sum_{k=0}^{m-1}\frac{e^{\frac{-\pi ik(m-1)}{m}}}{|1-e^{2i(\pi k/m+\theta)}|^{d-2}} + \gamma^{\bar{z}}c.c.\right] \ . \tag{3.27}$$

From this expression, we can deduce the following recursion relation for the two-point function:

$$G^F_{(1/m,d+2)}(2\theta) = \left((\partial_\theta^2 + d(d-2))\gamma^0(\gamma^z+\gamma^{\bar{z}}) + 2i(\gamma^0\gamma^z - \gamma^0\gamma^{\bar{z}})\partial_\theta\right)\frac{G^F_{(1/m,d)}(2\theta)}{8d(d-1)}. \tag{3.28}$$

To obtain the Rényi entropy we make the replacement $n = 1/m$ in the two point function and we use that $E_\psi = \frac{d-1}{2R}$ for free fermions on a sphere of radius R:

$$\delta S_n(\theta) = \frac{n}{1-n} \sum_i \left(\frac{\langle \psi_i \psi_i \rangle_n}{\langle \psi_i \psi_i \rangle_1} - 1 \right) e^{-(d-1)\beta/(2R)} + o\left(e^{-(d-1)\beta/(2R)}\right), \quad (3.29)$$

$$= \frac{n}{1-n} \operatorname{tr}(G^F_{(n,d)}(2\theta) G^F_{(1,d)}(2\theta)^{-1} - 1) e^{-(d-1)\beta/(2R)} + o(e^{-(d-1)\beta/(2R)}). \quad (3.30)$$

3.3.1 d=2

In $d = 1+1$ we can choose gamma matrices ($\gamma^0 = \sigma^3$ and $\gamma^1 = \sigma^1$) such that

$$\gamma^0 \gamma^z = \begin{pmatrix} 2 & 0 \\ 0 & 0 \end{pmatrix} \text{ and } \gamma^0 \gamma^{\bar{z}} = \begin{pmatrix} 0 & 0 \\ 0 & 2 \end{pmatrix}.$$

It is worth noting that it is convenient to have $\gamma^0\gamma^z$ diagonal, but is not necessary. Then the 2-point function is given by

$$G^F_{(1/m,2)}(2\theta) = \frac{1}{2} \sum_{k=0}^{m-1} \gamma^0 \left(\gamma^z \frac{\exp(\frac{-ik\pi(m-1)}{m})}{1 - \exp\left(2i(k\pi/m + \theta)\right)} + \gamma^{\bar{z}} \frac{\exp(\frac{ik\pi(m-1)}{m})}{1 - \exp\left(-2i(k\pi/m + \theta)\right)} \right)$$

$$= \gamma^0 \left(\gamma^z \frac{mi}{4} e^{-i\theta} \csc(m\theta) - \gamma^{\bar{z}} \frac{mi}{4} e^{i\theta} \csc(m\theta) \right) . \quad (3.31)$$

We can then calculate the Rényi entropies (and entanglement).

$$\begin{aligned} \delta S_n(\theta) &= \frac{n}{1-n} \operatorname{tr}(G^F_{(n,2)}(2\theta) G^F_{(1,2)}(2\theta)^{-1} - 1) e^{-\beta/(2R)} + o(e^{-\beta/(2R)}) \\ &= \frac{2}{1-n} \left(\sin(\theta) \csc(\theta/n) - n \right) e^{-\beta/(2R)} + o(e^{-\beta/(2R)}) , \end{aligned} \quad (3.32)$$

$$\delta S_{EE} = 2(1 - \theta \cot(\theta)) e^{-\beta/(2R)} + o(e^{-\beta/(2R)}) . \quad (3.33)$$

These agree with the known results for 2d CFTs [35] in general and for 2d fermions [30, 34] in particular.

3.3.2 d=4

In $d = 3 + 1$ we choose gamma matrices

$$\gamma^0 = \begin{pmatrix} \sigma^2 & 0 \\ 0 & -\sigma^2 \end{pmatrix} \text{ and } \gamma^1 = \begin{pmatrix} \sigma^1 & 0 \\ 0 & -\sigma^1 \end{pmatrix}.$$

In this case the 2-point function is given by

$$G^F_{(1/m,4)}(2\theta) = \frac{im}{8}(1 + 3m^2 + (m^2 - 1)\cos(2m\theta))\csc^3(m\theta)\gamma^0 \left(\gamma^z e^{-i\theta} - \gamma^{\bar{z}} e^{i\theta}\right) . \tag{3.34}$$

Repeating the calculation in $d = 2$ we get

$$\begin{aligned} \delta S_n(\theta) &= \frac{n}{1-n} \operatorname{tr}(G^F_{(n,4)}(2\theta) G^F_{(1,4)}(2\theta)^{-1} - 1) e^{-3\beta/(2R)} + o(e^{-3\beta/(2R)}) \\ &= \frac{4}{(1-n)n^2} \left((3 + n^2 - (n^2 - 1)\cos(2\theta/n))\csc^3(\theta/n)\sin^3(\theta) - 4n^3\right) e^{-3\beta/(2R)} \\ &\quad + o(e^{-3\beta/(2R)}) , \end{aligned} \tag{3.35}$$

$$\begin{aligned} \delta S_{EE}(\theta) &= \lim_{n\to 1} \frac{n}{1-n} \operatorname{tr}(G^F_{(n,4)}(2\theta) G^F_{(1,4)}(2\theta)^{-1} - 1) e^{-3\beta/(2R)} + o(e^{-3\beta/(2R)}) \\ &= 2(5 + \cos(2\theta) - 6\theta\cot(\theta)) e^{-3\beta/(2R)} + o(e^{-3\beta/(2R)}) . \end{aligned} \tag{3.36}$$

The second result correctly reproduces the entanglement entropy correction found for general conformal field theories on the sphere [36]. The result for $\delta S_n(\theta)$ is new.

3.3.3 d=3

In odd dimensions we can choose the same γ^z as we would use in one smaller dimension. Namely,

$$\gamma^0\gamma^z = \begin{pmatrix} 2 & 0 \\ 0 & 0 \end{pmatrix} \text{ and } \gamma^0\gamma^{\bar{z}} = \begin{pmatrix} 0 & 0 \\ 0 & 2 \end{pmatrix}.$$

Following previous work [37, 39], we may try to convert the denominator of the Green's function (3.27) to an integral in order to perform the sum over k. In the case of the scalar, the resulting expression can be analytically

continued to all m and thus in particular to $n = 1/m$. However, in the case of the fermion, some extra phases appear to spoil the analytic continuation. We are able to extract thermal corrections to entanglement entropy from an $n \to 1$ limit of the integral successfully. Thermal corrections to Rényi entropies remain out of reach however.

The first step in converting the sum to an integral is an integral representation of the cosecant used successfully in the analogous calculation for the scalars [37, 39]:

$$\int_0^\infty dx \frac{x^{\theta/\pi + k/m - 1}}{1+x} = \pi \csc(\theta + k\pi/m) \ . \tag{3.37}$$

From this integral representation, it directly follows that

$$\sum_{k=0}^{m-1} \frac{e^{-i\pi k(m-1)/m}}{\sin(\pi k/m + \theta)} = \frac{1}{\pi} \int_0^\infty dx \frac{x^{\theta/\pi - 1}}{1+x} \sum_{k=0}^{m-1} x^{k/m} e^{-i\pi k(m-1)/m} \tag{3.38}$$

$$= \frac{1}{\pi} \int_0^\infty dx \frac{x^{\theta/\pi - 1}}{1+x} \frac{(1 + e^{-i\pi m} x)}{1 + e^{i\pi/m} x^{1/m}} \ . \tag{3.39}$$

Using the representation (3.39) in the Green's function (3.27) for $d = 3$, we obtain

$$G^F_{(1/m,3)} = \frac{1}{8}(1 - i\partial_\theta)\gamma^0\gamma^z \frac{1}{\pi} \int_0^\infty dx \frac{x^{\theta/\pi - 1}}{1+x} \frac{e^{-i\pi m}(e^{im\pi} + x)}{1 + e^{i\pi/m} x^{1/m}} + \gamma^0\gamma^{\bar{z}} cc \ . \tag{3.40}$$

To get the entanglement entropy, we expand around $m = 1$:

$$G^F_{(1/m,3)} = (1 - i\partial_\theta)\frac{\gamma^0\gamma^z}{\pi} \int_0^\infty dx \, \frac{x^{\frac{\theta}{\pi}}}{1+x} \left(\frac{1}{x} - \frac{\log(x)}{1-x}(m-1) + O(m-1)^2 \right) + cc \tag{3.41}$$

$$= \gamma^0\gamma^z \left(i e^{-i\theta} \csc^2(\theta) - \frac{2e^{i\theta}\pi}{(1+e^{i\theta})^3}(m-1) + O(m-1)^2) \right) + cc \ . \tag{3.42}$$

The entanglement entropy correction is then constructed from a ratio of Green's functions

$$\delta S_{EE}(\theta) = \lim_{m \to 1} \frac{1}{m-1} \operatorname{tr}(G^F_{(1/m,3)}(2\theta) G^F_{(1,3)}(2\theta)^{-1} - 1) e^{-\beta/R} + o(e^{-\beta/R}) \tag{3.43}$$

$$= 4\pi \csc(\theta) \sin^4(\theta/2) e^{-\beta/R} + o(e^{-\beta/R}) \ . \tag{3.44}$$

This result matches the general case derived in Ref. [34].

While this integral representation gives the correct thermal corrections to the entanglement entropy, it appears to fail for the Rényi entropies. We suspect a reason is that the integral representation grows too quickly as a function of complex m to satisfy the assumptions of Carlson's Theorem. In other words, there will not be a unique analytic continuation. We can break the integral up into two pieces, one from $0 < x < 1$ and a second from $1 < x < \infty$, and then replace the two integrals with double sums:

$$\sum_{k=0}^{m-1} \frac{e^{-i\pi k(m-1)/m}}{\sin(\pi k/m + \theta)} = \sum_{p,q=0}^{\infty} (-1)^{p+q} m \left(\frac{e^{-im\pi} e^{-i\pi(q+1)/m}}{\pi(1+mp+q) - m\theta} + \frac{e^{-i\pi(q+1)/m}}{\pi(1+m+mp+q) - m\theta} + \frac{e^{i\pi q/m}}{\pi(mp+q) + m\theta} + \frac{e^{-im\pi} e^{i\pi q/m}}{\pi(m+mp+q) + m\theta} \right) .$$

In the case of the scalar, the phases in the numerator of this expression vanish, and the sum has better convergence properties. Here instead, for $m = iy$ pure imaginary, the sum has the same kind of growth as $\sin(\pi m)$, which vanishes for all integer m.[10]

3.3.4 Recursion relation for Entanglement entropy

We would also like to show that our recursion relation (3.28) is compatible with the recursion relation for the entanglement entropy found in Ref. [34]. We start by Taylor expanding the two-point function and relating it to the entanglement entropy[11]

$$G_{n,d}(2\theta) = G_d(2\theta) + \delta G_d(2\theta)(n-1) + \mathcal{O}(n-1)^2, \tag{3.45}$$

$$G_d(2\theta) = \gamma^0(\gamma^z e^{-i\theta} - \gamma^{\bar{z}} e^{i\theta}) \frac{i \csc^{d-1}(\theta)}{2^d}, \tag{3.46}$$

$$\delta S_{EE}(\theta) = g \frac{\delta G_d(2\theta)}{G_d(2\theta)} e^{-\beta E_\psi} + o(e^{-\beta E_\psi}). \tag{3.47}$$

We will proceed by induction and assume equation (3.6) in d dimensions. Equation (3.7) has the following recursion relation

$$I_d(\theta) - I_{d-2}(\theta) = -2\pi \frac{\mathrm{Vol}(S^{d-2})}{\mathrm{Vol}(S^{d-1})} \frac{\sin^{d-2}(\theta)}{(d-1)(d-2)}. \tag{3.48}$$

[10] See appendix C for an alternate integral representation of the sum.

[11] Here we are taking the case where $\gamma^0\gamma^z$ is diagonal so that the inverse is particularly simple.

Then using equation (3.6) and recalling that $\Delta = (d-1)/2$,

$$\delta G_d(2\theta) = \frac{d-1}{2} I_d(\theta) G_d(2\theta) \tag{3.49}$$

$$= \frac{d-1}{2} G_d(2\theta) \left(I_{d+2} + 2\pi \frac{\mathrm{Vol}(S^d)}{\mathrm{Vol}(S^{d+1})} \frac{\sin^d(\theta)}{(d+1)d} \right). \tag{3.50}$$

Acting on both sides with the operator in equation (3.28) and simplifying yields

$$\delta G_{d+2}(2\theta) = \frac{d+1}{2} I_{d+2}(\theta) G_{d+2}(2\theta). \tag{3.51}$$

We checked the entanglement entropy for both $d = 1+1$ and $d = 2+1$. Thus by induction the two recursion relations are in agreement for both even and odd dimensions.

3.4 Numerical Check

We are interested in numerically checking our results. As mentioned earlier a free fermion on a sphere does not suffer from the same boundary term ambiguities as the conformally coupled scalar [36]. The numerics for a free fermion should then directly give the general conformal field theory results. Using the convention $\bar{\Psi} = \Psi^\dagger \gamma^0$ the Hamiltonian and Lagrangian densities for a fermion in curved space are given by Γ

$$\mathcal{L} = \sqrt{-g} \bar{\Psi} (i \gamma^\lambda D_\lambda) \Psi, \tag{3.52}$$

$$\mathcal{H} = \sqrt{-g} \bar{\Psi} (i \gamma^j D_j) \Psi, \tag{3.53}$$

$$\{\Psi_\alpha(x), \Psi^\dagger_\beta(x')\} \sqrt{-g} = i \delta_{\alpha\beta} \delta(x - x') \tag{3.54}$$

Where D_λ is the covariant derivative on the manifold. This can be written explicitly in terms of the vierbein (e^λ_I) and spin connection $(\omega_{\lambda IJ})$.[12] We have defined the curved space gamma matrices and covariant spinor derivative

$$\gamma^\mu = \gamma^I e^\mu_I \ , \tag{3.55}$$

$$D_\mu = \partial_\mu + \frac{1}{8} \omega_{\mu IJ} [\gamma^I, \gamma^J] \ , \tag{3.56}$$

[12] We use capital Roman letters $I, J, K, \ldots$ for flat space-time indices, lower case Greek $\lambda, \mu, \nu, \ldots$ for curved space-time indices, lower case Greek $\alpha, \beta, \gamma, \ldots$ for spinor indices, and lower case Roman $i, j, k, \ldots$ for curved spatial indices.

where $\omega_{\mu IJ}$ is the spin connection. Using the torsion free Maurer-Cartan equation, $de^i + e^j \wedge \omega_j{}^i = 0$, we can extract the spin connection, the nonvanishing elements of which are

$$\omega^j{}_i = \cos(\theta_i) \left(\prod_{k=i+1}^{j-1} \sin\theta_k \right) d\theta_j \tag{3.57}$$

The general Hamiltonian in $d+1$ dimensions is then

$$\mathcal{H} = i\sqrt{-g}\bar{\Psi} \sum_{\ell=1}^{d} \gamma^\ell \left(\prod_{j=1}^{\ell-1} \csc(\theta_j) \right) \left(\partial_{\theta_\ell} + \frac{d-\ell}{2} \cot(\theta_\ell) \right) \Psi \tag{3.58}$$

where ℓ is a flat spatial index.

We can remove the cotangents and the volume factor in the commutation relation with the following definition $\Psi = \left(\prod_{j=1}^{d} \csc^{(d-j)/2}(\theta_j) \right) \psi$:

$$\{\psi_\alpha(x), \psi_\beta(x')\} = i\delta_{\alpha\beta}\delta(x-x') \ , \tag{3.59}$$

$$\mathcal{H} = \sum_{i=1}^{d} \prod_{j=1}^{i-1} \csc(\theta_j) \bar{\psi}\gamma^i \partial_{\theta_i} \psi \equiv \bar{\psi} \left(\gamma_1 \partial_{\theta_1} + \frac{1}{\sin(\theta_1)} \mathcal{O}_d \right) \psi \ . \tag{3.60}$$

To obtain a numerical result efficiently, we turn this Hamiltonian density into a $d = 1+1$ Hamiltonian. To this end, we integrate over θ_i for $i > 1$. We then calculate the spectrum of $\mathcal{O}$ where the lowest energy, smallest eigenvalue, gives the lowest order thermal correction to the Rényi entropies. For general d the result is

$$H_d = \int_0^\pi d\theta_1 \psi^\dagger \left(\gamma_0\gamma_1 \partial_{\theta_1} + \frac{(d-2)\gamma_0}{2\sin(\theta_1)} \right) \psi \tag{3.61}$$

as can be found in Ref. [42].

We discretize these Hamiltonians, turning the integral into a sum and the derivative into a finite difference. We then numerically calculate the entanglement and Rényi entropies in the same way as previous papers [14, 34, 37]. We find agreement with our analytical results for the entanglement entropy in both $d = 2+1$ and $d = 3+1$ (see Figure 7), and for the Rényi entropy in $d = 3+1$ (see Figure 8).

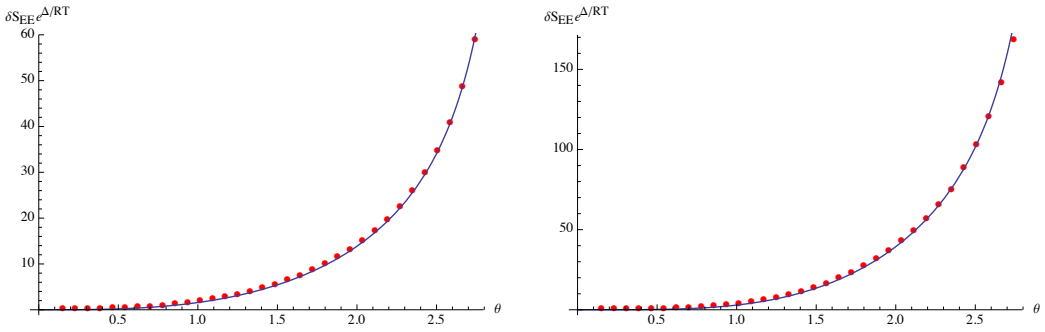

Figure 7: δS_{EE} in $d = 2 + 1$ (left), $3 + 1$ (right) with 200 grid points.

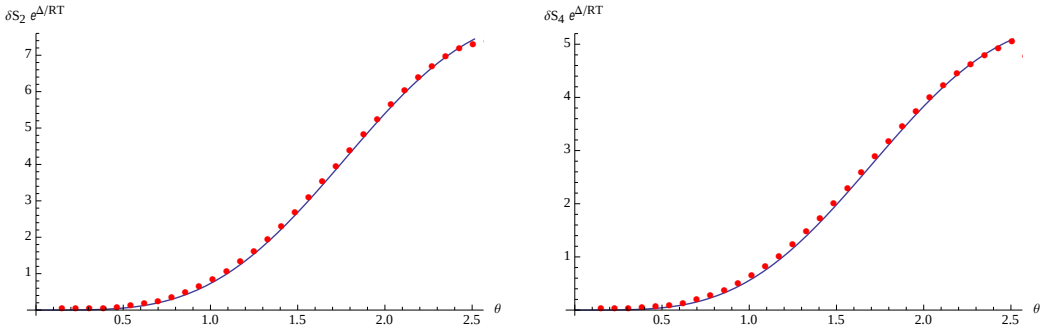

Figure 8: For $d = 3 + 1$, δS_2 (left) and δS_4 (right) with 200 grid points.

3.5 Discussion

In this chapter we extended to include massless free fermions the work in Ref. [37], which considered thermal corrections to Rényi and entanglement entropies for the conformally coupled scalar. This extension allowed a direct and successful comparison with Ref. [36] – which provided general results for thermal corrections to entanglement entropy for conformal field theories – without additional complications caused by boundary terms present for the conformally coupled scalar. We also were able to calculate thermal corrections to the Rényi entropies for the free fermion in even dimensions. We give the analytic result in $d = 1+1$ (3.32) and $d = 3+1$ (3.35) along with a recursion relation (3.28) which allows for computations of all even dimensions. In odd dimensions, we were unable to find an analytic continuation that would allow us to calculate thermal corrections to Rényi entropies, but we were able to reproduce the thermal corrections to entanglement entropy. Amusingly,

the situation is usually reversed, where one can compute Rényi entropies but the analytic continuation to entanglement entropy is not feasible.

It is possible that the methods used in this chapter and those in Ref. [37] could allow for corrections to be calculated for other free higher spin theories and possibly more generally for conformal field theories.

Part II
Fluids and the Riemann Problem

4 Relativistic Hydrodynamics and Non-Equilibrium Steady States

4.1 Background

The Riemann problem in hydrodynamics is an initial value problem where two equilibrium fluids are joined by a discontinuity. The solution for the case of relativistic fluids was first solved in 1948 [43]. It has since been studied in papers including [44, 45]. The key feature of these solutions is a rarefaction (adiabatic) region joined to a constant temperature region and then a shock discontinuity.[13]

The problem has seen renewed interest recently as an example of a steady state system which is not in thermal equilibrium (NESS). This type of NESS was first studied in 1+1 dimensional CFT's [47] and later extended to hydrodynamical descriptions of higher dimensional CFT's [48, 49]. Finally, it was considered for a CFT deformed by a relevant operator [50]. The papers [48, 50], however, miss the important rarefaction region and as a result their values for the NESS temperature as well as the rate of growth of the NESS are incorrect.[14]

[13]For a discussion of these issues in the context of the quark-gluon plasma, see for example ref. [46].

[14]The paper [49] restricts to a regime where the temperature difference is very small, and the difference between the two shock solution and the solution involving a rarefaction region correspondingly minuscule.

In this chapter we review both the older solution with the rarefaction region as well as the more recent solution which we call the two shock solution. Using a numerical simulation of relativistic hydrodynamics we show that the rarefaction solution matches the numerical simulation better than the two shock solution. We also consider a CFT deformed by a relevant operator. We calculate a phase diagram for the temperature of the NESS. The phase diagram we present differs from the two shock solution.

4.2 Ideal Hydrodynamics

We begin with the stress tensor of a perfect fluid and conserved currents

$$T^{\mu\nu} = (e+p)u^\mu u^\nu + p\eta^{\mu\nu}, \tag{4.1}$$

$$J_i^\mu = q_i u^\mu. \tag{4.2}$$

We mean perfect in the sense of having no dissipation. Here e is the energy density, q_i a charge density, and p the pressure. We have introduced a four velocity u^μ such that $u^2 = u^\mu u^\nu \eta_{\mu\nu} = -1$. At rest the fluid is described by $u^\mu = (1, \vec{0})$. We work in mostly plus signature with the Minkowski metric tensor $\eta^{\mu\nu} = (-,+,\ldots,+)$. The conservation equations of energy and momentum are given by

$$\partial_\mu T^{\mu\nu} = 0, \tag{4.3}$$

$$\partial_\mu J_i^\mu = 0. \tag{4.4}$$

The conservation equations are combined with an equation of state $e = e(p)$. In this chapter we will largely focus on a linear equation of state

$$p = c_s^2 e, \tag{4.5}$$

where c_s is the speed of sound. One important example for us is a conformal fluid in d spatial dimensions, where $c_s^2 = 1/d$.

We are interested in flows depending only on a single spatial variable, arbitrarily chosen to be x, and time. We will perform a change of variables to the local fluid velocity $v_i = u^i/u^t$. In these variables the stress tensor conservation equations become

$$\partial_t\left[(e+p)\gamma^2 - p\right] + \partial_x\left[(e+p)\gamma^2 v_x\right] = 0, \tag{4.6}$$

$$\partial_t\left[(e+p)\gamma^2 v_x\right] + \partial_x\left[(e+p)\gamma^2 v_x^2 + p\right] = 0, \tag{4.7}$$

$$\partial_t\left[(e+p)\gamma^2 \vec{v}_T\right] + \partial_x\left[(e+p)\gamma^2 v_x \vec{v}_T\right] = 0. \tag{4.8}$$

We have introduced $\gamma = 1/\sqrt{1 - v_x^2 - v_T^2}$ and also $\vec{v}_T$, the fluid velocity in the spatial directions perpendicular to x.

When there is a shock discontinuity we use the Rankine-Hugoniot jump condition to determine the relationship between conserved quantities on alternate sides of the shock [50, 51]. For a conservation law of the form

$$\partial_t Q(t,x) + \partial_x F(t,x) = 0, \tag{4.9}$$
$$u_s[Q] = [F], \tag{4.10}$$
$$[Q] = Q_L - Q_R, \tag{4.11}$$
$$[F] = F_L - F_R, \tag{4.12}$$

where Q_L (Q_R) and F_L (F_R) is the value of Q and F to the left (right) of the shock and u_s is the velocity of the shock. For the case of a perfect fluid, the jump conditions are given by

$$u_s[T^{tt}] = [T^{tx}], \tag{4.13}$$
$$u_s[T^{xt}] = [T^{xx}], \tag{4.14}$$
$$u_s[J_i^t] = [J_i^x]. \tag{4.15}$$

Equations like (4.15) can exhibit what are known as contact discontinuities. These have a jump in the conserved quantities. However, there is no transportation of particles across the discontinuity. In the case of (4.15), such a contact discontinuity can occur when $u_x/u_t = u_s$. The jump condition is trivially satisfied and the change in the conserved quantity can be arbitrary across the shock.

4.3 Double Shock solution

We are interested in solving the Riemann problem, where two semi-infinite fluids of different temperatures are brought into contact. An interesting feature of the resulting fluid flow is a non equilibrium steady state (NESS) that forms in the expanding region between the two semi-infinite fluids. Recently two papers [48, 50] have presented a solution that is not completely correct. Let us quickly review their work to see where the problem occurs.

They start with the EOS $p = c_s^2 e$. The initial conditions are that of two systems (with energies e_L and e_R) brought into thermal contact. They assume that two shocks propagate away from each other, leaving the NESS in between. The central region is assumed to have a constant fluid velocity

v. (We will suppress the x subscript on the fluid velocity v in what follows and set $v_T = 0$.) The conservation laws (4.13)-(4.15) imply

$$u_L = -c_s\sqrt{\frac{c_s^2\chi+1}{\chi+c_s^2}}, \quad u_R = c_s\sqrt{\frac{\chi+c_s^2}{c_s^2\chi+1}}, \tag{4.16}$$

$$e = \sqrt{e_L e_R}\ , \quad \frac{v}{c_s} = \frac{\chi-1}{\sqrt{(c_s^2\chi+1)(\chi+c_s^2)}}, \tag{4.17}$$

where $\chi = \sqrt{e_L/e_R}$. The velocity of the left and right moving shocks are u_L and u_R respectively.

This solution however is invalid because it violates the Entropy Condition [51]. This condition is most easily stated when the conservation conditions are written in characteristic form,

$$\partial_t\vec{u} + B(\vec{u})\partial_x\vec{u} = 0, \tag{4.18}$$

where here $\vec{u}(x,t) = (p(x,t), v(x,t))$. The eigenvalues $\lambda_\pm$ of B are

$$\lambda_\pm = \frac{v \pm c_s}{1 \pm vc_s^2}. \tag{4.19}$$

These characteristics correspond to the local right and left moving speeds of sound at a given space-time point in the fluid. (Reassuringly, $\lambda_\pm \to \pm c_s$ in the limit where the background fluid velocity vanishes, $v = 0$.)

The entropy condition requires that for solutions involving a shock, characteristics end on a shock discontinuity rather than begin on it. By ending on the shock, information is lost and entropy should increase. In contrast, in order for characteristics to begin on a shock, boundary conditions need to be specified, decreasing the entropy. More precisely, consider a right moving shock, $u_s > 0$. Let λ_R and λ_L be eigenvalues of B immediately to the right and left of the shock, respectively. We should take the eigenvalues corresponding to right moving characteristics. For the characteristics to end on the shock, it is necessary that

$$\lambda_L > u_s > \lambda_R\ . \tag{4.20}$$

A similar condition is also required for a left moving shock, taking now the left moving characteristic eigenvalues instead.

Rewriting the entropy condition (4.18) for the right moving shock yields

$$\frac{u_R^2 - c_s^2 + (1-c_s^2)c_s u_R}{c_s^2(u_R^2 - c_s^2) + u_R(1-c_s^2)} > u_R > c_s. \tag{4.21}$$

This condition is true for $u_R \in (c_s, 1)$, which is true for $\chi > 1$. Therefore a shock is a valid solution for the wave moving into the colder medium. However for $u_R \in (c_s^2, c_s)$, which is true for $\chi < 1$, neither inequality holds. Thus the entropy condition rules out a shock moving into the hotter region. (We could also analyze separately the left moving shock, but the physics is invariant under parity.)[15]

While we know from this analysis that the double shock solution is unphysical, it turns out to be very close to the actual solution in some situations. Given the simplicity of the double shock solution, it is interesting to consider adding a conserved charge. This addition requires us to include a contact discontinuity. A contact discontinuity is a discontinuity in one variable that travels at the local fluid velocity. For such a discontinuity the Rankine-Hugoniot jump condition is trivially satisfied and the change in the variable can be arbitrary. In this case the discontinuity is in the conserved charge. The result is the splitting of the NESS region into two NESS with distinct charges but equal velocities and pressures. The resulting charge densities are

$$q_1 = \frac{q_L\sqrt{c_s^2\chi + 1}}{\sqrt{\chi}\sqrt{c_s^2 + \chi}}, \tag{4.22}$$

$$q_2 = \frac{q_R\sqrt{\chi}\sqrt{c_s^2 + \chi}}{\sqrt{c_s^2\chi + 1}}. \tag{4.23}$$

where q_1 is the charge density in the region adjacent to q_L, q_2 is the charge density in the region adjacent to q_R.[16]

4.4 Adiabatic flow

We now need to replace the shock that does not satisfy the entropy condition with a smooth solution. The solution can be found in previous papers. As

[15] When $c_s = 1$, which holds for a conformal field theory in 1+1 dimensions, $u_R = \lambda_\pm = 1$ as well, and the entropy condition is satisfied (and saturated) for both the left and right moving shocks. We will see below that in this degenerate case, the two shock solution becomes identical with the solution involving a rarefaction wave.

[16] The entropy condition is trivially satisfied for shock discontinuities.

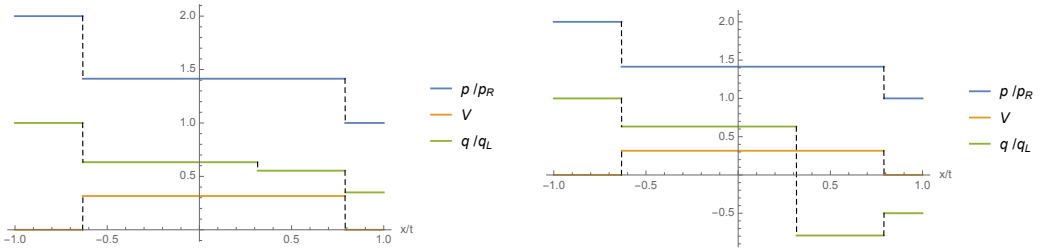

Figure 9: Plot of triple shock solutions. The regions from left to right are L, 1, 2 and R.

can be concluded by considering characteristics, the shock solution should be replaced with a fan of characteristics [44, 45, 51]. There is a characteristic for each value of the dimensionless ratio $\xi = x/t$. Therefore we will search for a solution that depends only on $\xi = x/t$. Such a solution would correspond to an adiabatic expansion.

It is simple to check that for $s = p^{1/(1+c_s^2)}$, eqs. (4.6–4.8) imply

$$\partial_t(s\gamma) + \partial(s\gamma v_x) = 0. \tag{4.24}$$

After switching to coordinates $\xi = x/t$, we can combine equations (4.8) and (4.24) and obtain

$$(\xi - v_x)\frac{d}{d\xi}(p^\kappa \gamma v_T) = 0 \ , \tag{4.25}$$

where we have defined

$$\kappa \equiv \frac{c_s^2}{1 + c_s^2} \ . \tag{4.26}$$

The solution in the adiabatic region is then

$$v_T = \frac{\alpha\sqrt{1-v_x(\xi)^2}}{\sqrt{\alpha^2+p^{2\kappa}}} \ , \tag{4.27}$$

$$v_x = \frac{\pm\left(\xi^2-1\right)c_s p^\kappa\sqrt{\alpha^2(1-c_s^2)+p^{2\kappa}}+\xi(c_s^2-1)\left(\alpha^2+p^{2\kappa}\right)}{\alpha^2(c_s^2-1)+\left(\xi^2c_s^2-1\right)p^{2\kappa}} \ , \tag{4.28}$$

$$p^\kappa = \frac{\alpha^2(c_s^2-1)\left(\frac{1-\xi}{\xi+1}\right)^{\mp\frac{c_s}{2}}}{4c_1} + c_1\left(\frac{1-\xi}{\xi+1}\right)^{\frac{\pm c_s}{2}} \ , \tag{4.29}$$

$$q = \exp\left(\int d\xi \frac{\frac{\alpha^2+p^{2\kappa}}{1-\xi^2}+\frac{\alpha^2\kappa\partial_x p}{p}+\frac{\alpha^2\kappa c_s p^{\kappa-1}\partial_x p}{\sqrt{p^{2\kappa}-\alpha^2(c_s^2-1)}}}{\alpha^2+p^{2\kappa}}\right) \ . \tag{4.30}$$

If we take the limit of zero tangential velocity ($\alpha = 0$), there are two solutions:

$$v_\pm(\xi) = \frac{c_s \pm \xi}{c_s\xi \pm 1} \ , \tag{4.31}$$

$$p_\pm(\xi) = \overline{p}\left(\frac{1-\xi}{1+\xi}\right)^{\pm\frac{1+c_s^2}{2c_s}} \ , \tag{4.32}$$

$$q_\pm(\xi) = \overline{q}\left(\frac{1-\xi}{1+\xi}\right)^{\pm\frac{1}{2c_s}} \ . \tag{4.33}$$

To solve the Riemann problem we need to match this adiabatic region onto a NESS region and a shock. Without loss of generality we can choose $p_L > p_R$. We then have a shock moving to the right at speed u_s. In the left region, the disturbance moves at the speed of sound as can be seen by setting $v_\pm = 0$. To the right of the shock $v = 0$ and $p = p_R$. To the left of the shock $v = V$ and $p = p_0$. Then the jump conditions are

$$p_0(c_s^2V(u_sV+1)+u_s-V)+p_Ru_s\left(V^2-1\right) = 0 \ , \tag{4.34}$$

$$p_0(c_s^2+V(c_s^2u_s+u_s-V))+p_Rc_s^2\left(V^2-1\right) = 0 \ . \tag{4.35}$$

Ideally when we put everything together we would get V and u_s as functions of χ. The best we were able to achieve were parametric expressions of V and

χ as functions u_s:

$$V = \frac{u_s^2 - c_s^2}{u_s(1-c_s^2)} \ , \tag{4.36}$$

$$\chi(u_s)^2 = \frac{(u_s - c_s^2)(c_s^2 + u_s)}{c_s^2(1-u_s^2)} \left(\frac{1+u_s}{1-u_s}\right)^{\frac{c_s^2+1}{2c_s}} \left(\frac{u_s - c_s^2}{c_s^2 + u_s}\right)^{\frac{c_s^2+1}{2c_s}} \ , \tag{4.37}$$

$$p_0 = p_L \left(\frac{(1-u_s)(u_s+c_s^2)}{(1+u_s)(u_s-c_s^2)}\right)^{\frac{c_s^2+1}{2c_s}} \ , \tag{4.38}$$

where $\chi = \sqrt{p_L/p_R}$. We can then add in the charge which has a contact discontinuity.

$$q_1 = q_L \left(\frac{(1-u_s)(u_s+c_s^2)}{(1+u_s)(u_s-c_s^2)}\right)^{\frac{1}{2c_s}} \ , \tag{4.39}$$

$$q_2 = \frac{q_R u_s \sqrt{u_s^2 - c_s^4}}{c_s^2 \sqrt{1-u_s^2}} \ . \tag{4.40}$$

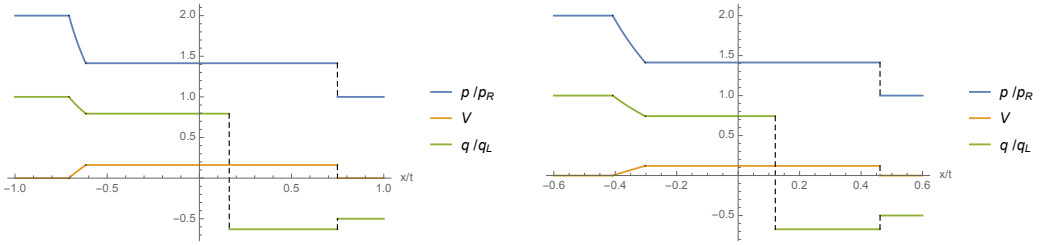

Figure 10: Plot of velocity, charge, and pressure profiles: left $c_s^2 = 1/2$, right $c_s^2 = 1/6$.

4.4.1 Simple Limits

While we only have a parametric solution in general, various limits take a simpler form. Consider the first the limit $c_s \to 1$. As $c_s^2 = 1/d$ for a conformal field theory, we can think about this limit as perturbing the number of spatial dimensions away from one, $d = 1+\epsilon$. In this case, the width of the rarefaction fan scales as

$$\delta\xi = \frac{1}{2}(\chi - 1)\epsilon + O(\epsilon^2) \ , \tag{4.41}$$

which vanishes as $\epsilon \to 0$. Indeed, the difference between the rarefaction solution and the two-shock solution is controlled by ϵ, with the differences

$$\delta v = 2f(\chi)\epsilon^2 + O(\epsilon^3) \ , \tag{4.42}$$

$$\delta u_R = f(\chi)\epsilon^3 + O(\epsilon^4) \ , \tag{4.43}$$

$$\delta p = \frac{p_L}{\chi^2(1+\chi)^4} f(\chi)\epsilon^2 + O(\epsilon^3) \ , \tag{4.44}$$

where we have defined the function of χ, positive for $\chi > 1$,

$$f(\chi) \equiv \frac{\chi}{8(1+\chi)^3}\left(1 - \chi + (1+\chi)\tanh^{-1}\frac{\chi-1}{\chi+1}\right) \ .$$

The quantities δv, δp and δu_R are the differences between the rarefaction solution and the two shock solution in velocity, pressure and shock speed respectively, e.g. $\delta v = v(\text{2-shock}) - v(\text{rarefaction})$. In this limit, the two-shock solution slightly overestimates the pressure and fluid velocity in the NESS, and also the right moving shock speed.

The non-relativistic limit $\chi \to 1$ of the rarefaction solution also approaches the two-shock solution. Let $p_L = p_R(1+\epsilon)$, $\epsilon \ll 1$, in which case

$$\delta\xi = \frac{(1-c_s^2)c_s}{2(1+c_s^2)}\epsilon + O(\epsilon^2), \tag{4.45}$$

$$\delta v = \frac{(1-c_s^2)^2 c_s}{384(1+c_s^2)^3}\epsilon^3 + O(\epsilon^4), \tag{4.46}$$

$$\delta p = p_L \frac{(1-c_s^2)^2}{384(1+c_s^2)^2}\epsilon^3 + O(\epsilon^4), \tag{4.47}$$

$$\delta u_R = \frac{(1-c_s^2)^3 c_s}{768(1+c_s^2)^3}\epsilon^3 + O(\epsilon^4), \tag{4.48}$$

where $\delta\xi$, δv, δp and δu_R are as before. In this limit, the two-shock solution again slightly overestimates the velocity and pressure in the NESS and the speed of the right moving shock.

While the two shock solution and the solution with a rarefaction region quickly approach each other in the limit $p_L \to p_R$, in the opposite limit where $\chi \gg 1$, the solutions have qualitatively different behavior. In both cases, the speed of the right moving shock approaches one, u_s, $u_R \to 1$, but

at a different rate. Let us assume a large χ ansatz where $u_s = 1 - \delta$. In the rarefaction case

$$\chi = \left(\frac{1}{\delta}\right)^{\frac{c_s^2+1}{4c_s}+\frac{1}{2}} \frac{1}{\sqrt{2}}\sqrt{\frac{1}{c_s^2} - c_s^2}\left(-2 + \frac{4}{1+c_s^2}\right)^{\frac{1+c_s^2}{4c_s}} (1 + O(\delta)) \ , \tag{4.49}$$

$$p = p_L \delta^{\frac{c_s^2+1}{2c_s}} \left(-2 + \frac{4}{1+c_s^2}\right)^{-\frac{1+c_s^2}{2c_s}} (1 + O(\delta)) \ , \tag{4.50}$$

$$v = 1 - \frac{1+c_s^2}{1-c_s^2}\delta + O(\delta^2) \ . \tag{4.51}$$

In contrast, for the two shock solution $\chi \sim \frac{1}{\delta}$ and $p \sim \sqrt{\delta}$.

Another important difference is that the size of the rarefaction region grows in this limit $\chi \gg 1$. The rightmost characteristic of the rarefaction fan approaches the location of the right moving shock:

$$\xi_R = 1 - \frac{1+c_s^2}{(1-c_s)^2}\delta + O(\delta^2) \ . \tag{4.52}$$

Thus the size of the NESS is correspondingly reduced. Indeed, for all practical purposes, the NESS probably disappears in this limit. An initial condition that is a step function is an idealization, and slightly smoothing the step function will destroy the NESS, as will viscous corrections, which smear out the shock.

4.5 Non-linear Equation of State

We can also consider the Riemman problem for nonlinear equations of state. For simplicity we will assume that $v_T = 0$. We consider a perturbation to the CFT by a relevant operator as in [50, 52],

$$S_{QFT} = S_{CFT} + \lambda' \int d^{d+1}x \, \mathcal{O}(x) \tag{4.53}$$

in the limit $\lambda/T^{d+1-\Delta} \ll 1$. For relevance and unitarity, we require $\frac{d-1}{2} \leq \Delta < d+1$. Such a perturbation should affect the equilibrium pressure and energy density at second order in λ'. Following ref. [52], we assume an ansatz

where

$$p = c\,T^{d+1}\left(1 - \frac{\lambda^2}{T^{2(d+1-\Delta)}}\right) \ , \tag{4.54}$$

$$e = c\,d\,T^{d+1}\left(1 - \alpha\frac{\lambda^2}{T^{2(d+1-\Delta)}}\right) \ , \tag{4.55}$$

where λ and λ' are proportional.[17] The Gibbs-Duhem relation $e + p = sT$ along with $s = \frac{dp}{dT}$ then imply that $\alpha = \frac{1}{d}(2\Delta - d - 2)$. Eliminating T, we can write an equation of state for e as a function of p:

$$e = pd + \epsilon\lambda^2 p^n \ , \tag{4.56}$$

where

$$\epsilon = 2c^{\frac{2(d+1-\Delta)}{d+1}}(d + 1 - \Delta) \ , \tag{4.57}$$

$$n = \frac{2\Delta}{d+1} - 1 \ . \tag{4.58}$$

Note that $\epsilon > 0$.

As in the case of a linear equation of state, we find an adiabatic solution and match it onto a NESS region and a shock. The equations of motion remain (4.6) and (4.7). We can solve these equations in a perturbative expansion in λ as follows:

$$p = p_0 + p_1\lambda^2, \quad v_x = v_0 + v_1\lambda^2. \tag{4.59}$$

Again there are two solutions

$$p_0^{\pm} = c_{0p}\left(\frac{1-\xi}{1+\xi}\right)^{\pm\frac{1+c_s^2}{2c_s}} \ , \tag{4.60}$$

$$v_0^{\pm}(\xi) = \frac{c_s \pm \xi}{\xi c_s \pm 1}, \tag{4.61}$$

$$p_1^{\pm} = -\epsilon\frac{c_s^2(2 - 2c_s^2 + n(1+c_s^2)(n + nc_s^2 - 2))c_{0p}^n}{2(n-1)(c_s^4 - 1)}\left(\frac{1-\xi}{1+\xi}\right)^{\pm n\frac{1+c_s^2}{2c_s}} \ , \tag{4.62}$$

$$v_1^{\pm} = \pm\epsilon\frac{n(\xi^2-1)c_s^3 c_{0p}^{n-1}}{2(\xi c_s \pm 1)^2}\left(\frac{1-\xi}{1+\xi}\right)^{\pm(n-1)\frac{1+c_s^2}{2c_s}} \ . \tag{4.63}$$

[17] We expect that a relevant perturbation should decrease the effective number of degrees of freedom of the theory and thus further decrease the entropy at low temperatures, explaining the minus sign in front of the correction to the pressure.

We are first interested in how fast the disturbance moves to the left (ξ_L). This can be found perturbatively in λ by requiring that $v_x(\xi_L) = 0$ and $p(\xi_L) = p_L$. The result is

$$\xi_L = -c_s + \frac{n p_L^{n-1} c_s^3}{2} \epsilon \lambda^2 \ , \tag{4.64}$$

$$c_{0p} = p_L \left(\frac{1+c_s}{1-c_s} \right)^{-(1+c_s^2)/2c_s} + \epsilon \lambda^2 p_L^n \frac{c_s^2 (n c_s^2 + n - 2)}{2(n-1)(1+c_s^2)} \left(\frac{1+c_s}{1-c_s} \right)^{-(1+c_s^2)/2c_s} . \tag{4.65}$$

Unfortunately, analytic solutions for the correction to the NESS pressure are not available. However, one can still do the calculation numerically with an interesting result. Unlike for the double shock solution presented in [50] the change to the NESS pressure is dependent on both Δ and p_L ($p_L > p_R = 1$) as opposed to only Δ in [50]. We do not have an analytic expression for the curve, but the phase diagrams are presented in Figure (11) for two different spacetime dimensions.

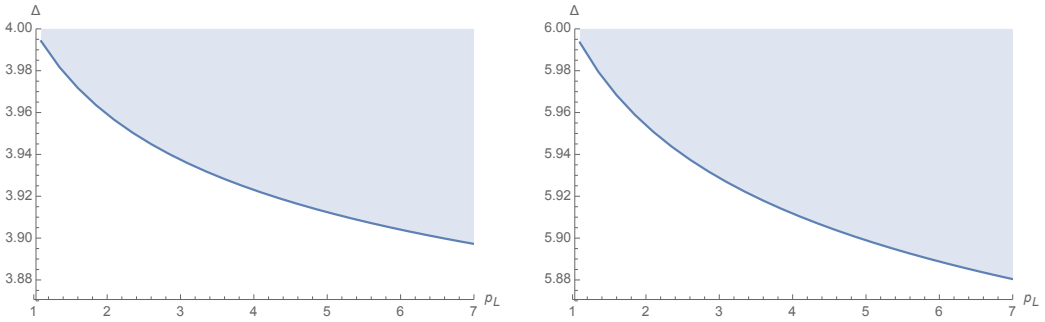

Figure 11: Phase diagrams for the change in P_{NESS} where the shaded region has $P_{NESS} < P_{CFT}$. The left is for $d = 3$ and the right $d = 5$.

In the two shock solution we can find the corrections analytically. We find

$$\delta v = \frac{(d+1)\left(\chi^n + \chi\right)\left((d+\chi)\chi^n - \chi(d\chi+1)\right)}{4\sqrt{d}\chi(d+\chi)^{3/2}(d\chi+1)^{3/2}} \epsilon \lambda^2, \tag{4.66}$$

$$\delta p = \frac{\left(\chi^n - \chi\right)\left((d+\chi)\chi^n - \chi(d\chi+1)\right)}{2d(d+1)\chi(\chi+1)} \epsilon \lambda^2. \tag{4.67}$$

The quantities δv and δp are the differences between the QFT and the CFT values of velocity and pressure respectively, e.g. $\delta v = v_{QFT} - v_{CFT}$. We note that $\delta p \geq 0$ for all relevant operators independent of χ, where the inequality is saturated for $\Delta = d + 1$.[18]

4.6 Numerical Check

We want to implement a numerical scheme to check our results. To do this we use the same hydrodynamic scheme as [53] which employed spectral methods. For simplicity we take $v_T = 0$. We start with

$$T^{\mu\nu} = (e + p)u^\mu u^\nu + p\eta^{\mu\nu} + \Pi^{\mu\nu} \tag{4.68}$$

where we define $\Pi^{\mu\nu}$ recursively[19] in a gradient expansion

$$\Pi^{\mu\nu} \;=\; -\eta\sigma^{\mu\nu} - \tau_\Pi \left[(D\Pi)^{\langle\mu\nu\rangle} + \frac{3}{2}\Pi^{\mu\nu}(\nabla \cdot u) \right] - \frac{\lambda_2}{\eta}\Pi^{\langle\mu}{}_\alpha \Omega^{\nu\rangle\alpha} \tag{4.69}$$

where $D \equiv u^\mu \nabla_\mu$.

Conformality implies tracelessness of $T^{\mu\nu}$ which in turn yields a relationship $e = d\,p$ between the energy density e and pressure p in d spatial dimensions. While μ in principle takes values from 0 to d, we let only u^0 and u^1 be nonzero. The vorticity is

$$\Omega^{\mu\nu} \equiv \frac{1}{2}\Delta^{\mu\alpha}\Delta^{\nu\beta}(\nabla_\alpha u_\beta - \nabla_\beta u_\alpha) \;, \tag{4.70}$$

where we have defined a projector onto a subspace orthogonal to the four velocity:

$$\Delta^{\mu\nu} \equiv \eta^{\mu\nu} + u^\mu u^\nu \;. \tag{4.71}$$

The shear stress tensor is

$$\sigma^{\mu\nu} \equiv 2\nabla^{\langle\mu} u^{\nu\rangle} \;. \tag{4.72}$$

[18] This result is not at odds with [50] because they consider temperature rather than pressure.

[19] The implicit definition of $\Pi^{\mu\nu}$ is Israel-Stewart like. Formally, higher than second order gradient corrections are present in the definition of $\Pi^{\mu\nu}$.

The angular brackets $\langle\rangle$ on the indices indicate projection onto traceless tensors orthogonal to the velocity

$$A^{\langle\mu\nu\rangle} \equiv \frac{1}{2}\Delta^{\mu\alpha}\Delta^{\nu\beta}(A_{\alpha\beta} + A_{\beta\alpha}) - \frac{1}{d}\Delta^{\mu\nu}\Delta^{\alpha\beta}A_{\alpha\beta} \ . \tag{4.73}$$

Note that with these definitions, both $\Pi^{\mu\nu}$ and $\Omega^{\mu\nu}$ are traceless and orthogonal to the velocity

$$u_\mu\Pi^{\mu\nu} = u_\mu\Omega^{\mu\nu} = 0 \ , \quad \Omega^\mu_\mu = \Pi^\mu_\mu = 0 \ .$$

Using $v_T = 0$ and flows that only depend on x and t, we know $\Pi^{xy} = 0$ and $\Omega^{xy} = 0$. The remaining one independent component of $\Pi^{\mu\nu}$ we choose to be $B = \Pi^{xx} - \Pi^{yy}$. We then use the two conservation equations and the implicit definiton of B to propagate forward in time.

We give the equation of state in terms of the energy density e and temperature T,

$$e = \left(\frac{4\pi T}{3}\right)^{d+1} \ , \tag{4.74}$$

and we start with the initial condition

$$u_x = 0, \tag{4.75}$$

$$T = \frac{T_R - T_L}{2}\tanh(\beta x) + \frac{T_R + T_L}{2}. \tag{4.76}$$

As can be seen in Figure (12) our solution with an adiabatic region matches well with the numerics. We accurately match the speed of the shock as well as the position of the adiabatic region. The matching is not perfect in the adiabatic region because the initial profile was not a perfect step function. The results were insensitive to the values of the dissipative coefficients η, τ_Π and λ_2. While the difference cannot be seen in the figures, we also calculated T^{tx}_{NESS} for the two analytic results and the numerics. The results are presented in Table (1)

4.7 Conclusion

We presented a review of previous work on the Riemann problem for a linear equation of state. The solution has the interesting feature of a steady

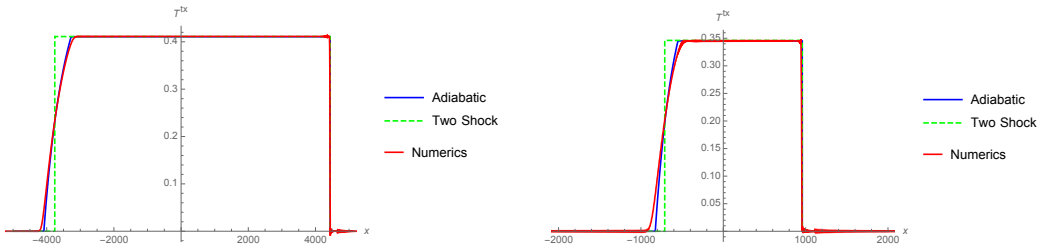

Figure 12: Plot comparing T^{tx} for the adiabatic solution and two shock solution to numerics. The left uses $p_L = 2.75$, $p_R = 1$, $\beta = \pi/100$ with 3001 grid points at $t = 5777$ (left) and $t = 1652$ (right).

d	Two shock	Adiabatic	Numerics
3	0.176587	0.176545	0.176551± 0.000006
5	0.14948	0.14936	0.149344±0.00009

Table 1: The average and standard deviation of T^{tx} over the flattest part of the NESS region compared with the theoretical values for $p_L = 1.75$, $p_R = 1$, $\beta = \pi/200$. The adiabatic solution presented in this chapter is a better fit than the two shock solution.

state region with a momentum flux. We contrast this solution with recent solutions [48, 50] that have appeared which incorrectly solved the Riemann problem by using a two shock ansatz. These papers had failed to consider the entropy condition and missed the adiabatic expansion region (rarefaction region) which exists between the hotter reservoir and the NESS. We also showed that for a conserved charge, the NESS region is actually two regions with different charges with a contact discontinuity separating them.

In the nonrelativistic limit ($\chi \to 1$) and the small dimension limit ($c_s \to 1$), the two shock solution leads to small errors in the value for the momentum flux of the NESS as well as in the velocity of the shock wave. We were able to show using a numerical simulation that the solution with the adiabatic region is preferred over the two shock solution. The adiabatic region was also a better match for the fluid profile than the shock propagating toward the high temperature reservoir.

Finally, we considered a CFT which had been perturbed by a relevant operator. The perturbation leads to a non-linear correction to the equation of state. Again we found the adiabatic solution which should be matched onto the NESS. Our solution gave a phase diagram for the correction to

the NESS temperature that depended on p_L and Δ the operator dimension. This diagram contrasted with the two shock solution where the only relevant parameter was the operator dimension.

One area for future investigation is adding viscosity to the solution. In general adding viscosity makes analytic solutions impossible. However, numerical simulations seem to show that the solution is very weakly affected by viscosity which gives hope that such a solution could be found. We are also interested in considering analytical solutions with smooth initial conditions to be better able to compare with our numerical results where the initial conditions are smooth by necessity (because we used spectral methods).

Perhaps the most interesting question is a rephrasing of the problem using the fluid-gravity correspondence [54] as a question about black-hole dynamics. In this context, the Riemann problem considered here maps to a solution to Einstein's equations in an asymptotically anti-de Sitter spacetime. The temperature of the fluid can be re-interpreted as the location of an apparent horizon of a black hole. Is there a gravitational counter-part of the entropy condition that we considered in this chapter? What is the gravity dual of the adiabatic region, and why is it required for consistency of the theory?

5 Riemann Problem for large d Black Holes

5.1 Introduction

The Riemann problem may provide a relatively simple setting in which to study the non-equilibrium physics of quantum field theory. The problem asks for the time evolution of piece wise constant initial conditions with a single discontinuity in the presence of some number of conservation laws, for example of energy, momentum, mass, or charge. In our case, we consider a fluid phase of a conformal field theory (CFT) with an initial planar interface, where the energy density jumps from e_L on the left of the interface to e_R on its right. We also allow for a discontinuity in the center of mass velocity of the fluid across the interface.

For simplicity, we will make a number of further restrictions. We assume a conformal field theory that has a dual gravity description via the AdS/CFT correspondence. A priori, this will allow us to study the system beyond the hydrodynamic limit. We also take the limit that the number of spatial

dimensions d is very large. In this limit, we find that the system is described by two conservation equations

$$\partial_t e - \partial_\zeta^2 e = -\partial_\zeta j \ , \qquad \partial_t j - \partial_\zeta^2 j = -\partial_\zeta \left(\frac{j^2}{e} + e \right) . \tag{5.1}$$

where e is, up to gradient corrections, the energy density and j the energy current. These equations are a special case of equations derived in ref. [55]. In these variables the Riemann problem amounts to a determination of e and j given an initial configuration of the form

$$(e, j) = \begin{cases} (e_L, j_L) & z < 0 \\ (e_R, j_R) & z > 0 \end{cases} . \tag{5.2}$$

By choosing an appropriate reference frame, we may set $j_L = 0$ without loss of generality.

As it happens, there are extensive treatments of this type of Riemann problem in hydrodynamics textbooks. See for example ref. [56]. Typically, a pair of rarefaction and/or shock waves form and move away from each other, creating in their wake a region with almost constant e and j. In recent literature, this intermediate region has been called a non-equilibrium steady state (NESS) [47, 57]. One of the main results of this chapter is a "phase" diagram (see figure 13) that describes, given the conservation equations (5.1) and initial conditions (5.2), which pair of waves are formed: rarefaction-shock (RS), shock-shock (SS), shock-rarefaction (SR), or rarefaction-rarefaction (RR). A physical reason for the preference of a rarefaction wave to a shock wave is entropy production.

Recent interest in this type of Riemann problem was spurred by a study of the problem in $1 + 1$ dimensional conformal field theory [47] where the evolution is completely determined by the conformal symmetry and a hydrodynamic limit need not be taken. Conservation and tracelessness of the stress tensor imply that the stress tensor is a sum of right moving and left moving parts. When $j_R = j_L = 0$ one finds a NESS in between the two asymptotic regions, characterized by an energy density $(e_R + e_L)/2$ and an energy current proportional to $e_R - e_L$. The NESS is separated from the asymptotic regions by outward moving shock waves traveling at the speed of light. (An extension of the analysis of [47] which includes a discontinuity in the center of mass velocity, holomorphic currents and chiral anomalies

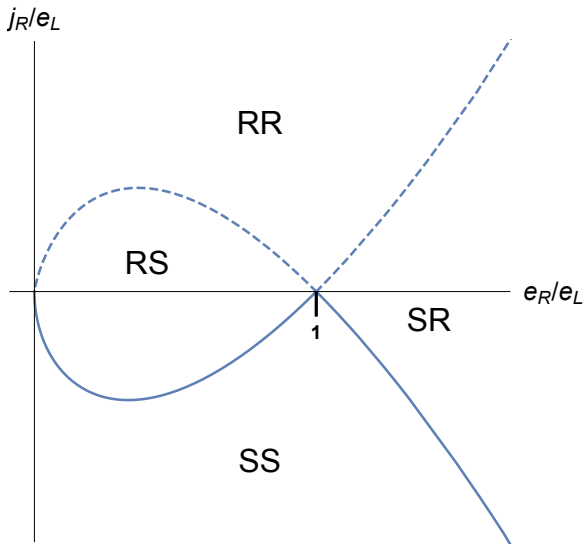

Figure 13: A phase diagram for the solution to the Riemann problem. Given a pair $(e_L, 0)$ and (e_R, j_R), the selection of shock and rarefaction waves is determined by the value of e_R/e_L and j_R/e_L. The dashed and solid lines are "critical": The dashed line indicates the values of (e_R, j_R) connected to $(e_L, 0)$ by a single rarefaction wave while the solid line indicates the values of (e_R, j_R) connected to $(e_L, 0)$ by a single shock wave.

can be found in [49]. An analysis of shock waves and their relation to two dimensional turbulence was carried out in [58].)

In more than two space-time dimensions, conformal symmetry alone is not enough to specify the evolution completely and one needs additional assumptions about the structure of the conserved currents. Recent work appealed to the gauge/gravity duality [48, 59, 60, 61], an analogy with $1+1$ dimensions [49], and hydrodynamics [48, 50, 62]. These papers focused on the case $j_R = j_L = 0$ and $e_L > e_R$ such that from a hydrodynamic perspective a left moving rarefaction wave and a right moving shock wave are expected to emerge.

The distinction between rarefaction and shock waves was ignored in some of these papers [48, 50, 49]. Indeed, when working with $2+1$ or $3+1$ dimensional conformal field theories, the difference between, say, an SS solution to the Riemann problem and an RS solution to the Riemann problem is very small for all but extreme initial energy differences. As the spacetime dimension d increases however, the difference between a rarefaction wave type of solution and a shock wave solution becomes significant.

Interestingly, a large d limit has independently been a topic of recent interest [55, 63, 64, 65, 66, 67, 68, 69, 70, 71, 72, 73, 74] in the study of black hole solutions to Einstein's equations. Of particular relevance to our work is the connection between black holes in asymptotically AdS spaces and hydrodynamics [75]. Certain strongly interacting conformal field theories are known to have dual classical gravitational descriptions. In the limit where these conformal field theories admit a hydrodynamic description, a solution to the relevant hydrodynamic equations can be mapped to a solution of Einstein's equations, in a gradient expansion where physical quantities change slowly in space and time. Transport coefficients such as shear viscosity are fixed by the form of Einstein's equations. Thus, one may study the Riemann problem in conformal field theories with a large number of dimensions by studying an equivalent Riemann-like problem involving an initially discontinuous metric of a black hole in an asymptotically AdS background.

Given that extensive analyses of conservation equations like (5.1) can be found in many hydrodynamics textbooks and papers, one can legitimately ask why we bother to redo the analysis here. The reason is that when working in a large number of dimensions, one can solve for the black hole metric exactly, independent of the derivative expansion (which is naturally truncated), thus obtaining an exact solution to the Riemann problem which includes possible viscous terms and is in general valid even when gradients of thermodynamic

quantities are large (as is the case with discontinuous initial conditions).

Our work is organized as follows. In section 5.2, we rederive the equations (5.1) by taking a large d limit of Einstein's equations. We show how to rewrite them as the conservation condition on a stress-tensor, $\partial_\mu T^{\mu\nu} = 0$. In section 5.3, we compare the large d stress tensor and equations of motion to those arising from the fluid-gravity correspondence [75]. We find that both eqs. (5.1) and the stress tensor $T^{\mu\nu}$ are equivalent to the hydrodynamic equations that come from the fluid-gravity correspondence at large d, at least up to and including second order gradient corrections. In the same section we also construct an entropy current J^μ_S using an area element of the black hole horizon and show that the divergence of the entropy current is positive $\partial_\mu J^\mu_S \geq 0$ in this large d limit. In section 5.4, we solve the Riemann problem for eqs. (5.1) and derive the phase diagram given in figure 13. Finally, we conclude in section 5.5 with some directions for future research. Appendix D contains a short calculation of the entropy produced across a shock, while apppendix E contains plots of auxiliary numerical results.

5.2 The holographic dual of the Riemann problem for large d

We wish to construct a holographic dual of the Riemann problem. Consider the Einstein Hilbert action

$$S = -\frac{1}{2\kappa^2}\int \sqrt{-g}\left(R + \frac{(d-2)(d-1)}{L^2}\right)\mathrm{d}^d x\,. \tag{5.3}$$

A canonical stationary solution of the resulting equations of motion is the black brane solution

$$\mathrm{d}s^2 = 2\mathrm{d}t\,\mathrm{d}r - r^2\left(1 - \left(\frac{4\pi T}{(d-1)r}\right)^{d-1}\right)\mathrm{d}t^2 + r^2\mathrm{d}x_\perp^2\,, \tag{5.4}$$

where T is an integration constant which denotes the Hawking temperature. The solution (5.4) is dual to a thermal state of a conformal field theory with temperature T. For instance, the thermal expectation value of the stress

tensor in such a state is given by

$$\langle T^{\mu\nu}\rangle = \begin{pmatrix} (d-2)P(T) & 0 & \dots & 0 \\ 0 & P(T) & \dots & 0 \\ \vdots & \vdots & \ddots & \vdots \\ 0 & 0 & \dots & P(T) \end{pmatrix} \tag{5.5}$$

where

$$P(T) = p_0 \left(\frac{4\pi T}{d-1}\right)^{d-1} \tag{5.6}$$

is the pressure with p_0 a theory dependent dimensionless parameter.

As discussed in [61] a dual description of the Riemann problem necessitates an initial black hole configuration which is held at some fixed temperature T_L for all $z < 0$ and at a different temperature T_R for $z > 0$. This would correspond to a configuration where the expectation value of the stress tensor is given by (5.5) with $T = T_L$ for $z < 0$ and by (5.5) with $T = T_R$ for $z > 0$. Since the initial black hole is out of equilibrium it will evolve in time. Its dual description will provide a solution for the time evolution of the stress tensor which we are after. Thus, our goal is to solve the equations of motion following from (5.3) and use them to construct the dual stress tensor.

An ansatz for the metric which is compatible with the symmetries and our initial conditions is given by

$$\mathrm{d}s^2 = \mathrm{d}t(2\mathrm{d}r - g_{tt}\mathrm{d}t - 2g_{tz}\mathrm{d}z) + g_{zz}\mathrm{d}z^2 + g_{\perp\perp}\mathrm{d}x_\perp^2\,, \tag{5.7}$$

where the metric components are functions only of t, r, and z. (A more general ansatz which involves a transverse velocity can be found in [55].) A numerical solution of the equations of motion for g_{tt}, g_{tz} and g_{ii} ($i = x_\perp$ or z) with smoothened initial conditions has been obtained for $d = 4$ in [61] for relatively small initial temperature differences, $(T_L - T_R)/(T_L + T_R) < 1$. A solution for finite $d > 4$ and for large temperature differences, $(T_L - T_R)/(T_L + T_R) \sim 1$ is challenging.

In this work we use the methods developed in [55, 63] (see also [64, 65, 66, 67, 68, 69, 70, 71, 72]) to address the Riemann problem in the limit that d is very large. Such a limit can be understood as follows. In an appropriate

gauge, the near boundary expansion of the metric gives

$$\begin{aligned} g_{tt} &= r^2 + \mathcal{O}(r^{3-d}) \ , \\ g_{tz} &= \mathcal{O}(r^{3-d}) \ , \\ g_{ii} &= r^2 + \mathcal{O}(r^{3-d}) \, . \end{aligned} \tag{5.8}$$

Thus, in the large d limit at any finite value of r, the spacetime looks like the AdS vacuum. Only by keeping $R = r^n$ finite with $n \equiv d-1$ will the $O(r^{-n})$ corrections to the metric remain observable. Our strategy is to solve the equations of motion in the finite R region subject to the boundary conditions (5.8). Following [55], we also use the scaling $x_\perp = \chi/\sqrt{n}$ and $z = \zeta/\sqrt{n}$ so that in this coordinate system the line element takes the form

$$\mathrm{d}s^2 = \mathrm{d}t(2\mathrm{d}r - g_{tt}\mathrm{d}t - 2g_{t\zeta}\mathrm{d}\zeta) + g_{\zeta\zeta}\mathrm{d}\zeta^2 + g_{\perp\perp}\mathrm{d}\chi_\perp^2 \, , \tag{5.9}$$

where

$$\begin{aligned} \frac{g_{tt}}{r^2} &= \sum_{k=0} \frac{E^{(k)}}{n^k} \ , \\ g_{t\zeta} &= \sum_{k=1} \frac{J^{(k)}}{n^k} \ , \\ \frac{g_{ii}}{r^2} &= \frac{1}{n} + \sum_{k=2} \frac{g_i^{(n)}}{n^k} \, . \end{aligned} \tag{5.10}$$

(In a slight abuse of notation i is now either $\chi_\perp$ or ζ.) We have used the letters E and J to emphasize these quantities' (soon to be seen) close connection with an energy density and energy current in the dual hydrodynamic description.

One can now solve the equations of motion order by order in $1/n$. The equations of motion are simply Einstein's equations in the presence of a negative cosmological constant:

$$R_{MN} = -(d-1)g_{MN} \ , \tag{5.11}$$

setting $L = 1$ for convenience. Let a and b index the t, r, and ζ directions only, while i and j index the remaining perpendicular directions. Furthermore, let $\tilde{R}_{ab}$ be the Ricci tensor with respect to the three dimensional metric

in the t, r, and ζ directions. Then

$$R_{ab} = \tilde{R}_{ab} + \frac{d-3}{4}(\partial_a \log g_{\perp\perp})(\partial_b \log g_{\perp\perp}) - \frac{d-3}{2}\frac{\nabla_a \partial_b g_{\perp\perp}}{g_{\perp\perp}} \ , \quad (5.12)$$

$$R_{ij} = \delta_{ij}\left(\frac{5-d}{4}\frac{(\partial_a g_{\perp\perp})(\partial^a g_{\perp\perp})}{g_{\perp\perp}} - \frac{1}{2}\nabla^a \partial_a g_{\perp\perp}\right) \ . \quad (5.13)$$

Imposing that the boundary metric is Minkowski and choosing a near boundary expansion of the form (5.8) we find

$$\begin{aligned}
\frac{g_{tt}}{r^2} &= 1 - \frac{e}{R} - \frac{1}{n}\left(\frac{e_2}{R} + \frac{\log R}{R}\partial_\zeta j + \frac{j^2}{2R^2}\right) + O(n^{-2}) \ , \\
g_{t\zeta} &= \frac{1}{n}\frac{j}{R} + \frac{1}{n^2}\left(\frac{j_2}{R} + \frac{\log R}{R}\left(\partial_\zeta\left(\frac{j^2}{e}\right) + 2f\right) + \frac{j^3}{2R^2 e}\right) + O(n^{-3}) \ , \\
\frac{g_{\zeta\zeta}}{r^2} &= \frac{1}{n} + \frac{1}{n^2}\frac{j^2}{Re} + O(n^{-3}) \ , \\
\frac{g_{\perp\perp}}{r^2} &= \frac{1}{n} - \frac{1}{n^3}\frac{j^2}{Re} + O(n^{-4}) \ ,
\end{aligned} \quad (5.14)$$

where the $\mathcal{O}(n^{-2})$ correction to g_{tt} and the $\mathcal{O}(n^{-3})$ contributions to $g_{\zeta\zeta}$ are too long to write explicitly. The functions e and j are functions of t and ζ only and must satisfy the additional constraints (5.1). Equations (5.1) are identical to those obtained in [55, 63]. We can rewrite them in terms of a conservation law

$$\partial_\mu T^{\mu\nu} = 0 \quad (5.15)$$

where

$$T^{\mu\nu} = \begin{pmatrix} e & j - \partial_\zeta e \\ j - \partial_\zeta e & e + \frac{j^2}{e} - 2\partial_\zeta j + \partial_\zeta^2 e \end{pmatrix} + \begin{pmatrix} \partial_\zeta^2 g & -\partial_\zeta \partial_t g \\ -\partial_\zeta \partial_t g & \partial_t^2 g \end{pmatrix} . \quad (5.16)$$

where g is an arbitrary function. Likewise, the functions e_2 and j_2 must also satisfy a set of equations which can be obtained from the conservation of

$$T_2^{\mu\nu} = \begin{pmatrix} e_2 & \left(\frac{j^2}{e} + e - e_2 - 2j'\right)' + j + j_2 \\ \left(\frac{j^2}{e} + e - e_2 - 2j'\right)' + j + j_2 & T^{11} \end{pmatrix} + \begin{pmatrix} \partial_\zeta^2 g_2 & -\partial_\zeta \partial_t g_2 \\ -\partial_\zeta \partial_t g_2 & \partial_t^2 g_2 \end{pmatrix} . \quad (5.17)$$

where

$$T^{11} = 2\left(1-\left(\frac{j}{e}\right)'\right)\left(\frac{j}{e}\right)' e(\log(e)-3)+e+e_2\left(1-\frac{j^2}{e^2}\right)+2j_2\frac{j}{e} + \left(e_2-4e-6\frac{j^2}{e}+4j'\right)''-2\left(j_2-3j-\frac{j^3}{e^2}\right)'+\frac{j^2}{e}\left(\frac{j}{e}\right)' . \quad (5.18)$$

We will use $'$ and ∂_ζ interchangeably in what follows.

5.3 Comparison with hydrodynamics

Let us pause to understand (5.16). Within the context of the gauge-gravity duality it is possible to construct a solution to the Einstein equations which is perturbative in t, ζ and $\chi_\perp$ derivatives of the metric components [75]. Such a perturbative solution to the equations of motion, which is available for any dimension d [76, 77], allows for a dual description of the theory in terms of fluid dynamical degrees of freedom.

5.3.1 Stress tensor from fluid-gravity correspondence

To construct the dual hydrodynamic description of a slowly varying black hole, we boost the black hole solution (5.4) by a constant velocity u^μ in the t, z, $x_\perp$ directions. The resulting line element is given by

$$\mathrm{d}s^2_{(0)} = 2u_\mu \mathrm{d}x^\mu \mathrm{d}r - r^2\left(1-\left(\frac{4\pi T}{(d-1)r}\right)^{d-1}\right)u_\mu u_\nu \mathrm{d}x^\mu \mathrm{d}x^\nu + r^2\left(\eta_{\mu\nu}+u_\mu u_\nu\right)\mathrm{d}x^\mu \mathrm{d}x^\nu . \quad (5.19)$$

Allowing for u^μ and T to become spacetime dependent implies that (5.19) will get corrected. By setting gradients of u^μ and T to to be small, one can solve for the corrections to (5.19) order by order in derivatives so that the line element will take the schematic form

$$\mathrm{d}s^2 = \mathrm{d}s^2_{(0)} + \mathrm{d}s^2_{(1)} + \ldots \quad (5.20)$$

where $\mathrm{d}s^2_{(i)}$ denotes the ith order gradient corrections to the line element.

The stress tensor $T^{\mu\nu}$ which is dual to (5.19) takes the form

$$T^{\mu\nu} = \sum_i T^{\mu\nu}_{(i)} \quad (5.21)$$

also expanded in gradients. One finds [76, 77]

$$T^{\mu\nu}_{(0)} = P(T)\left((d-1)u^\mu u^\nu + \eta^{\mu\nu}\right) \tag{5.22}$$

which is nothing but a boosted version of (5.5) and then, in the Landau frame,

$$\begin{aligned} T^{\mu\nu}_{(1)} &= -2\eta\sigma_{\mu\nu} \ , \\ T^{\mu\nu}_{(2)} &= \frac{(d-1)\eta}{2\pi T}\left[(1-\tau_0)u\cdot\mathcal{D}\sigma^{\mu\nu} + \sigma^\lambda{}_\mu\sigma_{\lambda\nu} - \frac{\sigma^{\alpha\beta}\sigma_{\alpha\beta}}{d-2}P_{\mu\nu} - \tau_0\left(\omega_\mu{}^\lambda\sigma_{\lambda\nu} + \omega_\nu{}^\lambda\sigma_{\mu\lambda}\right)\right] \end{aligned} \tag{5.23}$$

with

$$\begin{aligned} P^{\mu\nu} &= \eta^{\mu\nu} + u^\mu u^\nu \ , \\ \sigma_{\mu\nu} &= \frac{1}{2}P_\mu{}^\alpha P_\nu{}^\beta\left(\partial_\alpha u_\beta + \partial_\beta u_\alpha\right) - \frac{1}{d-2}P^{\mu\nu}\partial_\alpha u^\alpha \ , \\ \omega_{\mu\nu} &= \frac{1}{2}P^{\mu\alpha}P^{\nu\beta}\left(\partial_\alpha u_\beta - \partial_\beta u_\alpha\right) \ , \\ u\cdot\mathcal{D}\sigma_{\mu\nu} &= P_\mu{}^\alpha P_\nu{}^\beta u^\lambda\partial_\lambda\sigma_{\alpha\beta} + \frac{\partial_\alpha u^\alpha}{d-2}\sigma_{\mu\nu} \ , \end{aligned} \tag{5.24}$$

and

$$\eta = \frac{(d-1)P}{4\pi T} \ , \qquad \tau_0 = \int_1^\infty \frac{y^{d-3}-1}{y(y^{d-1}-1)}dy = \frac{1}{2} + O(d^{-2})\,. \tag{5.25}$$

(Note that our definition of $\sigma_{\mu\nu}$ is somewhat unconventional.) An initial analysis of third order gradient corrections has been carried out in [78] for $d = 5$. A full analysis of all third order transport terms for arbitrary dimension d is currently unavailable.

Since (5.16) has been obtained from a large d limit of a gravitational dual theory, we expect that (5.16) coincides with (5.21) when the former is expanded in derivatives and the latter is expanded around large $n = d-1$. In short, we expect that taking a gradient expansion commutes with taking a large d limit. To make a direct comparison let us consider the hydrodynamic stress tensor (5.21) in the t, ζ, $\chi_\perp$ coordinate system where the metric tensor takes the form

$$ds^2 = -\mathrm{d}t^2 + \frac{\mathrm{d}\zeta^2}{n} + \frac{\mathrm{d}\chi_\perp^2}{n} \ . \tag{5.26}$$

One important effect of this rescaling is to keep the sound speed to be an order one quantity.

Scaling the spatial component of the velocity field by $1/\sqrt{n}$, viz.,

$$u^\mu = \frac{1}{\sqrt{1-\frac{\beta^2(t,\zeta)}{n}}}\left(1,\, \beta(t,\zeta)\right) \,, \tag{5.27}$$

and maintaining that $\epsilon = (d-2)P$ is finite in the large d limit, we find,

$$\begin{aligned} \sigma^{\mu\nu} &= n\partial_\zeta\beta\, \delta^\mu_\zeta \delta^\nu{}_\zeta + \mathcal{O}(n^0) \\ u\cdot\mathcal{D}\sigma^{\mu\nu} &= n\left(\beta\partial_\zeta^2\beta + \partial_t\partial_\zeta\beta\right)\, \delta^\mu_\zeta\delta^\nu{}_\zeta + \mathcal{O}(n^0) \\ \sigma^\lambda{}_\mu\sigma_{\lambda\nu} - \frac{\sigma^{\alpha\beta}\sigma_{\alpha\beta}}{d-2}P_{\mu\nu} &= n\left(\partial_\zeta\beta\right)^2\, \delta^\mu_\zeta\delta^\nu{}_\zeta + \mathcal{O}(n^0) \end{aligned} \tag{5.28}$$

and thus,

$$T^{\mu\nu} = \begin{pmatrix} \epsilon & \beta\epsilon \\ \beta\epsilon & \epsilon(1+\beta^2)+p \end{pmatrix} + \mathcal{O}\left(n^{-1}\right) \tag{5.29}$$

where

$$p = -2\epsilon\partial_\zeta\beta + 2\epsilon(\partial_\zeta\beta)^2 + \epsilon\beta\partial_{\zeta^2}\beta + \epsilon\partial_\zeta\partial_t\beta + \mathcal{O}\left(\partial^3\right) \tag{5.30}$$

and $\mathcal{O}\left(\partial^3\right)$ denotes third order and higher derivative corrections. Note that this constitutive relation for the stress tensor includes and encodes the large d limit of the transport coefficients (5.25).

Now, we insert the redefinitions

$$\begin{aligned} e &= \epsilon - \frac{1}{2}\partial_\zeta^2\epsilon \,, \\ j &= \beta\epsilon + \partial_\zeta\epsilon + \frac{1}{2}\partial_t\partial_\zeta\epsilon \,, \\ g &= \frac{1}{2}\epsilon \end{aligned} \tag{5.31}$$

into the large d constitutive relation for the stress tensor (5.16), use the large d stress tensor conservation equations (5.1), and throw out terms that have three or more derivatives. We claim that in this fashion, we recover the stress tensor (5.29) in the gradient expansion. Note that while the conservation equations (5.1) are of second order in gradients of ζ and t, the stress tensor includes at least second order gradients.

5.3.2 Entropy from Gravity

Within the context of our forthcoming analysis, it is instructive to compute the dual entropy production rate which is associated with the evolution of the horizon. Due to its teleological nature, it is usually difficult to identify the location of the event horizon. However, in the large d limit the analysis is somewhat simplified. Let us look for a null surface of the form $R = r_h(t, \zeta)$. The normal to such a surface is

$$\Xi_M \mathrm{d}x^M = \mathrm{d}R - \partial_t r_h \mathrm{d}t - \partial_\zeta r_h \mathrm{d}\zeta \ . \tag{5.32}$$

Demanding that $\Xi^2\Big|_{R=r_h} = 0$ implies, to leading order in the large d limit, that

$$r_h = e \, . \tag{5.33}$$

The spacetime singularity which exists in our solution implies that an event horizon must be present. Since the only null surface available is (5.33), it must be the location of the event horizon. Subleading corrections to the location of the event horizon are given by

$$\begin{aligned} r_h &= e + \frac{1}{n}\left(\frac{4je' - 2(e')^2 - j^2}{2e} + e_2 - 2j' + 2e'' + j'\log(e)\right) \\ &\equiv e + \frac{1}{n} r_{h\,1} \ . \end{aligned} \tag{5.34}$$

To compute the change in the black hole entropy over time we compute the area form of the event horizon. Following the prescription of [79], we find that

$$\mathbf{A} = \frac{\epsilon_{\mu_1 \ldots \mu_d}}{(d-1)!} J_S^{\mu_1} \mathrm{d}x^{\mu_2} \wedge \ldots \wedge \mathrm{d}x^{\mu_d} \tag{5.35}$$

where

$$J_S^\mu = \frac{\sqrt{h}}{4G_N} \frac{N^\mu}{N^t} \tag{5.36}$$

where h is the spatial (t = constant) part of the induced metric on the horizon

$$H_{\mu\nu}\mathrm{d}x^\mu \mathrm{d}x^\nu = g_{MN}\mathrm{d}x^M \mathrm{d}x^N\Big|_{R=r_h} \tag{5.37}$$

and N^μ is defined via

$$\Xi^M \partial_M = N^R \partial_R + N^\mu \partial_\mu \, . \tag{5.38}$$

A short computation yields

$$\begin{aligned}\sqrt{h} &= n^{-\frac{n-1}{2}}\left(e+\frac{1}{n}\left(r_{h\,1}-e\ln e\right)\right)\ ,\\ N_\mu \mathrm{d}x^\mu &= -\partial_t e\,\mathrm{d}t-\partial_\zeta e\,\mathrm{d}\zeta\ .\end{aligned} \tag{5.39}$$

Thus,

$$\begin{aligned}&\tilde{J}^\mu_S = 16\pi G_N n^{\frac{n-1}{2}} J^\mu_S = \frac{4\pi}{n}\left(e,\quad j-e',\quad \ldots\right)\\ &+\frac{4\pi}{n^2}\left(r_{h\,1}-e\ln e,\quad \left(\tfrac{j^2}{2e^2}+\log e\right)(2e'-j)+\left(\tfrac{j^2}{e}\right)'\log e+j_2-r'_{h\,1},\quad \ldots\right)\end{aligned} \tag{5.40}$$

where we have normalized the entropy density so that it is compatible with our conventions for the energy density.

The second law of black hole thermodynamics amounts to

$$\partial_\mu J^\mu_S \geq 0\ . \tag{5.41}$$

In our large d limit we find that

$$\partial_\mu \tilde{J}^\mu_S = \frac{8\pi e}{n^2}\left[\partial_\zeta\left(\frac{j-\partial_\zeta e}{e}\right)\right]^2\ . \tag{5.42}$$

The expectation from hydrodynamics, to second order in derivatives, is that the divergence of the entropy current is given by

$$\partial_\mu \tilde{J}^\mu_S = \frac{2\eta}{T}\sigma^2\,. \tag{5.43}$$

(See for example (8) of ref. [80].) This expectation matches (5.42) on the nose. Note that to leading order in the large d limit the entropy current vanishes. This somewhat surprising feature of the large d limit follows from the fact that entropy production terms are suppressed by inverse powers of the dimension in the large d limit.

5.4 Near equilibrium steady states

We now analyze the dynamics controlled by the partial differential equations (5.1) which encode the dynamics of an out of equilibrium black hole (5.7)

and its dual stress tensor (5.16). Various related holographic analyses can be found in [53, 81, 82, 83, 84, 85, 86, 87, 88, 89]. As discussed in the introduction, the particular question we would like to address is a Riemann problem: What is the time evolution following from an initial condition (5.2)? We are particularly interested in the steady state solution which will emerge at late times. For convenience we will consider a reference frame for which $j_L = 0$. Indeed, if $e(x,t)$ and $j(x,t)$ satisfy the conservation equations (5.1), then so do $e(x-vt,t)$ and $j(x-vt,t)+ve(x-vt,t)$. Thus, for constant values of e and j, we can choose a v such that j will be set to zero. The non-relativistic nature of the boost symmetry reflects the fact that the large d limit we have taken is effectively a non-relativistic limit where the speed of light $c \sim \sqrt{d}$ has been pushed off to infinity.

5.4.1 Rarefaction waves vs. shock waves

Before addressing the Riemann problem in its entirety let us consider a simplified system which is less constrained. Consider (5.16) with gradient terms neglected. The resulting expression is the large d limit of the energy momentum tensor of an inviscid fluid which is known to support (discontinuous) shock waves [56] for any finite value of d. Indeed, consider a single discontinuous shock wave moving with velocity s. Conservation of energy and momentum imply

$$s[T^{tt}] = [T^{t\zeta}] \ , \qquad s[T^{t\zeta}] = [T^{\zeta\zeta}] \ , \tag{5.44}$$

where $[Q] = Q_l - Q_r$ and $Q_{r/l}$ specify the value of Q to the left or right of the shock respectively.[20] The conservation conditions (5.44) are very general and are often referred to as the Rankine-Hugoniot (RH) relations. In our setup they reduce to

$$\begin{aligned} se_l - j_l &= se_r - j_r \ , \\ sj_l - \left(e_l + \frac{j_l^2}{e_l}\right) &= sj_r - \left(e_r + \frac{j_r^2}{e_r}\right) \ , \end{aligned} \tag{5.45}$$

where $e_{r/l}$ and $j_{r/l}$ are the energy density and current immediately to the right or left of the shock. While these Rankine-Hugoniot relations hold for

[20] In this section we use subscripts r and l to denote values of quantities to the right or left of the shock. In other sections we use subscripts R and L to denote quantities in the right and left asymptotic regions. In the latter case there is generally an interpolating region which we denote with a 0 subscript.

an arbitrary, piece-wise continuous fluid profile, in what follows, we are interested in the much simpler situation where e and j are constant functions away from the shocks. Amusingly, e_r satisfies a cubic equation,[21]

$$(e_l j_r - e_r j_l)^2 = e_l e_r (e_l - e_r)^2 \ , \tag{5.46}$$

a plot of which as a function of j_r resembles a fish: fixing (e_l, j_l), each value of s is mapped to a point on the (e_r, j_r) plane. The collection of such points is given by a fish-like curve, an example of which is given in the left panel of figure 14.

We make two observations about the fish. The vacuum $(e_r, j_r) = (0, 0)$ always lies on the cubic (5.46), corresponding to the fact that a shock can interpolate between any value of (e_l, j_l) and the vacuum. Also $(e_r, j_r) = (e_l, j_l)$ is the point of self-intersection of the cubic and has $s = \pm 1 + j_l/e_l$. The physical content of this observation is that when (e_r, j_r) is close to (e_l, j_l) but still lies on the cubic, we can find a close approximation to the fluid profile by linearizing the equations of motion. As we will describe in greater detail below, linearized fluctuations correspond to damped sound modes, and indeed the two regions can be connected by sound waves propagating at the local sound speed $s = \pm 1 + j_l/e_l$.

The shock solutions we found all solve the conservation equations (5.45). However, some of these solutions are unphysical in the following sense. Let us boost to a frame where the shock speed vanishes, $s = 0$. In half of the shock solutions, a quickly moving fluid at low temperature is moving into a more slowly moving fluid at higher temperature, converting kinetic energy into heat and producing entropy. We will refer to these shocks as "good" shocks. The other half of the solutions correspond to the time reversed process where a slowly moving fluid at high temperature moves into a rapidly moving but cooler fluid, turning heat into kinetic energy. This second solution, as we shall see shortly, should be discarded.

Strictly speaking, entropy is conserved in the large d limit (see the discussion following equation (5.43)). A more formal way of understanding why one should discard the bad shocks is to restore the gradient corrections but

[21] In general d, one finds the relation

$$\sinh^2(\alpha_l - \alpha_r) = \frac{d-2}{(d-1)^2} \frac{(\epsilon_l - \epsilon_r)^2}{\epsilon_l \epsilon_r} \ ,$$

where $\beta = \tanh \alpha$ is the fluid velocity.

take a limit where these are small. et us assume that in the frame where the shock velocity is zero there is an approximately stationary configuration such that time derivatives are much smaller than spatial derivatives. Boosting back to a shock with velocity s, we expect that e and j depend only on the combination $\zeta - st$, i.e., $j(t,\zeta) = j(\zeta - st)$ and likewise, $e(t,\zeta) = e(\zeta - st)$. The equations of motion (5.1) become ordinary differential equations which can be integrated once to obtain

$$\begin{aligned} e' &= -s(e - e_l) + (j - j_l) \,, \\ j' &= -s(j - j_l) + \left(e + \frac{j^2}{e} - e_l - \frac{j_l^2}{e_l} \right) \,. \end{aligned} \tag{5.47}$$

We have picked the two integration constants such that e' and j' vanish in the left asymptotic region. The Rankine-Hugoniot conditions (5.45) imply that e' and j' also vanish in the right asymptotic region. As e' and j' themselves vanish in the left and right asymptotic regions, we can describe e' and j' well near these points by looking at a gradient expansion. Near the left asymptotic region

$$\begin{aligned} \begin{pmatrix} e' \\ j' \end{pmatrix} &\approx \begin{pmatrix} -s & 1 \\ 1 - \frac{j_l^2}{e_l^2} & \frac{2j_l}{e_l} - s \end{pmatrix} \begin{pmatrix} e - e_l \\ j - j_l \end{pmatrix} \\ &\equiv M_l \begin{pmatrix} e - e_l \\ j - j_l \end{pmatrix} \,. \end{aligned} \tag{5.48}$$

There is a similar looking equation for e' and j' near the right asymptotic region

$$\begin{pmatrix} e' \\ j' \end{pmatrix} \approx M_r \begin{pmatrix} e - e_r \\ j - j_r \end{pmatrix} \,. \tag{5.49}$$

The solutions near (e_l, j_l) and near (e_r, j_r) have an exponential nature with the sign of the exponents depending on the eigenvalues of M_l and M_r appearing on the right hand side of (5.48) and (5.49) given by

$$\lambda_{r\,\pm} = \pm 1 + \frac{j_r}{e_r} - s \,, \qquad \lambda_{l\,\pm} = \pm 1 + \frac{j_l}{e_l} - s \,. \tag{5.50}$$

We now observe that the signs of the eigenvalues of M_l and M_r determine whether the shock is a viable solution to the equations of motion.

- If both eigenvalues of M_l are negative, then e' and j' will not vanish as $x \to -\infty$. Thus we require that at least one eigenvalue of M_l is positive in order for a shock solution to exist.

- If we assume there is exactly one positive eigenvalue, then $1 + j_l/e_l > s$ and $-1 + j_l/e_l < s$. Note that the value $1 + j_l/e_l$ corresponds to the slope of one of the characteristics (i.e. the local speed of one of the sound waves), and this condition implies that this characteristic will end on the shock. Since λ_{l-} is assumed to be negative, we have to tune one of the two integration constants of the system of differential equations to zero. This tuning means that generically the solution to the right of the shock will be a linear combination of both of the solutions near (e_r, j_r). If both solutions are to be used, then it had better be that both eigenvalues of M_r are negative. (Otherwise, it will not be true that e' and j' vanish in the limit $x \to \infty$.) In particular, the larger of the two eigenvalues must be negative, which implies that $1 + j_r/e_r < s$. (In terms of characteristics, both will end on the shock.) Thus, we find the constraint
$$1 + j_r/e_r < s < 1 + j_l/e_l \,. \tag{5.51a}$$

- If both eigenvalues of M_l are positive, we still need at least one negative eigenvalue of M_r to be able to connect the solutions in the left and right asymptotic regions. Moreover, for M_r to have two negative eigenvalues would be inconsistent with momentum conservation (5.45). An analysis similar to the previous one yields
$$-1 + j_r/e_r < s < -1 + j_l/e_l \,. \tag{5.51b}$$

The constraints (5.51) choose the good shocks over the bad ones.

Since bad shocks are not allowed, one may inquire as to the time evolution of a discontinuity with initial conditions which would have generated a bad shock. As it turns out, bad shocks can be replaced by the more physical rarefaction solutions [56]. The rarefaction solution assumes that between the asymptotic regions specified by (e_l, j_l) and (e_r, j_r), there is an interpolating solution where e and j are functions of $\xi = \zeta/t$. As was the case for the shock wave, given e_l and j_l, there is a one parameter family of allowed values of e_r and j_r. These are given by
$$\begin{aligned} e_r =& e_l \exp\left(\pm j_l/e_l - 1 \mp \xi_r\right) \,, \\ j_r =& e_l(\pm 1 + \xi_r) \exp\left(\pm j_l/e_l - 1 \mp \xi_r\right) \,. \end{aligned} \tag{5.52}$$

The curve traced by (e_r, j_r) also resembles a fish, and for moderate values of the shock parameters e_r and j_r it closely follows the cubic curve corresponding to a shock solution. (See the central panel of figure 14.) The vacuum $(0,0) = (e_r, j_r)$ solution can always be connected to (e_l, j_l) through a rarefaction wave. The self-intersection point $(e_r, j_r) = (e_l, j_l)$ has $\xi = \mp 1 + j_l/e_l$, again corresponding to a sound wave type interpolation between the two regions $(e_r, j_r) \approx (e_l, j_l)$.

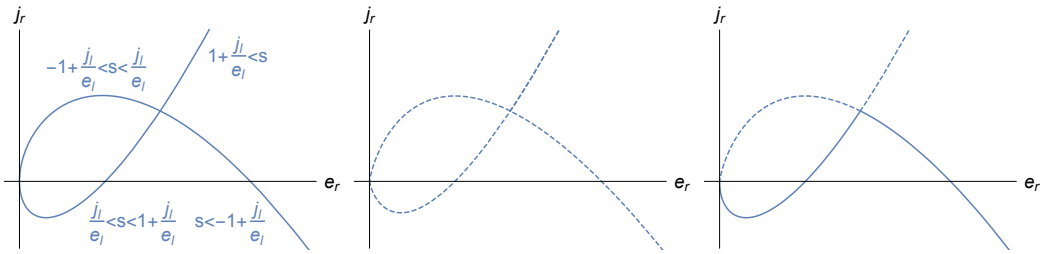

Figure 14: (Left panel) The solid blue curve corresponds to the solution to the Rankine-Hugoniot condition for (e_l, j_l). Points on the curve correspond to different values of s in (5.45). The regions $j_l/e_l < s < j_l/e_l + 1$ and $s < j_l/e_l - 1$ correspond to good shocks satisfying (5.51a) and (5.51b) respectively. (Center panel) The dashed line, which almost overlaps with the blue line at places, parameterizes the rarefaction solution (5.52) also associated with (e_l, j_l). (Right panel) A plot of possible values of (e_r, j_r) for a given a pair (e_l, j_l) with good shocks preferred over the rarefaction solution and the rarefaction solution preferred over bad shocks.

Given that bad shocks are replaced by rarefaction waves, one should remove from the fish diagram (left panel of figure 14) the portion of the curve which corresponds to bad shocks and replace it with a curve corresponding to a rarefaction solution (central panel of figure 14). The resulting curve can be found on the right panel of figure 14: the belly of the fish and the lower part of its tail corresponds to a good shock and its back and upper tail to a rarefaction solution. One may compute the curve explicitly by imposing (5.51), but it can also be understood from a graphical viewpoint as we now explain.

Recall that the self intersection point of the shock wave fish (solid curve on the left panel of figure 14) corresponds to a shock velocity, s, which takes the values of the local speed of sound, $\pm 1 + j_l/e_l$. On the tail, s is either larger than $1 + j_l/e_l$ (upper tail) or smaller than $-1 + j/e$ (lower tail). Thus,

on the tails, the eigenvalues are either both positive or both negative. The top portion of the tail has $\lambda_{\pm l} < 0$ while the bottom portion of the tail has $\lambda_{\pm l} > 0$. As a result, the top portion of the tail must be replaced by a rarefaction wave while the bottom portion can be a shock. To decide which portion of the body of the shock fish to replace by a rarefaction wave, one must study $\lambda_{\pm r}$.

Consider a second fish which exhibits the solution to the cubic (5.46) for a given value of (e_r, j_r). We will call this second fish an r-fish and the first an l-fish. Similar to the analysis of the tail of the l-fish, we find that the bottom portion of the tail of the r-fish should be constructed from a rarefaction solution while the top portion from a shock.

Consider an r-fish whose point of self intersection lies somewhere on the body of the l-fish. When the r-fish is drawn so that it intersects the back of the l-fish, the bottom portion of the r-fish's tail will go through the point of self-intersection of the l-fish (see the left panel of figure 15). As the bottom portion of the tail of the r-fish is a rarefaction, the region (e_r, l_r) can be connected to (e_l, j_l) by a rarefaction. Reciprocally, since we're describing a single shock or rarefaction interface between two regions, the back of the l-fish should be replaced by a rarefaction wave. We can run the argument again for an r-fish drawn to intersect the belly of the l-fish. We conclude that the belly of the l fish must be a shock (see the right panel of figure 15).

5.4.2 Solving the Riemann problem using ideal hydrodynamics

Armed with our understanding of shock waves and rarefaction solutions, let us now tackle the Riemann problem we set out to solve. At $t = 0$, we consider a pair $(e_L, 0)$ which describes the fluid for $z < 0$ and another pair (e_R, j_R) describing the fluid for $z > 0$. For a single interpolating shock or rarefaction, we have seen that given $(e_L, 0)$ there is a one parameter family of solutions that determine (e_R, j_R). Thus, generically, there will not be a single shock or rarefaction solution that joins $(e_L, 0)$ to an arbitrary (e_R, j_R). However, we can connect the two regions using a pair of shock and/or rarefaction waves. That is, we could connect $(e_L, 0)$ to an intermediate regime with values of e and j given by (e_0, j_0) using a shock or rarefaction wave and another shock wave or rarefaction wave to connect the intermediate regime to the right asymptotic region (e_R, j_R). In all cases, given the initial conditions, the pair of rarefaction and/or shock waves should be such that they move away from

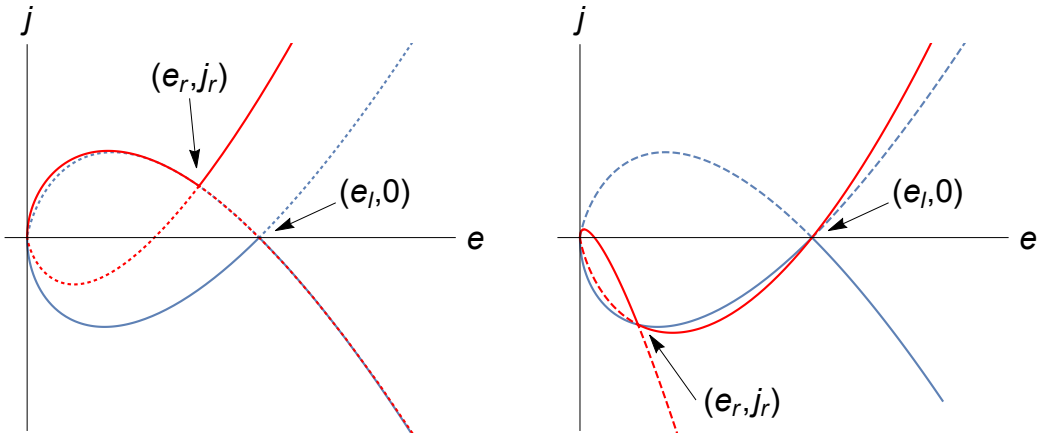

Figure 15: A graphical determination of the "good shocks" and "bad shocks". The red fish corresponds to (e_r, j_r) while the blue fish is built from $(e_l, 0)$. See the main text for a discussion.

each other.

The strategy for determining which type of solution is allowed is to prefer good shocks over rarefaction solutions and rarefaction solutions over bad shocks. Thus, given a pair $(e_L, 0)$ and (e_R, j_R) we need to establish which of the four possibilities for the time evolution of the initial state is allowed: two shocks (SS), a rarefaction wave followed by a shock (RS), or the remaining two configurations which we will denote by SR and RR.

To understand the possible solutions to the Riemann problem, let us first consider two fish diagrams: one associated with $(e_l, j_l) = (e_L, 0)$ (the l-fish) and another with $(e_r, j_r) = (e_R, j_R)$ (the r-fish). The points of overlap of the diagrams will give us the possible value of e_0 and j_0. We will always choose a point where the two disturbances are moving away from each other. See, for example, figure 16.

Instead of plotting the r- and l-fishes, we can obtain closed form expressions for the various types of solutions by solving (5.51) and (5.52) on a case by case basis. In the following we provide some simple examples of such expressions.

- **RS configurations.** As an example of the RS case, we take $(e_L, 0)$ and $(e_R, 0)$ as the asymptotic regions with $e_L > e_R$. The SR case is a left-right reflection of the RS case and therefore does not warrant further discussion.

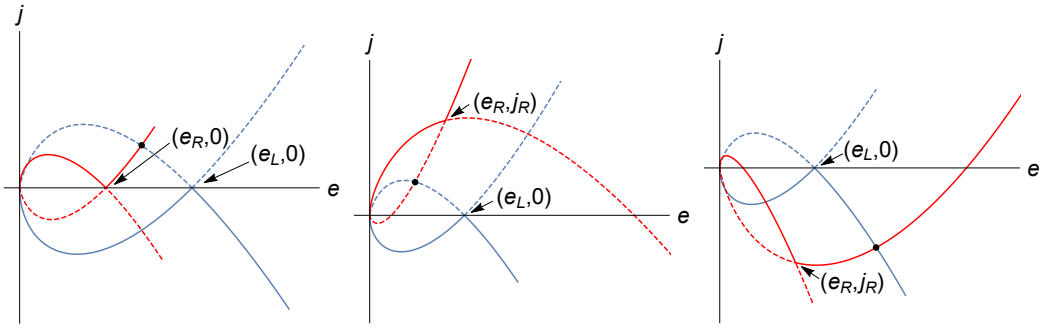

Figure 16: Some diagramatic solutions to the Riemann problem. The blue fish corresponds to $(e_L, 0)$ while the red fish to (e_R, j_R). The solid line is a shock and the dashed line a rarefaction. The intermediate region is indicated by a black dot. Left panel: The shock solution of the right asymptotic region overlaps with the rarefaction solution of the left asymptotic region, so we get an SR type configuration. Center panel: The rarefaction solution of the left and right regions overlap creating an RR type solution. Right panel: An SS type solution.

To estimate the values of e_0 and j_0 we can follow the strategy laid out in [62, **?**]. For the left region we use the solution (5.52) with $e_l = e_L$, $j_l = 0$, $e_r = e_0$ and $j_r = j_0$. For the right region we use (5.45) with $e_l = e_0$, $j_l = j_0$, $e_r = e_R$ and $j_r = 0$. We find

$$\begin{aligned} e_0 &= e_R s^2 \ , \\ j_0 &= e_R s(s^2 - 1) \ , \\ 0 &= \frac{1}{s} - s - \log\left(\frac{e_R}{e_L} s^2\right) \ , \end{aligned} \tag{5.53}$$

which, unsurprisingly, coincides with the large d limit of the hydrodynamic analysis of [62, **?**].

As pointed out in [62] the rarefaction solution will cover the location of the original shock discontinuity whenever

$$\frac{e_L}{e_R} \geq \left(\frac{1+\sqrt{5}}{2}\right)^2 \exp(1) \sim 7.11655 \ . \tag{5.54}$$

At the point $\zeta = 0$ in the rarefaction wave, the values of e and j are time independent (since any function of ζ/t will have a fixed point at

$\zeta = 0$). Moreover for a conserved stress tensor $T^{\mu\nu} = T^{\mu\nu}\left(\frac{\zeta}{t}\right)$, the first spatial derivative of $T^{t\zeta}$ and the first and second spatial derivatives of $T^{\zeta\zeta}$ vanish at this fixed point. Thus, one may think of the pressure at the fixed point as a "short" steady state for long enough times. "Short" implies that the region is of small spatial extent. From this perspective one has split steady states for large enough initial temperature differences. The values of e and j at the short steady state are given by

$$e_s = j_s = e_L \exp(-1)\,. \tag{5.55}$$

- **SS configurations.** A simple example of the SS case has $(e_L, 0)$ on the left and (e_L, j_R) on the right with $j_R < 0$. We compute the NESS by gluing two shock waves to an intermediate region with $(e, j) = (e_0, j_0)$, similar to the RS case. Setting $\beta = j_R/e_L$, the intermediate NESS is given by

$$e_0 = \frac{e_L}{8}(8 + \beta^2 - \beta\sqrt{16+\beta^2})\ , \quad \frac{j_0}{e_0} = \frac{\beta}{2}\ , \tag{5.56}$$

and the shock velocities for the left and right moving shocks, s_L and s_R respectively, are given by

$$s_L = \frac{1}{4}(\beta - \sqrt{16+\beta^2})\ , \tag{5.57}$$

$$s_R = \frac{1}{4}(3\beta + \sqrt{16+\beta^2})\ . \tag{5.58}$$

- **RR configurations.** Using $e_L = e_R$ and $j_R > 0$, we can find simple solutions that involve two rarefaction waves.[22] In this case, the NESS

[22] As it turns out in the RR phase, there is a simple expression for the steady state for all values of e_L, e_R, j_L and j_R,

$$e_0 = \sqrt{e_L e_R}\exp\left(\frac{j_L}{2e_L} - \frac{j_R}{2e_R}\right)\ , \quad j_0 = \frac{e_0}{2}\left(\xi_+ + \xi_-\right)\ ,$$

where

$$\xi_+ - \xi_- = 2\,, \qquad \xi_+ + \xi_- = \frac{j_L}{e_L} + \frac{j_R}{e_R} - \log\frac{e_R}{e_L}\ .$$

A fixed point associated with a left moving rarefaction solution occurs whenever

$$\frac{e_R}{e_L} \le \exp\left(\frac{j_L}{e_L} + \frac{j_R}{e_R} - 2\right) \quad \text{with} \quad e_s = j_s = e_L \exp\left(-1 + \frac{j_L}{e_L}\right)\ ,$$

is characterized by

$$e_0 = e_L \exp\left(-\frac{j_R}{2e_L}\right) , \qquad j_0 = \frac{j_R}{2} \exp\left(-\frac{j_R}{2e_L}\right) , \tag{5.59}$$

where the left moving rarefaction wave extends from $\xi = -1$ to $\xi = \xi_-$ while the right moving rarefaction wave extends from $\xi = \xi_+$ to $\xi = 1$ with

$$\xi_+ - \xi_- = 2 , \qquad \xi_+ + \xi_- = \frac{j_R}{e_R} , \tag{5.60}$$

Similar to the RS case we find that there is a fixed point associated with the left moving wave whenever

$$\frac{j_R}{2e_L} \geq 1 , \tag{5.61}$$

with

$$e_s = j_s = e_L \exp(-1) . \tag{5.62}$$

We claim that given $(e_L, 0)$, the "phase diagram" of figure 13 immediately allows us to choose the correct configuration of shocks and rarefaction waves for any (e_R, j_R). Indeed, following figure 16, the location of the self intersection point of the r-fish will determine the nature of the intersection of the r- and l-fish: if the intersection point of the r-fish lies above the l-fish we will always get an RR solution; if the intersection point of the r-fish is below the l fish we get an SS solution; and RS and SR solutions will correspond to an intersection point of the r-fish in the body or tail of the l-fish respectively. Conformal invariance dictates that the phase diagram can depend on the only two dimensionless parameters of this problem, and we obtain the phase diagram in figure 13.

Note that even though the r-fish and the l-fish intersect at $(0, 0)$, we can always rule out an intermediate point that corresponds to a vacuum. The vacuum intersection point is always along the bodies of the two fish where we have $\lambda_{-,l/r} < 0 < \lambda_{+,l/r}$. As discussed, we can not in general connect the two asymptotic solutions if we do not have two eigenvalues of the same sign (positive for l and negative for r) in one of the regions.

---

and a fixed point associated with the right moving rarefaction solution occurs whenever

$$\frac{e_R}{e_L} \geq \exp\left(\frac{j_L}{e_L} + \frac{j_R}{e_R} + 2\right) \quad \text{with} \quad e_s = -j_s = e_R \exp\left(-1 + \frac{j_R}{e_R}\right) .$$

5.4.3 A numerical solution to the Riemann problem.

In the previous sections we have obtained predictions for the evolution of e and j starting from an initial configuration (5.2) and assuming that gradient corrections to the equations of motion are small. It is somewhat unfortunate that this assumption stands in stark contrast to the discontinuous jump in the initial state and one may inquire whether the analysis of the previous section is relevant for the problem at hand. In order to resolve this issue we solve the full equations of motion (5.1) numerically. We give numerical examples of the RR, SS, and RS phases described above. To our numerical accuracy, the difference in e_0 and j_0 between the ideal case which we have studied analytically and the case with gradients included which has been obtained numerically appears to disappear in the long time limit.

As it turns out, the equations (5.1) are easy to evolve numerically with canned PDE solvers, such as Mathematica's NDSolve routine [90]. To obtain various solutions one can evolve the initial condition

$$e = \langle e \rangle \left(1 + \delta e \tanh(c \sin(2\pi x/L))\right) \ , \tag{5.63}$$

$$j = \langle j \rangle \left(1 + \delta j \tanh(c \sin(2\pi x/L))\right) \ , \tag{5.64}$$

in a periodic box of length L. (In appendix E, we use a more elaborate piecewise continuous initial condition.) For c sufficiently large, the initial condition approaches a square wave. As long as the disturbance has not travelled a distance of order L, causality ensures that the behaviour of e and j are very close to that of an infinite system where the values of e and j in the asymptotic region are fixed at some constant value. If we denote these asymptotic values as e_L and e_R then

$$\delta e = \frac{e_L - e_R}{e_L + e_R} \quad \text{and} \quad \langle e \rangle = \frac{1}{2}\left(e_L + e_R\right) . \tag{5.65}$$

We can similarly define $\langle j \rangle$ and δj.

In figures 17, 18, and 19, we have plotted typical results for numerical solutions to (5.1), corresponding to RS, SS, and RR configurations. The resulting values of e and j seem to approach the predicted values of e_0 and j_0 at long times—at least as far as our numerical precision can be trusted (see appendix E). In particular, in the RS case, we approach the steady state value (5.53); in the SS case, we approach (5.56); and in the RR case, we approach (5.59). As we discuss in greater detail in the next section, one

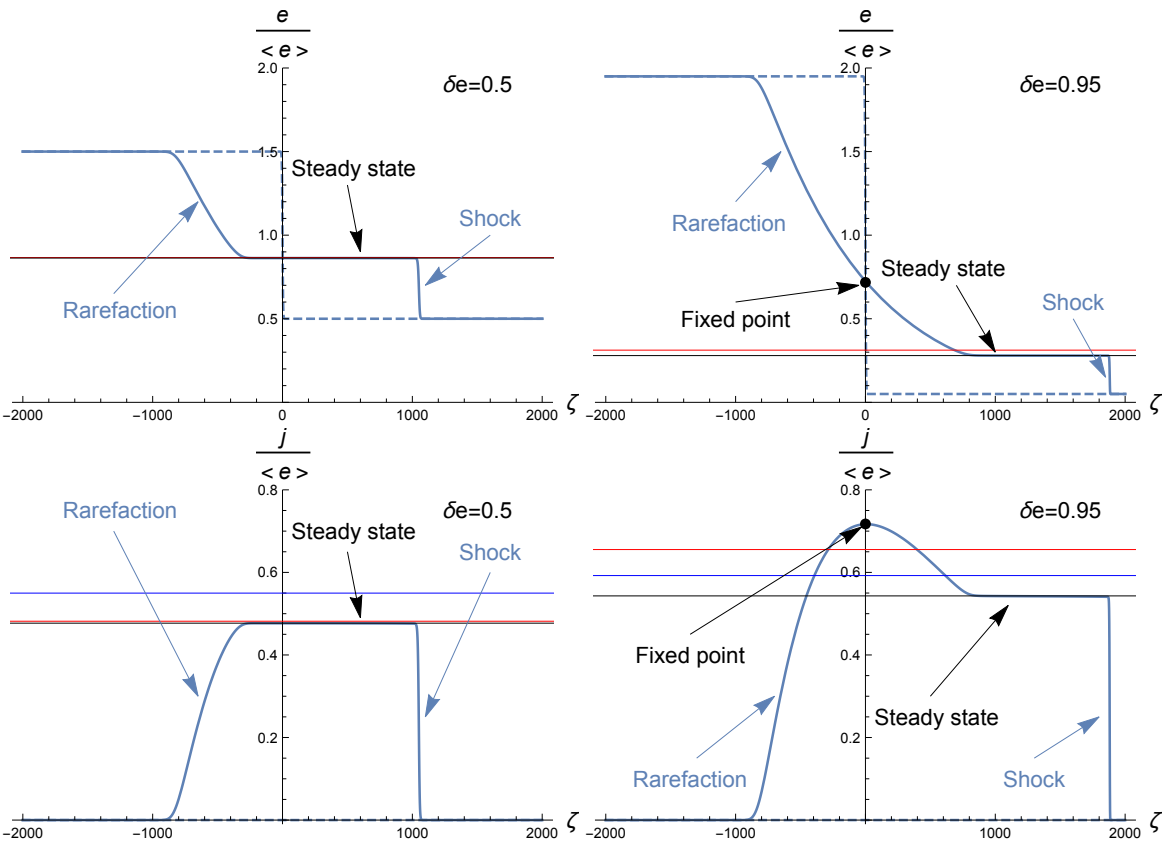

Figure 17: A numerical solution to the Riemann problem. The plots were obtained starting with an initial condition (E.5) with $L = 8000$, $c = 300$ and $\langle j \rangle = 0$. Only one half of the box, centered around the origin, is depicted. The dashed curve corresponds to values of e and j at $t = 0$ while the solid curve corresponds to values of e and j at $t = 800$. The black, red and blue horizontal lines correspond to the predicted near equilibrium steady state associated with a rarefaction wave and shock pair (c.f., equation (5.53)), a bad shock and good shock pair (c.f., references [48, 49]), and a non thermodynamic shock pair (c.f., reference [49]) respectively. The fixed point associated with a rarefaction solution which exists for $\delta e \geq 0.7536\ldots$ is represented by a black dot.

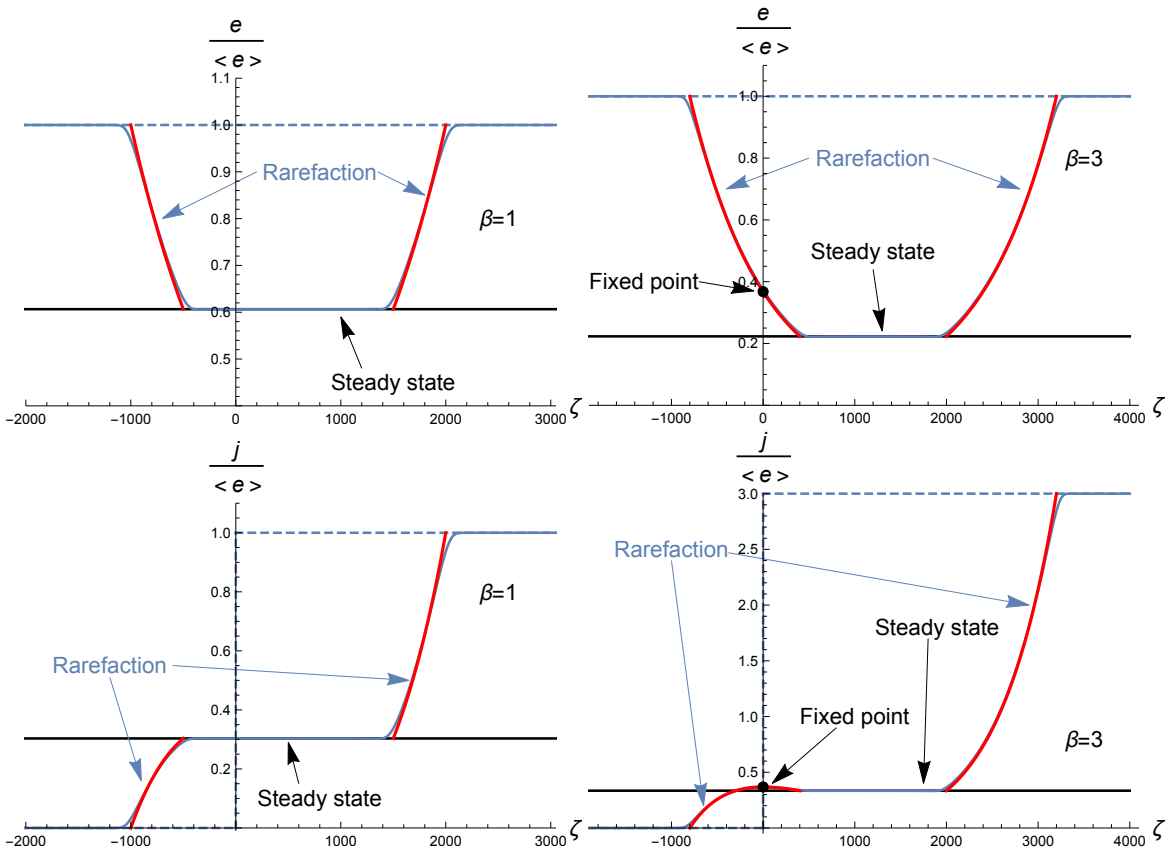

Figure 18: Two numerical solutions to the Riemann problem in the RR case. The plots were obtained starting with a constant e initial condition, $j_L = 0$, and fixed $\beta = j_R/e_L$, with $L = 8000$ and $c = 200$. The dashed line corresponds to the solution at $t = 0$ and the solid blue line at $t = 1000$. The solid red curves are the rarefaction waves in the ideal limit, without gradient corrections. The horizontal black line is the predicted steady state value.

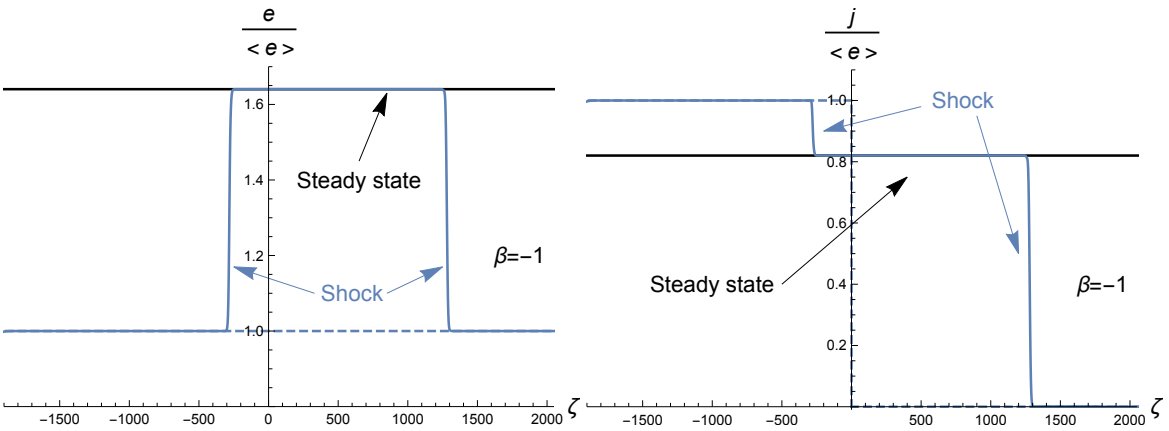

Figure 19: A numerical solution to the Riemann problem in the SS case. The plots were obtained starting with a constant e initial condition, $j_R = 0$, and $\beta = -j_L/e_L = -1$, with $L = 8000$ and $c = 200$. The dashed line corresponds to the solution at $t = 0$ and the solid blue line at $t = 1000$. The horizontal black line is the predicted steady state value.

place where gradient effects show up and do not disappear as a function of time is in the shock width.

One may speculate that the agreement between the predicted steady state in the absence of gradient corrections and the numerical results is asscoiated to the fact that the gradient corrections, even though order one in our system of units, come with dimensionful coefficients. In the language of the renormalization group, they conform to irrelevant couplings. Perhaps it is for this reason that at long enough time and in a large enough box, we may be able to ignore these corrections for the most part.

5.4.4 Restoring gradient corrections

In this section, we try to gain a better handle over the gradient corrections and their affect on the predicted steady state values. The analysis here is incomplete and approximate. To overcome the deficiencies of paper and pencil estimates, we include some numerical solutions to the conservation equations (5.1) that provide support for the estimates. We will consider separately corrections to each of the features we found in the idealized limit: the steady state and asymptotic regions with constant e and j, a shock wave, a rarefaction wave, and the discontinuity at the edge of the rarefaction.

Corrections to constant regions Corrections to a constant e and j region are easiest to analyze. Assuming the fluctuations are small, we look for linearized solutions of the form $e = e_0 + \delta e \exp(-i\omega t + ik\zeta)$ and $j = j_0 + \delta j \exp(-i\omega t + ik\zeta)$. We find two propagating modes

$$\omega = \left(\pm 1 + \frac{j_0}{e_0}\right) k - ik^2 \ . \tag{5.66}$$

These two modes are damped sound modes whose speed is shifted by the fluid velocity $\beta = j/e$. The gradient corrections appear here in the form of the damping term ik^2 in the dispersion relation. Given this result, we anticipate that we will be able to correct a constant e and j region by taking an appropriate linear superposition of sound waves. The damping suggests that at long times the solution can only involve constant e and constant j.

As a side comment, an odd thing about these mode relations is that they are exact. Recall that in first order viscous hydro, we would typically solve an equation of the form $\omega^2 + i\Gamma k^2\omega - k^2 = 0$ for ω, in the case of vanishing background fluid velocity. If this equation were treated as exact, the solutions for ω would be non linear in k and therefore have higher order contributions, i.e. $O(k^3)$, $O(k^4)$, etc., when expanded around small k.

Corrections to shocks The gradient corrections should act to smooth a shock and give it some characteristic width. We estimate this width in a frame in which the shock is not moving, i.e. $s = 0$. In this frame, $j_r = j_l$ and $e_r e_l = j_l^2$. We can find a solution for the shock profile in the case where the shock is weak $e_r \sim e_l$:

$$e = \langle e \rangle \left[1 + \delta e \tanh\left(\frac{\zeta \delta e}{2}\right) - \frac{\delta e^2}{2} \operatorname{sech}\left(\frac{\zeta \delta e}{2}\right)^2 \log\cosh\left(\frac{\zeta \delta e}{2}\right) + O(\delta e^3)\right] , \tag{5.67}$$

$$j = \langle j \rangle \left[1 \qquad\qquad + \frac{\delta e^2}{2} \operatorname{sech}\left(\frac{\zeta \delta e}{2}\right)^2 + O(\delta e^3)\right] , \tag{5.68}$$

where we have defined

$$\langle e \rangle \equiv \frac{e_r + e_l}{2} , \quad \delta e \equiv \frac{e_r - e_l}{e_r + e_l} , \quad \text{and} \quad \langle j \rangle \equiv \frac{j_r + j_l}{2} \ .$$

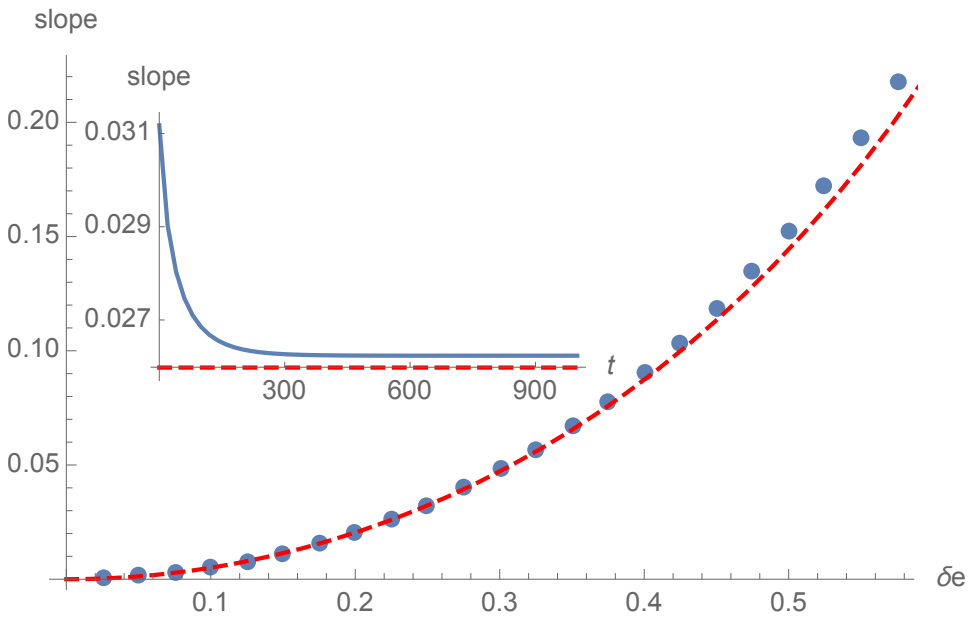

Figure 20: A numerical simulation of stationary shocks. We start from an initial condition $e = \langle e \rangle (1 + \delta e \tanh(c \sin(2\pi x/L)))$, $j = 1$ with parameters $L = 8000$ and $c = 1.2(L\delta e/4\pi)$. We chose e_r and e_l to produce a stationary shock ($e_l = \frac{\sqrt{1-\delta e}}{\sqrt{1+\delta e}}$, $e_r = \frac{\sqrt{1+\delta e}}{\sqrt{1-\delta e}}$) using the RH relations. We then plot the value of the slope of the shock after the system has settled into a steady state. This is compared with the weak shock solution (5.67), given by the dashed red line. The inset plot shows the relaxation from the initial conditions to the steady state for $\delta e = 0.23$.

We can see in figure 20 that even for values of $\delta e \sim 1/2$, that $\langle e \rangle \delta e^2/2$ appears to be a good estimate for the slope of the shock.[23] In appendix D, we show that this shock profile produces, at the correct subleading order in a large d expansion, the correct (positive) amount of entropy predicted by the RH relations.

Corrections to a rarefaction We will perform two estimates of gradient corrections to the rarefaction wave. The first estimate is a correction to the

[23] We found that when $\delta e = 0.8$ the relative error between (5.67) and the numerical solution grew to $\sim 13\%$. As δe gets closer to one numerical error is more difficult to control.

interior of the wave far from the edges where it joins onto constant e and j regions. The second estimate is a correction to the discontinuity where the rarefaction joins a constant region. For the first estimate, we assume an ansatz for the long time behavior of the rarefaction wave:

$$\begin{aligned} e &= e_0(\xi) + \frac{\log t}{t} e_l(\xi) + \frac{1}{t} e_1(\xi) + O((\log t)^2/t^2) \ , \\ j &= j_0(\xi) + \frac{\log t}{t} j_l(\xi) + \frac{1}{t} j_1(\xi) + O((\log t)^2/t^2) \ , \end{aligned}$$

where

$$e_0 = c_1 \exp(\mp\xi) \ , \quad j_0 = (\pm 1 + \xi) c_1 \exp(\mp\xi) \ , \tag{5.69}$$

$$e_l = 2c_1 \exp(\mp\xi) - \frac{1}{2} c_2 \exp(\mp\xi/2) \ , \quad j_l = \xi e_l \ , \tag{5.70}$$

$$j_1 = \pm \exp(\mp\xi)(c_1 - c_2 \exp(\pm\xi/2)) + \xi e_1 \ . \tag{5.71}$$

With an appropriate choice for the integration constant c_1, the expressions for e_0 and j_0 become the same as we had before (5.52). There are subleading corrections that scale as $1/t$ and $\log(t)/t$ that depend on a second integration constant c_2 and an arbitrary function $e_1(\xi)$, both presumably set by the initial conditions. Note that the combination $\xi e - j$ is independent of the arbitrary function $e_1(\xi)$ at order $1/t$. In figure 21, the numerics confirm that the corrections to $\xi e - j$ do indeed scale as $1/t$.

Last, we would like to heal the discontinuity at the edge of a rarefaction wave. The tanh function we found above heals the discontinuity in the shock case, making the question of what happens at the edge of a shock less pressing. Consider a case where the rarefaction wave meets a steady state at $\zeta = 0$, with the rarefaction region to the right and the steady state to the left. (We can always move the meeting point away from $\zeta = 0$ by boosting the solution $\zeta \to \zeta + vt$.) With the intuition that the second order gradients in the conservation equations are dominant and render the behavior similar to that of a heat equation with $1/\sqrt{t}$ broadening, we look for an approximate late time solution of the form

$$e = e_0 + \frac{1}{\sqrt{t}} e_1(\chi) + O(t^{-1}) \ , \tag{5.72}$$

$$j = j_0 + \frac{j_1}{\sqrt{t}} + \frac{1}{t} j_2(\chi) + O(t^{-3/2}) \ , \tag{5.73}$$

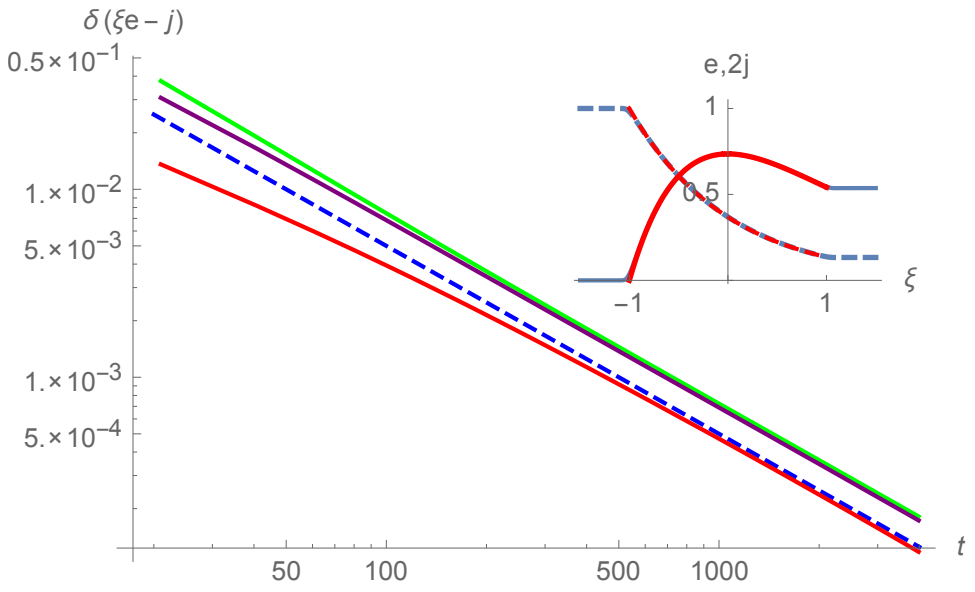

Figure 21: A plot of $\delta(\xi e - j)$ vs. time at three different points in a single rarefaction wave. The quantity $\delta(\xi e - j)$ is the difference between the zeroth order prediction (5.52) and numerics. The rarefaction wave spreads from $\xi_l = -1$ to $\xi_r = 1$. The three points correspond to $\xi = -1/2$ (red), $\xi = 0$ (purple) and $\xi = 1/2$ (green). The dashed line $1/(2t)$ is a guide to the eye. Inset: the rarefaction profile at $t = 3000$. Dashed lines correspond to e while the solid lines correspond to j. The blue curve is numeric, while the red curve is the ideal result (5.52).

defining $\chi \equiv \zeta/\sqrt{t}$. We find that $j_0 = \pm e_0$, that j_1 is constant, and that

$$j_2'(\chi) = \mp \frac{e_1(\chi) e_1'(\chi)}{e_0} + \left(4 \frac{e_1'}{e_0} \pm 1 \right) j_1 \ .$$

Note that the relation $j_0 = \pm e_0$ is consistent with a rarefaction meeting a steady state region at $\zeta = 0$. These relations for the j_i lead to a second order, nonlinear differential equation for e_1:

$$e_1'' + \left(\frac{\chi}{2} + \frac{\pm e_1 - j_1}{e_0} \right) e_1' + \frac{e_1}{2} \mp \frac{j_1}{4} = 0 \ . \tag{5.74}$$

Remarkably, this equation can be written as a total derivative and integrated to yield

$$\pm \frac{e_1^2}{2e_0} + e^{-\chi^2/4} \partial_\chi (e^{\chi^2/4} e_1) - \frac{j_1 e_1}{e_0} \mp \frac{j_1}{4} \chi = c_1 \ , \tag{5.75}$$

where c_1 is another integration constant. The integration constants reflect a translation symmetry of both e_1 and χ. We can shift $\chi \to \chi + j_1/e_0$ and $e_1(\chi) \to e_1(\chi - j_1/e_0) \pm j_1/2$. The shifts send $j_1 \to 0$ and $c_1 \to c_1 \mp 3j_1^2/8e_0$ in the equation (5.75). If we apply the boundary condition that both $e_1(\chi)$ and $e_1'(\chi)$ vanish in the steady state region $\chi \to -\infty$, then we must set $c_1 = 0$, and the resulting first order differential equation becomes separable. To match onto the rarefaction region, we require that $e_1' \to \pm e_0$ as $\chi \to \infty$. This boundary condition fixes the remaining integration constant associated with the first order equation (5.75), and the solution for e_1 is then

$$e_1 = \pm \frac{2 e_0 e^{-\chi^2/4}}{\sqrt{\pi} \operatorname{erfc}(\chi/2)} \ . \tag{5.76}$$

As we choose the rarefaction region to match onto the steady state at $\chi = 0$, we conclude that the integration constant j_1 in the original differential equation must be zero as well. We can check numerically that a $1/\sqrt{t}$ scaling is consistent with the behavior at the endpoints of a rarefaction solution. See figure 22.

5.5 Discussion

We presented a solution to the Riemann problem for the conservation equations (5.1). Through fluid-gravity and the AdS/CFT correspondence, these

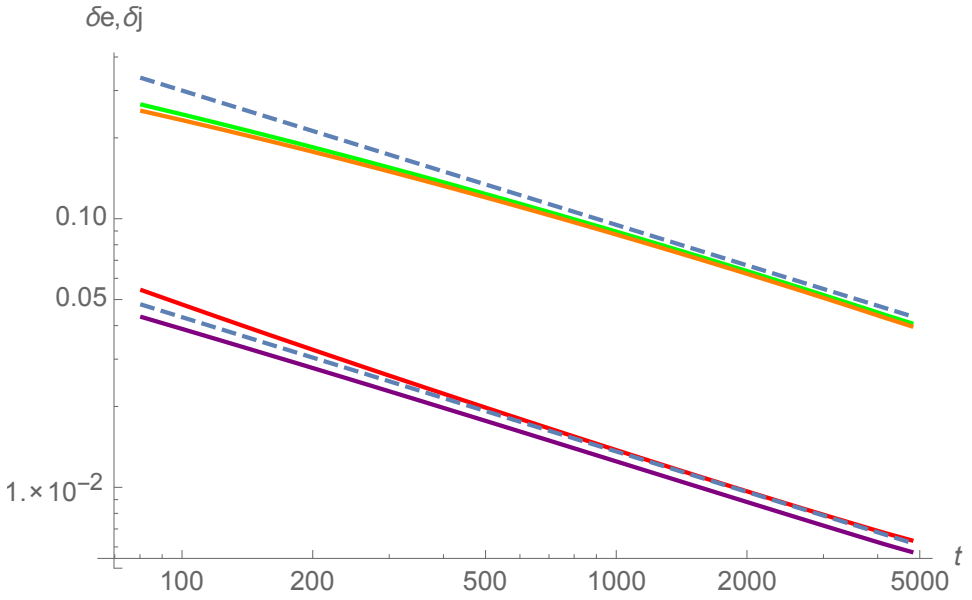

Figure 22: A log log plot of δe,δj vs. time at the endpoints of a rarefaction wave, where $\delta e = e - e_0$ and $\delta j = j - j_0$ and e_0 and j_0 are from the zeroth order prediction (5.52). As in figure 21 the rarefaction wave spreads from $\xi_l = -1$ to $\xi_r = 1$. The four curves correspond to $e(1)$ (red), $e(-1)$ (purple) and $j(1)$ (green) and $j(-1)$ (orange). The dashed lines $0.43t^{-1/2}$ and $3t^{-1/2}$ are a guide to the eye.

equations describe, in a large d limit, both the dynamics of a black hole horizon and also the dynamics of a strongly interacting conformal field theory.

There are a number of possible future directions for research. The simplest is perhaps to include a transverse velocity. With a transverse velocity, in addition to the shock and rarefaction waves, there will in general be a contact discontinuity [43, 44, 45]. It is known (and perhaps intuitive given the similarity to a counter flow experiment), that the contact discontinuity is in general unstable to the development of turbulence [91]. It would be interesting to see what precisely happens in our large d limit. Another more complicated extension is the inclusion of a conserved charge. The large d equations of motion in the presence of a conserved charge are available from ref. [63]. Once again, a contact discontinuity is expected, as seen in the previous chapter, although whether such a discontinuity is stable or unstable to turbulence is unclear. More ambitiously, one could consider what happens for the holographic dual of a superfluid or superconductor [68, 74, 92, 93, 94, 95, 96].

Another possible direction is the addition of higher curvature terms to the dual gravitational description. One could presumably tune the d dependence of these terms such that higher order gradient corrections appear in the conservation equations (5.1) and also such that the first and second order transport coefficients are tuned away from the values examined in this chapter.

Perhaps the most interesting direction for future study is the connection to black hole dynamics. What can we learn about black holes through the connection to hydrodynamics in a large d limit?

6 Conclusion and Outlook

In this dissertation we looked at finite temperature field theories in and out of equilibrium. The two parts of this dissertation study opposite ends of statistical mechanics. Entanglement entropy captures information about the short distance nature of field theories. On the other end of the spectrum fluids ignore short distance nature the QFT in favor of studying long distance features. There are interesting directions of research in both topics.

- **Entanglement** While entanglement and Rényi entropies are very useful for measuring entanglement of the ground state as temperature increases the entanglement entropy is contaminated by thermal entropy. While the method presented in Chapter 3 does not suffer from

this problem, in general, entanglement negativity[97, 98] is a better quantity for studying entanglement. As yet there is no known simple holographic calculation for negativity. In addition, there are plenty of open problems for specific CFTs.

- **Fluids** Fluid dynamics is an old and well studied area in physics and math. Yet there is still much that needs to be uncovered. Fundamental questions about existence and smoothness of solutions to fluid equations is one of the unsolved Millennium Problems. Turbulence and instabilities of fluid flows are interesting from a theoretical viewpoint and are also important for real world applications e.g. airplane wing design.

- **Gravity** Following the discovery of gauge/gravity duality solutions to classic general relativity problems can now give great insight into previously intractable problems. The duality between classical gravity and strongly coupled QFTs has lead to a profusion of semi-empirical studies of quark gluon plasmas. It also opens the door for similar studies in condensed matter theory e.g. high temperature superconductors.

Discoveries in early 20th century left physicists with years of interesting problems to investigate. More was understood about the physical world in that century than in the rest of human history. As the 21st century begins a new set of questions, combined with old ones, will keep physicist interested for decades to come.

A Classical Fluid Equations Derivation

We use the following definitions

Table 2: Definitions of fluid related quantities.

ρ	Fluid density.
$\mathbf{u}$	Local fluid velocity
$\mathbf{F}$	Force on a fluid element
τ	Stress on a fluid element

A.1 Newton's second law

Let us derive the Navier-Stokes equations. First let us define a pathline as the trajectory that an infinitesimal part of the fluid follows. Then we can define the fluid flow, $\mathbf{\Phi}(\mathbf{t}, \mathbf{x})$, as the pathlines of all infinitesimal parts of the fluid. Then the velocity is given by

$$\mathbf{u}(t, x) = \frac{d}{dt}\mathbf{\Phi}(t, \mathbf{x}). \tag{A.1}$$

Let us then consider the Jacobian, $J(t, \mathbf{x})$, of fluid flow. Taking a time derivative we obtian

$$\begin{aligned} \partial_t \partial_{x_j} \phi_i &= \partial_{x_j} v_i, \\ &= (\partial_{x_i} v_i)(\partial_{x_j} \phi_i), \end{aligned} \tag{A.2}$$

where $\mathbf{\Phi} = (\phi_1, \phi_2...)$ and i,j run over spatial directions. Then the derivative of the Jacobian is then

$$\partial_t J(t, \mathbf{x}) = J(t, \mathbf{x}) \nabla \cdot v. \tag{A.3}$$

We can then prove the Transport Theorem, for some general function $q(t, \mathbf{x})$,

$$\frac{d}{dt} \int_{\mathbf{\Phi}(t,W)} d\mathbf{x} q(t, \mathbf{x}) = \int_{\mathbf{\Phi}(t,W)} d\mathbf{x} \left(\partial_t q(t, \mathbf{x}) + \nabla \cdot (q\mathbf{u}) \right). \tag{A.4}$$

Recalling that the definition of the fluid flow

$$\frac{d}{dt}\int_{\mathbf{\Phi}(t,W)} d\mathbf{x} q(t,\mathbf{x}) = \frac{d}{dt}\int_W d\mathbf{x_0} q(t,\mathbf{\Phi}(t,\mathbf{x}_0)J(t,\mathbf{x}_0), \tag{A.5}$$

$$= \int_W d\mathbf{x_0}(\partial_t q + (\nabla q)\cdot\mathbf{u} + q\nabla\cdot\mathbf{u})J(t,\mathbf{x}_0), \tag{A.6}$$

$$= \int_{\mathbf{\Phi}(t,W)} d\mathbf{x}(\partial_t q + \nabla\cdot(q\mathbf{u})). \tag{A.7}$$

Let us first apply this to the density. Classically, mass is conserved and therefore

$$\frac{d}{dt}\int_V d\mathbf{x}\rho = 0, \tag{A.8}$$

$$\int_V d\mathbf{x}(\partial_t\rho + \nabla\cdot(\rho\mathbf{u})) = 0. \tag{A.9}$$

Next applying Newton's second law to a volume element V of the fluid

$$\frac{d}{dt}\int_V d\mathbf{x}\,\rho\mathbf{u} = \int_V d\mathbf{x}\,\rho\mathbf{F} + \int_{\partial V}\tau\cdot\hat{\mathbf{n}}. \tag{A.10}$$

Where $\mathbf{F}$ is the force and τ is the stress matrix on the fluid element. We can apply the Transport Theorem to this to obtain

$$\int_V d\mathbf{x}\,[\partial_t(\rho\mathbf{u}) + (\nabla(\rho\mathbf{u}))\cdot\mathbf{u} + \rho\mathbf{u}\nabla\cdot\mathbf{u})] = \int_V d\mathbf{x}(\mathbf{F}\rho + \nabla\cdot\tau). \tag{A.11}$$

Combining Equations (A.9) and (A.11) and noting that they must be true for any fluid element considered we get the Euler equations

$$\begin{aligned}&\partial_t\rho = \nabla\cdot(\rho\mathbf{u}),\\ &\rho(\partial_t\mathbf{u} + \mathbf{u}\cdot\nabla\mathbf{u}) = \rho F + \nabla\cdot\tau.\end{aligned} \tag{A.12}$$

A.2 Boltzmann Equation

Let us give a derivation of the Euler equations from a microscopic view point. Let us define the $f(t, \mathbf{x}, \mathbf{u})$ as the distribution function in phase space. Then the total particle number and number density are given by

$$N = \int d\mathbf{x} d\mathbf{u} f(t, \mathbf{x}, \mathbf{u}), \tag{A.13}$$

$$n = \int d\mathbf{u} f(t, \mathbf{x}, \mathbf{u}). \tag{A.14}$$

After a short time dt and in the absence of collisions the distribution is to

$$f(t + dt, \mathbf{x} + \mathbf{u}dt, \mathbf{u} + (\mathbf{F}/m)dt), \tag{A.15}$$

where $\mathbf{F}$ is the external force and m is the mass of the fluid particles. This can be viewed as the coordinate change

$$x' = x + \mathbf{u}dt, \tag{A.16}$$

$$u' = u + \frac{\mathbf{F}}{m}dt. \tag{A.17}$$

In the absence of collisions there should be no change in the number of particles in each area of phase. Therefore

$$f(t + dt, \mathbf{x} + \mathbf{u}dt, \mathbf{u} + (\mathbf{F}/m)dt)d\mathbf{x}'d\mathbf{u}' - f(t, \mathbf{x}, \mathbf{u})d\mathbf{x}d\mathbf{u} = 0. \tag{A.18}$$

Expanding the left hand side to first order in dt yields the collision-less Boltzmann equation

$$\partial_t f + \mathbf{u} \cdot \nabla_{\mathbf{x}} f + \frac{\mathbf{F}}{m} \cdot \nabla_{\mathbf{u}} f = 0. \tag{A.19}$$

When we allow for two point collisions it is possible to write down the additional term that appears on the right hand side of equation (A.19). Such collisions take two particles out of one part of phase space into another with

rates depending upon the cross section $\sigma(\omega)$. The particles lost in one part of phase space are given by

$$\frac{\partial f_1}{\partial t}\Big|_{\text{out}} = \int d\mathbf{u}_2 \int d\Omega\sigma(\Omega) f_2 f_1 |\mathbf{u}_1 - \mathbf{u}_2|, \tag{A.20}$$

$$f_i = f(t, \mathbf{x}, \mathbf{u}_i), \tag{A.21}$$

and they scatter into

$$\frac{\partial f_1}{\partial t}\Big|_{\text{in}} = \int d\mathbf{u}_2 \int d\Omega\sigma(\Omega) f_2' f_1' |\mathbf{u}_1' - \mathbf{u}_2'| \tag{A.22}$$

$$f_i' = f(t, \mathbf{x}, \mathbf{u}_i'). \tag{A.23}$$

For elastic collisions $|\mathbf{u}_1' - \mathbf{u}_2'| = |\mathbf{u}_1 - \mathbf{u}_2|$ and so the correction to Equation A.19 is given by

$$\frac{\partial f_1}{\partial t}\Big|_{\text{coll}} = \int d\mathbf{u}_2 \int d\Omega\sigma(\Omega)(f_2' f_1' - f_2 f_1)|\mathbf{u}_1 - \mathbf{u}_2|. \tag{A.24}$$

The average value of a test function ϕ can be obtained from the distribution function

$$\langle\phi\rangle = \frac{1}{n}\int d\mathbf{u}\phi f. \tag{A.25}$$

By multiplying Equation A.19 by ϕ and integrating over $d\mathbf{u}$ and then integrating each term by parts we get the transport equation,

$$\partial_t(n\langle\phi\rangle) + \nabla_x \cdot (n\langle\phi\mathbf{u}\rangle) - n\langle\mathbf{u}\cdot\nabla_{\mathbf{x}}\phi\rangle - \frac{n}{m}\langle\mathbf{F}\cdot\nabla_{\mathbf{u}}\phi\rangle - \frac{n}{m}\langle(\nabla_{\mathbf{u}}\cdot F)\phi\rangle = 0. \tag{A.26}$$

Replacing ϕ with m, $m\mathbf{u}$ and $m|\mathbf{u}-\mathbf{v}|^2/2$ we obtain

$$\partial_t\rho + \nabla\cdot(\rho\mathbf{v}) = 0 \tag{A.27}$$

$$\partial_t(\rho v_i) + \nabla\cdot(\rho v_i\mathbf{v}) - \frac{\rho}{m}F_i + \sum_j \partial P_{ij} = 0 \tag{A.28}$$

$$\partial_t(\rho\epsilon) + \nabla\cdot(\rho\epsilon\mathbf{v}) + \nabla\cdot\mathbf{q} + \sum_{i,j} P_{ij}\Lambda_{ij} = 0, \tag{A.29}$$

where we used the fact that all of the test functions are conserved quantities and so the collision integral is zero. We also made the following definitions

$$\begin{aligned}
\rho &= mn, \\
P_{ij} &= \rho\langle(u_i - v_j)(u_j - v_i)\rangle, \\
\epsilon &= \frac{1}{2}\langle|\mathbf{u} - \mathbf{v}|^2\rangle, \\
\Lambda_{ij} &= \frac{1}{2}(\partial_{x_j} v_i + \partial_{x_i} v_j), \\
\mathbf{q} &= \frac{1}{2}\rho\langle(\mathbf{u} - \mathbf{v})|\mathbf{u} - \mathbf{v}|^2\rangle.
\end{aligned} \tag{A.30}$$

To evaluate these we make the assumption of small mean free path. Such a system is always in local thermal equilibrium and so the distribution f must be the Maxwell-Boltzmann Distribution. Then there are two integrals to do; one is odd and therefore zero and the other is Gaussian,

$$\mathbf{q} = 0 \tag{A.31}$$

$$P_{ij} = \rho\left(\frac{m}{2\pi k_B T}\right)^{3/2} \int d|\mathbf{u} - \mathbf{v}|(u_i - v_j)(u_j - v_i) \exp\left(-\frac{m}{2k_B T}|\mathbf{u} - \mathbf{v}|^2\right) \tag{A.32}$$

$$= p\delta_{ij}. \tag{A.33}$$

Plugging P and $\mathbf{q}$ back into (A.30) we obtain the Euler equations for an ideal fluid

$$\partial_t \rho + \nabla \cdot (\rho \mathbf{v}) = 0 \tag{A.34}$$

$$\partial_t(\rho v_i) + \nabla \cdot (\rho v_i \mathbf{v}) - \frac{\rho}{m} F_i + \nabla p = 0 \tag{A.35}$$

$$\rho(\partial_t \epsilon + \mathbf{v} \cdot \nabla \epsilon) + p \nabla \cdot \mathbf{v} = 0. \tag{A.36}$$

Had we kept higher order corrections we would have also gotten the viscous terms in the Navier Stokes equations. The same approach can be taken for the relativistic Boltzmann equation. If we again take the zero mean free path limit the resulting equations are for a relativistic perfect fluid.

B Computing Traces in the Continuum Limit

The basic technique used in computing $\mathrm{tr}\, C_e^2$, $\mathrm{tr}\, C_o^2$ and $\langle\psi|C_e^2|\psi\rangle$ in the continuum limit $N \to \infty$ with n/N held fixed was to replace sums with integrals. However, there are three wrinkles in this procedure, two of which have already been hinted at in the text. The first is that we were not able to perform the integrals obtained by taking the continuum limit of the mode sums over a and b. Thus, we first performed the mode sums over a and b explicitly yielding sums over cotangents. For example, performing the mode sums for eq. (2.25) yields,

$$\begin{aligned}
8N^2(\tilde{C}_e^2)_{jk} &= \Big[\cot\frac{\pi}{N}(s+j+1/2)+\cot\frac{\pi}{N}(s-j+1/2)\Big]\times \\
&\quad\Bigg[\sum_{b=1}^{N-1}\csc\frac{\pi b}{N}-2\sum_{l=1}^{s}\cot\frac{\pi}{N}(l-1/2) \\
&\quad-\sum_{l=1}^{|k|}\Big(\cot\frac{\pi}{N}(s+l-1/2)-\cot\frac{\pi}{N}(s-l+1/2)\Big)\Bigg] \\
&\quad+\sum_{l=1}^{s}\Big[\cot\frac{\pi}{N}(l+j-1/2)+\cot\frac{\pi}{N}(l-j-1/2)\Big]\times \\
&\quad\Big[\cot\frac{\pi}{N}(l+k-1/2)+\cot\frac{\pi}{N}(l-k-1/2)\Big]\ , \qquad \text{(B.1)}
\end{aligned}$$

while performing the mode sums for eq. (2.26) gives

$$\begin{aligned}
(\tilde{C}_o^2)_{jk} &= \frac{1}{4N^2}\sum_{l=1}^{s}\Big[\cot\frac{\pi}{N}(j+l-1/2)-\cot\frac{\pi}{N}(j+s+1/2)+ \\
&\qquad+\cot\frac{\pi}{N}(j-l+1/2)-\cot\frac{\pi}{N}(j-s-1/2)\Big]\times \\
&\qquad\times\Big[\cot\frac{\pi}{N}(k+l-1/2)+\cot\frac{\pi}{N}(k-l+1/2)\Big] \qquad \text{(B.2)}
\end{aligned}$$

The second wrinkle is that naive integral approximations of the cotangent sums often include singular regions. Our strategy in this case was to add and subtract a sum that we could perform analytically but whose integral approximation had the same singular region. This procedure was already used in the text to perform the sum (2.23). The third wrinkle is that the integral approximations of the cotangent sums were often difficult to perform.

Changing variables and using discrete symmetries reduced the integrals to known results in most cases. However, in two cases, we had to perform an integral we could not find in the books.

Let us first sketch the computation of $\mathrm{tr}\, C_o^2$, i.e. the trace of (B.2). Several of the terms in the sum have the structure

$$I_{\pm\pm} = \frac{1}{N^2} \sum_{k,j=1}^{s} \cot \frac{\pi}{N}(k \pm (j-1/2)) \cot \frac{\pi}{N}(k \pm (j-1/2)) \ . \tag{B.3}$$

To perform these sums, we make the change of variables $x = k + j$ and $y = k - j$. Using the same technique in eq. (2.23) to regularize the singular regions of the integral approximations, one straightforwardly finds

$$I_{++} = -\frac{1}{4} - \frac{s^2}{N^2} + \frac{1}{\pi^2}\left[\ln \frac{2N \tan(\pi s/N)}{\pi} + 1 + \gamma\right] + O(1/N) \tag{B.4}$$

$$I_{--} = s - \frac{s^2}{N^2} - \frac{2}{\pi^2}\left[\ln \frac{4N \sin(\pi s/N)}{\pi} + 1 + \gamma\right] + O(1/N^2) \tag{B.5}$$

$$I_{+-} = I_{-+} = \frac{1}{8} + O(\log N/N) \ . \tag{B.6}$$

An intermediate result necessary for the computation of I_{+-} is

$$\frac{1}{N}\sum_{k=1}^{n}(-1)^k \cot \frac{\pi}{N}(k-1/2) = -\frac{1}{2} + \frac{(-1)^n}{2N} \cot\left(\frac{\pi n}{N}\right) + O(1/N^3) \ . \tag{B.7}$$

The remaining pieces of $\mathrm{tr}\, C_o^2$ can be rearranged in the following way

$$\begin{aligned} & 2\sum_{k,j=1}^{s}\left(\cot\frac{\pi}{N}(k+j-1/2) + \cot\frac{\pi}{N}(k-j+1/2)\right) \times \\ & \times \left(\cot\frac{\pi}{N}(k-s-1/2) + \cot\frac{\pi}{N}(k+s+1/2)\right) \\ & = -\left(\sum_{y=0}^{2s} \cot\frac{\pi}{N}(y+1/2)\right)^2 - \sum_{y=0}^{2s} \cot^2\frac{\pi}{N}(y+1/2) \\ & \quad +2\sum_{y=0}^{2s}\sum_{x=2s-y}^{2s} \cot\frac{\pi}{N}(y+1/2)\cot\frac{\pi}{N}(x+1/2) \ . \end{aligned} \tag{B.8}$$

The first sum on the r.h.s. of eq. (B.8) we performed in (2.23). The second sum can be performed using the same techniques:

$$\frac{1}{N^2}\sum_{k=1}^{n}\cot^2\frac{\pi}{N}(k-1/2)=\frac{1}{2}+O(1/N)\ . \tag{B.9}$$

The third sum requires more work and reduces to one of the two integrals we could not find in tables. Up to $\log N/N$ corrections, we may replace the third sum by the following integral:

$$I(b)\equiv\int_0^1\int_{1-x}^1\cot(bx)\cot(by)\,dy\,dx\ , \tag{B.10}$$

where

$$\frac{1}{N^2}\sum_{y=0}^{2s}\sum_{x=2s-y}^{2s}\cot\frac{\pi}{N}(y+1/2)\cot\frac{\pi}{N}(x+1/2)=\left(\frac{2s}{N}\right)^2 I\left(\frac{2\pi s}{N}\right)+O(\log N/N)\ . \tag{B.11}$$

The integral over dy is trivial:

$$I(b)=\frac{1}{b}\int_0^1\cot(bx)\log\frac{\sin(b)}{\sin(b(1-x))}dx\ . \tag{B.12}$$

We find that $I'(b)b+2I(b)=-1$ and that in the small b limit $I(b)=\pi^2/6b^2+O(1)$. From these two facts, we deduce that[24]

$$I(b)=\frac{\pi^2}{6b^2}-\frac{1}{2}\ . \tag{B.13}$$

The quanties $\mathrm{tr}\,C_e^2$ and $\langle\psi|C_e^2|\psi\rangle$ may be computed in an analogous way. As can be seen in eq. (B.1), there was one mode sum we were forced to do in the continuum limit:

$$\frac{1}{N}\sum_{b=1}^{N-1}\csc\frac{\pi b}{N}=\frac{2}{\pi}\left(\gamma+\ln\frac{2N}{\pi}\right)+O(1/N^2)\ . \tag{B.14}$$

All of the other mode sums we were able to perform explicitly. The remaining sums over cotangents are similar to cases treated above. We spare the reader

[24]We would like Dan Gulotta for showing us how to perform this integral and also the integral (B.15).

almost all of the remaining details. In the computation of $\langle\psi|C_e^2|\psi\rangle$, we came across a second novel integral:

$$J(b) = \int_0^1 \left[\log \frac{\sin(b(1+x))}{\sin(b(1-x))}\right]^2 dx \ . \tag{B.15}$$

Similar to the strategy in computing $I(b)$, we find that $J''(b)+2J'(b)/b = -8$ and that in the small b limit $J(b) = \pi^2/3 + O(b^2)$. Thus we deduce that

$$J(b) = \frac{1}{3}(\pi^2 - 4b^2) \ . \tag{B.16}$$

C Alternate Formulation of d=3 Sum

In our effort to find the Rényi entropies in odd dimensions we came across an alternate form of the sum in Equation (3.38).

$$\sum_{k=0}^{m-1} \frac{e^{-\pi i k(m-1)/m}}{\sin(\pi k/m+\theta)} = e^{-i\theta}\left(\cot(m\theta) + i - 2\frac{1}{\sin(m\theta)}\sum_{k=1/2}^{m/2-1}\frac{\sin[2k(\theta-\pi/2m)]}{\sin(\pi k/m)}\right). \tag{C.1}$$

This alternate representation is essentially a Fourier series on the shifted interval $\frac{\pi}{2m} < \theta < 2\pi + \frac{\pi}{2m}$.

Using the same integral form for the cosecant used for $d = 3$ we can rewrite this new sum as an integral.

$$\sum_{k=1/2}^{m/2-1}\frac{\sin[2k(\theta-\pi/2m)]}{\sin(\pi k/m)} = \frac{1}{\pi}\sum_{k=1/2}^{m/2-1}\int_0^\infty dx \frac{x^{k/m}}{x(1+x)}\sin[2k(\theta-\pi/2m)]. \tag{C.2}$$

The integral can be evaluated for individual values of $n = 1/m$. This rewriting of the sum seems to have different issues with analytic continuation than those that plagued Equation (3.39). It appears to reproduce correctly the $n = 2$ thermal correction to the Rényi entropy (see Figure 23), but fails for the others and for the entanglement entropy.

Equation (C.1) gives the following results for the first couple of Rényi entropies

$n=2$	$2\sin(\theta/2)^3$
$n=3$	$\frac{4}{3}\left[2+\cos\left(\frac{2\theta}{3}\right)\right]\sin^2\left(\frac{\theta}{3}\right)$

(Note that the $n = 3$ result is not reproduced by our numerics.)

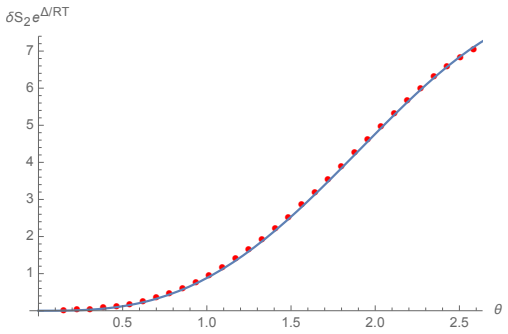

Figure 23: For $d = 2 + 1$, δS_2 with 200 grid points.

D Comment About Entropy Production Across a Shock

In the ideal limit, in addition to conservation of energy and momentum, we can write down a conservation condition for the entropy current, $\partial_\mu \tilde{J}^\mu_S = 0$ where

$$\tilde{J}^\mu_S = (\epsilon + p)u^\mu/T. \tag{D.1}$$

This conservation condition would naively seem to lead to an additional Rankine-Hugoniot relation across a single shock. As is well known in the hydrodynamics community (see for example [62]), since shocks create entropy this third Rankine-Hugoniot relation is violated. Let us parameterize a possible violation of the additional Rankine-Hugoniot relation by Δ.

$$\Delta = s[\tilde{J}^t_S] - [\tilde{J}^\zeta_S] \tag{D.2}$$

where the square brackets are the same as those in (5.44). One finds

$$\Delta = \frac{2\pi}{\sqrt{e_r e_l} d^2}\left(e_r^2 - e_l^2 - 2e_r e_l \log\left(\frac{e_r}{e_l}\right)\right) + O(d^{-3}) \ . \tag{D.3}$$

Equation (D.3) can be obtained by using a large d expression for the entropy current (5.40) along with the Rankine-Hugoniot relations for energy and momentum, (5.44) supplemented by (5.16) and (5.17). Note that in the asymptotic regions, the gradient terms will all vanish. (It is also possible to start with a finite d result, as done in the previous chapter or for example ref. [62], and then take a large d limit directly.)

The non-conservation of entropy (D.3) can be captured by the leading viscous corrections to the shock width (5.67) when the energy difference is small. Indeed, using (5.42)

$$\partial_\mu \tilde{J}^\mu_S = \frac{8\pi}{d^2}\frac{j_0^2 (e')^2}{e^3} + O(d^{-3}) = \frac{2\pi j_0^2 \delta e^4}{d^2\langle e\rangle}\,\mathrm{sech}\left(\frac{\zeta\delta e}{2}\right)^4 + O(\delta e^5, d^{-3})\ . \quad \text{(D.4)}$$

Integrating this divergence over the ζ direction leads to

$$\int \partial_\mu \tilde{J}^\mu_S \mathrm{d}\zeta = \frac{16\pi\langle e\rangle \delta e^3}{3d^2} + O(\delta e^4, d^{-3})\ , \quad \text{(D.5)}$$

which agrees with a small δe expansion of (D.3).

E A bestiary of plots

In section 5.4.3 we studied the numerical solutions to the Riemann problem for various initial energy and velocity profiles associated with RR, RS and SS type solutions. In what follows we provide additional evidence that at late times the full numerical solution to the Riemann problem approaches the appropriate predicted steady state values e_0 and j_0 and fixed point values e_s and j_s.

E.1 RR configurations

To generate an RR configuration we used the initial data

$$e = 1\,, \qquad j = \begin{cases} f(\zeta) & 0 \le \zeta < \ell/4 \\ 0 & \ell/4 \le \zeta < L/2 - \ell/4 \\ f(\zeta - L/2 - \ell/2) & L/2 - \ell/4 \le \zeta < L/2 + \ell/4 \\ j_* & L/2 + \ell/4 \le \zeta < L - \ell \\ f(\zeta - L) & L - \ell \le \zeta < L \end{cases} \quad \text{(E.1)}$$

where

$$f(\zeta) = \frac{1}{2} j_* \left(1 - \tanh\left(c \sin\left(\frac{2\pi\zeta}{\ell}\right)\right)\right)\ . \quad \text{(E.2)}$$

The analysis of section 5.4.2 predicts a steady state of the form

$$e_0 = \exp\left(-j_*/2\right) \qquad j_0 = \frac{j_*}{2}\exp\left(-j_*/2\right)\ . \quad \text{(E.3)}$$

Once $j_* \geq 2$ one should find a fixed point with $e_s = j_s = \exp(-1)$. We find that the numerical solution approaches the predicted states via power law behavior, see figure 24.

E.2 SS configurations

To generate an SS configuration we used the initial data (E.1) with $j_* < 0$. The analysis of section 5.4.2 predicts a steady state of the form

$$e_0 = \frac{1}{8}(8 + j_*^2 - j_*\sqrt{16 + j_*^2}) \ , \quad \frac{j_0}{e_0} = \frac{j_*}{2} \ . \tag{E.4}$$

See figure 25 for a comparison with the numerical data.

E.3 RS configurations

To generate an RS configuration we used the initial data

$$j = 0 \, , \qquad e = \begin{cases} f(\zeta) & 0 \leq \zeta < \ell/4 \\ e_* & \ell/4 \leq \zeta < L/2 - \ell/4 \\ f(\zeta - L/2 - \ell/2) & L/2 - \ell/4 \leq \zeta < L/2 + \ell/4 \\ 1 & L/2 + \ell/4 \leq \zeta < L - \ell \\ f(\zeta - L) & L - \ell \leq \zeta < L \end{cases} \tag{E.5}$$

where

$$f(\zeta) = \frac{1}{2}\left(1 + e_*\right) + \frac{1}{2}\left(e_* - 1\right) \tanh\left(c \sin\left(\frac{2\pi\zeta}{\ell}\right)\right) + e_* \, . \tag{E.6}$$

The analysis of section 5.4.2 predicts a steady state of the form

$$e_0 = s^2 \ , \quad j_0 = s(s^2 - 1) \ . \tag{E.7}$$

with

$$0 = \frac{1}{s} - s - \log\left(\frac{s^2}{e_*}\right) \ . \tag{E.8}$$

According to the same analysis, once $e_* \geq \left(\frac{1+\sqrt{5}}{2}\right)^2 \exp(1)$ we will obtain a fixed point at the origin with $e_s = j_s = \exp(-1)$. An analysis of the late time behavior of the numerical solution can be found in figure 26.

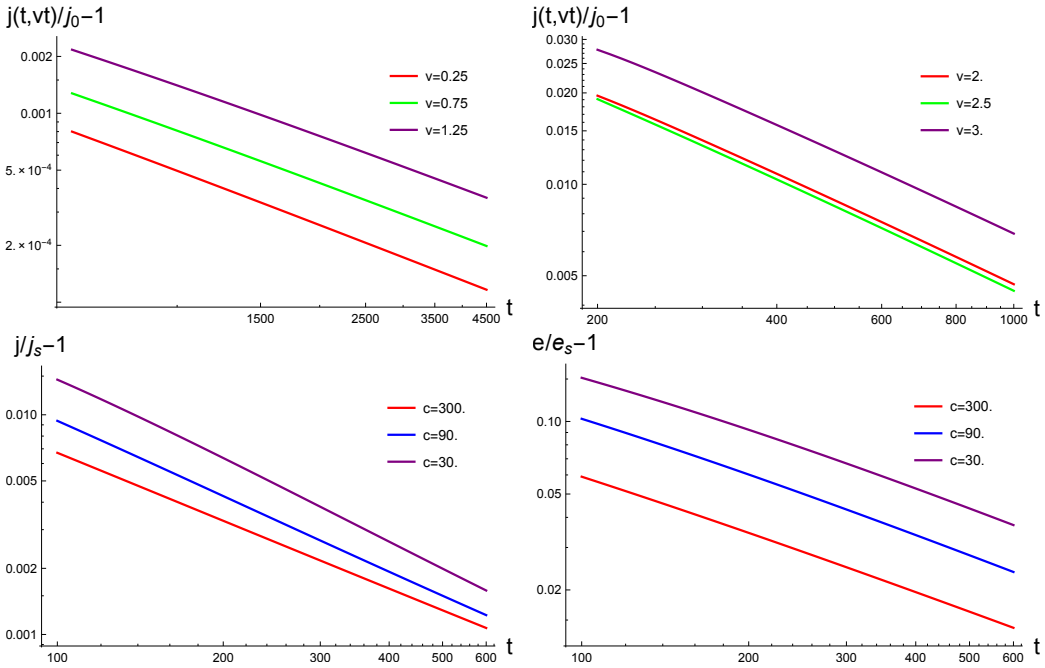

Figure 24: Late time behavior of the steady state and fixed point for RR type configurations. Top plots: The deviation of $j(t, \zeta = vt)$ from the predicted steady state value j_0 for various values of v. The initial conditions are given by (E.1) with $L = 20000$, $\ell = 8000$, and $c = 300$ and $j_* = 1.8$ for the top left plot and $L = 8000$, $\ell = 2000$, $c = 100$ and $j_* = 5$ for the top right plot. Both the results roughly fit a $\sim t^\alpha$ asymptotic behavior with $\alpha \sim 0.9$. Bottom plots: The deviation of e and j from the predicted fixed point value at $\zeta = 0$ for various values of c. The initial conditions are given by (E.1) with $L = 16000$, $\ell = 4000$ and $j_* = 3$. Both the time dependence of $e/e_s - 1$ and $j/j_s - 1$ can be fit to a power law, $\sim t^\alpha$. For the energy density one finds that α gradually increases to $\alpha \sim 0.8$ as one approaches $c = 300$. For the energy current α decreases to $\alpha \sim 1.1$ at $c = 300$.

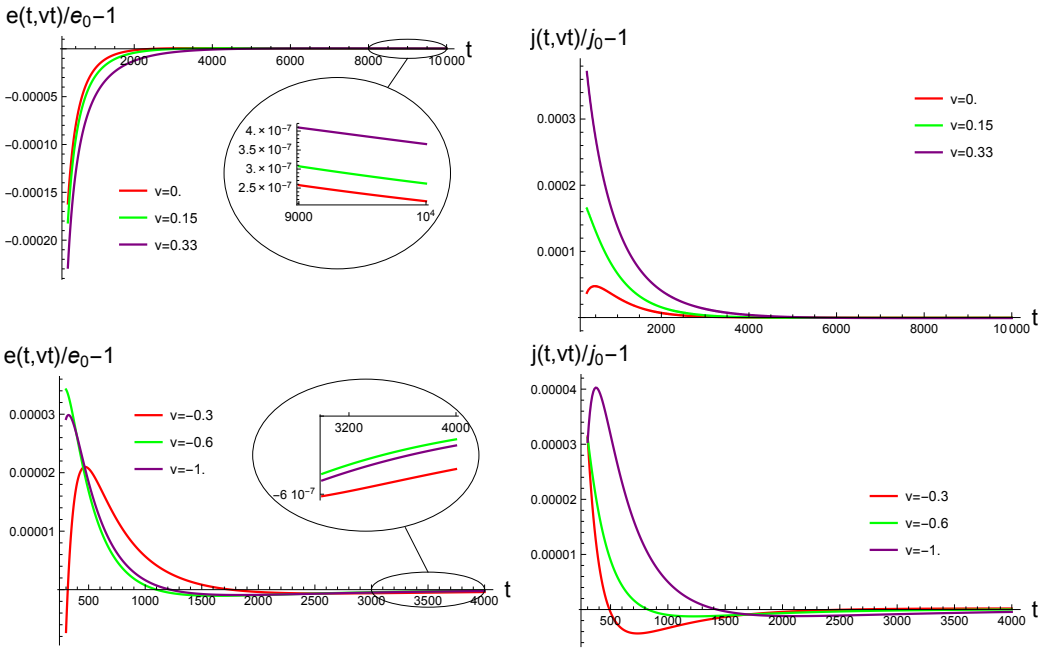

Figure 25: Late time behavior of the steady state and fixed point for SS type configurations. The plots show the deviation of $e(t, \zeta = vt)$ and $j(t, \zeta = vt)$ from the predicted steady state values e_0 and j_0 for various values of v. The initial conditions are given by (E.1) with $L = 40000$ (top) or $L = 20000$ (bottom), $\ell = 2000$ and $c = 100$. The top plots correspond to $j_* = -0.5$ and the bottom ones to $j_* = -2$. We expect that numerical error is of order $10^{-7} - 10^{-8}$.

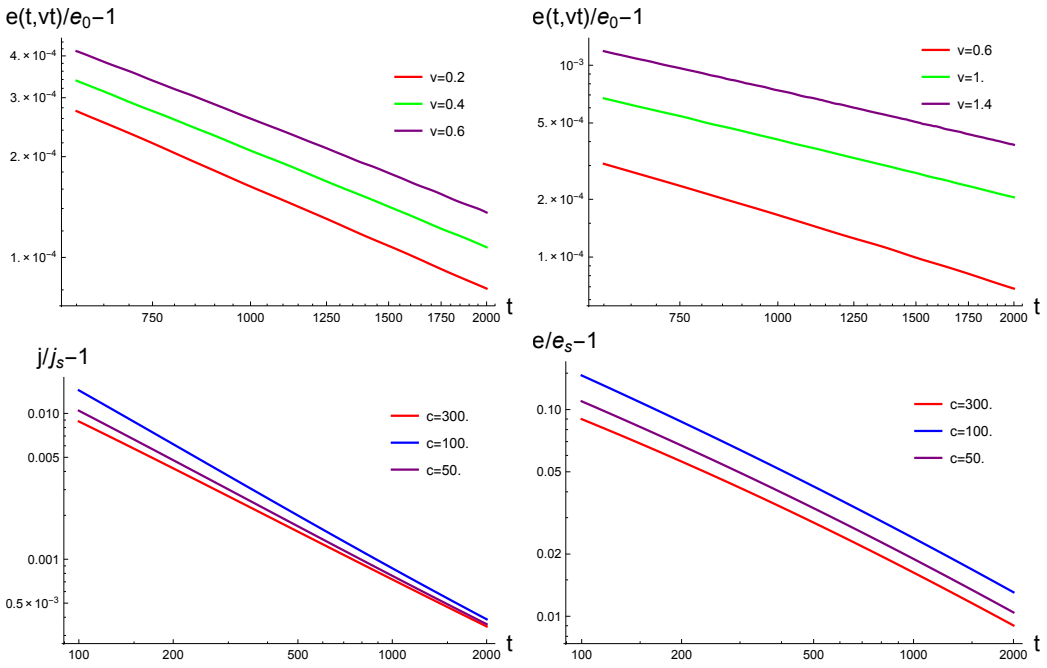

Figure 26: Late time behavior of the steady state and fixed point for RS type configurations. Top plots: The deviation of $e(t, \zeta = vt)$ from the predicted steady state value e_0 for various values of v. The initial conditions are given by (E.5) with $L = 16000$, $\ell = 2000$, and $c = 100$ and $e_* = 4$ for the top left plot and $e_* = 9$ for the top right plot. Bottom plots: The deviation of e and j from the predicted fixed point value at $\zeta = 0$ for various values of c. The initial conditions are given by (E.1) with $L = 16000$, $\ell = 4000$ and $e_* = 9$. Both the time dependence of $e/e_s - 1$ and $j/j_s - 1$ can be fit to a power law, $\sim t^\alpha$. For the energy density one finds $\alpha \sim 0.77$. For the energy current $\alpha \sim 1.1$.

E.4 Error analysis

In sections E.1 and E.3 we have fit the late time approach of the data to the predicted steady state and (or) fixed point values to a power law behavior. The fit was done using Mathematica's NonLinearModelFit routine [90]. In detail, the late time data was discretized into order 1 time steps which were then fit to a a/t^{α} curve with a and α as parameters. The standard errors for the fit were usually of order 10^{-3} to 10^{-4}. Fits involving very small values of the slope parameter c in (E.2) and (E.6) (c.f., the bottom plots of figures 24 and 26) often had large standard errors.

References

[1] Maxwell, James Clerk. A Treatise on Electricity and Magnetism: Y James Clerk Maxwell. Oxford: Clarendon, 1873. Print.

[2] A. G. Riess et al. [Supernova Search Team Collaboration], Astron. J. 116, 1009 (1998); S. Perlmutter et al. [Supernova Cosmology Project Collaboration], Astrophys. J. 517, 565 (1999).

[3] B. P. Abbott *et al.* [LIGO Scientific and Virgo Collaborations], Phys. Rev. Lett. **116**, no. 6, 061102 (2016) doi:10.1103/PhysRevLett.116.061102 [arXiv:1602.03837 [gr-qc]].

[4] Bernoulli, Daniel. Hydrodynamica, Sive De Viribus Et Motibus Fluidorum Commentarii. Opus Academicum Ab Auctore, Dum Petropoli Ageret, Congestum. Argentorati: Sumptibus J.R. Dulseckeri, 1738. Print.

[5] L. Hadjiivanov, I. Todorov, "Quantum entanglement," [arXiv 1506.04262]

[6] Nielsen, Michael A., and Isaac L. Chuang. Quantum Computation and Quantum Information. Cambridge: Cambridge UP, 2010.

[7] M. Srednicki, "Entropy and area," Phys. Rev. Lett. **71**, 666 (1993) [hep-th/9303048].

[8] L. Bombelli, R. K. Koul, J. Lee and R. D. Sorkin, "A Quantum Source of Entropy for Black Holes," Phys. Rev. D **34**, 373 (1986).

[9] H. Casini and M. Huerta, "Entanglement and alpha entropies for a massive scalar field in two dimensions," J. Stat. Mech. **0512**, P12012 (2005) doi:10.1088/1742-5468/2005/12/P12012 [cond-mat/0511014].

[10] S. Ryu and T. Takayanagi, "Holographic derivation of entanglement entropy from AdS/CFT," Phys. Rev. Lett. **96**, 181602 (2006) [hep-th/0603001].

[11] H. Casini and M. Huerta, "A c-theorem for the entanglement entropy," J. Phys. A **40**, 7031 (2007) [cond-mat/0610375].

[12] H. Casini and M. Huerta, "On the RG running of the entanglement entropy of a circle," Phys. Rev. D **85**, 125016 (2012) [arXiv:1202.5650 [hep-th]].

[13] P. Calabrese and J. Cardy, "Entanglement entropy and conformal field theory," J. Phys. A **42**, 504005 (2009) [arXiv:0905.4013 [cond-mat.stat-mech]].

[14] I. Peschel and V. Eisler, "Reduced density matrices and entanglement entropy in free lattice models," J. Phys. A **42**, 504003 (2009) [arXiv:0906.1663 [cond-mat]].

[15] P. Calabrese and J. L. Cardy, "Entanglement entropy and quantum field theory," J. Stat. Mech. **0406**, P06002 (2004) [hep-th/0405152].

[16] V. E. Korepin, "Universality of Entropy Scaling in One Dimensional Gapless Models," Phys. Rev. Lett. **92**, 096402 (2004).

[17] I. Peschel, J. Phys. A: Math. Gen. **36**, L205 (2003) [arXiv:cond-mat/0212631]; M. C. Chung and I. Peschel, Phys. Rev. B **62**, 4191 (2000) [arXiv:cond-mat/0004222].

[18] B. Doyon, "Bi-partite Entanglement Entropy in Massive Two-Dimensional Quantum Field Theory," Phys. Rev. Lett. **102**, 031602 (2009) [hep-th/0803.1999v2].

[19] J.L. Cardy, and O.A. Castro-Alvaredo, and B. Doyon, "Form Factors of Branch-Point Twist Fields in Quantum Integrable Models and Entanglement Entropy," J. Stat. Phys. **130**,129 (2008) [hep-th/0706.3384].

[20] A. Botero and B. Reznik, "Spatial structures and localization of vacuum entanglement in the linear harmonic chain," Phys. Rev. A **70**, 052329 (2004) [quant-ph/0403233].

[21] E. Witten, "Anti-de Sitter space, thermal phase transition, and confinement in gauge theories," Adv. Theor. Math. Phys. **2**, 505 (1998) [hep-th/9803131].

[22] C. P. Herzog, "A Holographic Prediction of the Deconfinement Temperature," Phys. Rev. Lett. **98**, 091601 (2007) [hep-th/0608151].

[23] I. Klebanov, D. Kutasov, A. Murugan, "Entanglement as a Probe of Confinement," Nuc.. Phys. B. **796**, 274 (2008) [hep-th/0709.2140].

[24] P. V. Buividovich, M. I. Polikarpov, "Numerical study of entanglement entropy in SU(2) lattice gauge theory," Nuc. Phys. B. **802**, 458 (2008) [hep-lat/0802.4247].

[25] A. Velytsky, "Entanglement entropy in d+1 SU(N) gauge theory," Phys. Rev. D. **77**, 085021 (2008) [hep-th/0801.4111].

[26] Y. Nakagawa, A. Nakamura, S. Motoki and V. I. Zakharov, "Quantum entanglement in SU(3) lattice Yang-Mills theory at zero and finite temperatures," PoS LATTICE **2010**, 281 (2010) [arXiv:1104.1011 [hep-lat]].

[27] S. Cacciatori, F. Costa and F. Piazza, "Renormalized Thermal Entropy in Field Theory," Phys. Rev. D **79**, 025006 (2009) [arXiv:0803.4087 [hep-th]].

[28] T. J. Osborne and M. A. Nielsen, "Entanglement in a simple quantum phase transition," Phys. Rev. A **66**, 032110 (2002).

[29] G. Vidal, J. I. Latorre, E. Rico and A. Kitaev, "Entanglement in quantum critical phenomena," Phys. Rev. Lett. **90**, 227902 (2003) [quant-ph/0211074].

[30] T. Azeyanagi, T. Nishioka and T. Takayanagi, "Near Extremal Black Hole Entropy as Entanglement Entropy via AdS(2)/CFT(1)," Phys. Rev. D **77**, 064005 (2008) [arXiv:0710.2956 [hep-th]].

[31] T. Barrella, X. Dong, S. A. Hartnoll and V. L. Martin, "Holographic entanglement beyond classical gravity," JHEP **1309**, 109 (2013) [arXiv:1306.4682 [hep-th]].

[32] S. Datta and J. R. David, "Rényi entropies of free bosons on the torus and holography," JHEP **1404**, 081 (2014) [arXiv:1311.1218 [hep-th]].

[33] B. Chen and J. q. Wu, "Single interval Renyi entropy at low temperature," JHEP **1408**, 032 (2014) [arXiv:1405.6254 [hep-th]].

[34] C. P. Herzog and T. Nishioka, "Entanglement Entropy of a Massive Fermion on a Torus," JHEP **1303**, 077 (2013) [arXiv:1301.0336 [hep-th]].

[35] J. Cardy and C. P. Herzog, "Universal Thermal Corrections to Single Interval Entanglement Entropy for Two Dimensional Conformal Field Theories," Phys. Rev. Lett. **112**, no. 17, 171603 (2014) [arXiv:1403.0578 [hep-th]].

[36] C. P. Herzog, "Universal Thermal Corrections to Entanglement Entropy for Conformal Field Theories on Spheres," JHEP **1410**, 28 (2014) [arXiv:1407.1358 [hep-th]].

[37] C. P. Herzog and J. Nian, "Thermal Corrections to Rényi Entropies for Conformal Field Theories," arXiv:1411.6505 [hep-th].

[38] P. Candelas and J. S. Dowker, "Field Theories On Conformally Related Space-times: Some Global Considerations," Phys. Rev. D **19**, 2902 (1979).

[39] J. Cardy, "Some results on the mutual information of disjoint regions in higher dimensions," J. Phys. A **46**, 285402 (2013) [arXiv:1304.7985 [hep-th]].

[40] M. E. Peskin and D. V. Schroeder, "An Introduction to quantum field theory," Reading, USA: Addison-Wesley (1995) 842 p

[41] F. T. J. Epple, "Induced gravity on intersecting branes," JHEP **0409**, 021 (2004) [hep-th/0408105].

[42] R. Camporesi and A. Higuchi, "On the Eigenfunctions of the Dirac operator on spheres and real hyperbolic spaces," J. Geom. Phys. **20**, 1 (1996) [gr-qc/9505009].

[43] A. H. Taub, "Relativistic Rankine-Hugoniot equations," Physical Review **74.3**, 328 (1948).

[44] K. W. Thompson, "The special relativistic shock tube," Journal of Fluid Mechanics **171**, 365-375, (1986).

[45] P. Mach and M. Pietka, "Exact solution of the hydrodynamical Riemann problem with nonzero tangential velocities and the ultrarelativistic equation of state," Phys. Rev. E **81**, 046313 (2010) [arXiv:0905.0349 [math-ph]].

[46] D. H. Rischke, S. Bernard and J. A. Maruhn, "Relativistic hydrodynamics for heavy ion collisions. 1. General aspects and expansion into vacuum," Nucl. Phys. A **595**, 346 (1995) [nucl-th/9504018].

[47] D. Bernard and B. Doyon, "Energy flow in non-equilibrium conformal field theory," J. Phys. A **45**, 362001 (2012) [arXiv:1202.0239 [cond-mat.str-el]].

[48] M. J. Bhaseen, B. Doyon, A. Lucas and K. Schalm, "Far from equilibrium energy flow in quantum critical systems," Nature Physics 11, XXX (2015) [arXiv:1311.3655 [hep-th]].

[49] H. C. Chang, A. Karch and A. Yarom, "An ansatz for one dimensional steady state configurations," J. Stat. Mech. **1406**, no. 6, P06018 (2014) [arXiv:1311.2590 [hep-th]].

[50] R. Pourhasan, "Non-equilibrium steady state in the hydro regime," arXiv:1509.01162 [cond-mat.stat-mech].

[51] Lawrence C. Evans, *Partial differential equations*, volume 19 of *Graduate Studies in Mathematics*, American Mathematical Society, 2^{nd} edition, 2010.

[52] A. Buchel, L. Lehner, R. C. Myers and A. van Niekerk, JHEP **1305**, 067 (2013) [arXiv:1302.2924 [hep-th]].

[53] K. Balasubramanian and C. P. Herzog, Class. Quant. Grav. **31**, 125010 (2014) [arXiv:1312.4953 [hep-th]].

[54] V. E. Hubeny, S. Minwalla and M. Rangamani, "The fluid/gravity correspondence," arXiv:1107.5780 [hep-th].

[55] R. Emparan, R. Suzuki and K. Tanabe, Phys. Rev. Lett. **115**, no. 9, 091102 (2015) doi:10.1103/PhysRevLett.115.091102 [arXiv:1506.06772 [hep-th]].

[56] J. Smoller. Shock Waves and Reaction-Diffusion Equations - 1982. Springer.

[57] D. Bernard and B. Doyon, arXiv:1603.07765 [cond-mat.stat-mech].

[58] X. Liu and Y. Oz, JHEP **1103**, 006 (2011) doi:10.1007/JHEP03(2011)006 [arXiv:1006.0494 [hep-th]].

[59] I. Bakas, K. Skenderis and B. Withers, Phys. Rev. D **93**, no. 10, 101902 (2016) doi:10.1103/PhysRevD.93.101902 [arXiv:1512.09151 [hep-th]].

[60] E. Megias, PoS EPS **-HEP2015**, 366 (2015) [arXiv:1510.04219 [hep-th]].

[61] I. Amado and A. Yarom, JHEP **1510**, 015 (2015) doi:10.1007/JHEP10(2015)015 [arXiv:1501.01627 [hep-th]].

[62] A. Lucas, K. Schalm, B. Doyon and M. J. Bhaseen, arXiv:1512.09037 [hep-th].

[63] R. Emparan, K. Izumi, R. Luna, R. Suzuki and K. Tanabe, arXiv:1602.05752 [hep-th].

[64] S. Bhattacharyya, A. De, S. Minwalla, R. Mohan and A. Saha, JHEP **1604**, 076 (2016) doi:10.1007/JHEP04(2016)076 [arXiv:1504.06613 [hep-th]].

[65] S. Bhattacharyya, M. Mandlik, S. Minwalla and S. Thakur, JHEP **1604**, 128 (2016) doi:10.1007/JHEP04(2016)128 [arXiv:1511.03432 [hep-th]].

[66] R. Emparan, R. Suzuki and K. Tanabe, JHEP **1306**, 009 (2013) doi:10.1007/JHEP06(2013)009 [arXiv:1302.6382 [hep-th]].

[67] R. Emparan, D. Grumiller and K. Tanabe, Phys. Rev. Lett. **110**, no. 25, 251102 (2013) doi:10.1103/PhysRevLett.110.251102 [arXiv:1303.1995 [hep-th]].

[68] R. Emparan and K. Tanabe, JHEP **1401**, 145 (2014) doi:10.1007/JHEP01(2014)145 [arXiv:1312.1108 [hep-th]].

[69] R. Emparan and K. Tanabe, Phys. Rev. D **89**, no. 6, 064028 (2014) doi:10.1103/PhysRevD.89.064028 [arXiv:1401.1957 [hep-th]].

[70] R. Emparan, R. Suzuki and K. Tanabe, JHEP **1406**, 106 (2014) doi:10.1007/JHEP06(2014)106 [arXiv:1402.6215 [hep-th]].

[71] R. Emparan, R. Suzuki and K. Tanabe, JHEP **1407**, 113 (2014) doi:10.1007/JHEP07(2014)113 [arXiv:1406.1258 [hep-th]].

[72] R. Emparan, R. Suzuki and K. Tanabe, JHEP **1504**, 085 (2015) doi:10.1007/JHEP04(2015)085 [arXiv:1502.02820 [hep-th]].

[73] T. Andrade, S. A. Gentle and B. Withers, arXiv:1512.06263 [hep-th].

[74] A. M. Garca-Garca and A. Romero-Bermdez, JHEP **1509**, 033 (2015) doi:10.1007/JHEP09(2015)033 [arXiv:1502.03616 [hep-th]].

[75] S. Bhattacharyya, V. E. Hubeny, S. Minwalla and M. Rangamani, JHEP **0802**, 045 (2008) doi:10.1088/1126-6708/2008/02/045 [arXiv:0712.2456 [hep-th]].

[76] M. Haack and A. Yarom, JHEP **0810**, 063 (2008) doi:10.1088/1126-6708/2008/10/063 [arXiv:0806.4602 [hep-th]].

[77] S. Bhattacharyya, R. Loganayagam, I. Mandal, S. Minwalla and A. Sharma, JHEP **0812**, 116 (2008) doi:10.1088/1126-6708/2008/12/116 [arXiv:0809.4272 [hep-th]].

[78] S. Grozdanov and N. Kaplis, Phys. Rev. D **93**, no. 6, 066012 (2016) doi:10.1103/PhysRevD.93.066012 [arXiv:1507.02461 [hep-th]].

[79] S. Bhattacharyya, V. E. Hubeny, R. Loganayagam, G. Mandal, S. Minwalla, T. Morita, M. Rangamani and H. S. Reall, JHEP **0806**, 055 (2008) doi:10.1088/1126-6708/2008/06/055 [arXiv:0803.2526 [hep-th]].

[80] D. T. Son and P. Surowka, Phys. Rev. Lett. **103**, 191601 (2009) doi:10.1103/PhysRevLett.103.191601 [arXiv:0906.5044 [hep-th]].

[81] P. M. Chesler, N. Kilbertus and W. van der Schee, JHEP **1511**, 135 (2015) doi:10.1007/JHEP11(2015)135 [arXiv:1507.02548 [hep-th]].

[82] P. M. Chesler and L. G. Yaffe, Phys. Rev. D **82**, 026006 (2010) doi:10.1103/PhysRevD.82.026006 [arXiv:0906.4426 [hep-th]].

[83] P. M. Chesler and L. G. Yaffe, Phys. Rev. Lett. **106**, 021601 (2011) doi:10.1103/PhysRevLett.106.021601 [arXiv:1011.3562 [hep-th]].

[84] E. Shuryak, Phys. Rev. C **86**, 024907 (2012) doi:10.1103/PhysRevC.86.024907 [arXiv:1203.6614 [hep-ph]].

[85] P. M. Chesler and L. G. Yaffe, JHEP **1407**, 086 (2014) doi:10.1007/JHEP07(2014)086 [arXiv:1309.1439 [hep-th]].

[86] P. Figueras and T. Wiseman, Phys. Rev. Lett. **110**, 171602 (2013) doi:10.1103/PhysRevLett.110.171602 [arXiv:1212.4498 [hep-th]].

[87] S. Fischetti, D. Marolf and J. E. Santos, Class. Quant. Grav. **30**, 075001 (2013) doi:10.1088/0264-9381/30/7/075001 [arXiv:1212.4820 [hep-th]].

[88] R. Emparan and M. Martinez, JHEP **1309**, 068 (2013) doi:10.1007/JHEP09(2013)068 [arXiv:1307.2276 [hep-th]].

[89] S. Khlebnikov, M. Kruczenski and G. Michalogiorgakis, Phys. Rev. D **82**, 125003 (2010) doi:10.1103/PhysRevD.82.125003 [arXiv:1004.3803 [hep-th]].

[90] Wolfram Research, Inc., Mathematica, Version 10.4, Champaign, IL (2016).

[91] P. Mach, AIP Conf. Proc. **1458**, 459 (2012) doi:10.1063/1.4734459 [arXiv:1104.3751 [math-ph]].

[92] S. S. Gubser, Phys. Rev. D **78**, 065034 (2008) doi:10.1103/PhysRevD.78.065034 [arXiv:0801.2977 [hep-th]].

[93] S. A. Hartnoll, C. P. Herzog and G. T. Horowitz, Phys. Rev. Lett. **101**, 031601 (2008) doi:10.1103/PhysRevLett.101.031601 [arXiv:0803.3295 [hep-th]].

[94] S. A. Hartnoll, C. P. Herzog and G. T. Horowitz, JHEP **0812**, 015 (2008) doi:10.1088/1126-6708/2008/12/015 [arXiv:0810.1563 [hep-th]].

[95] C. P. Herzog, N. Lisker, P. Surowka and A. Yarom, JHEP **1108**, 052 (2011) doi:10.1007/JHEP08(2011)052 [arXiv:1101.3330 [hep-th]].

[96] C. P. Herzog, P. K. Kovtun and D. T. Son, Phys. Rev. D **79**, 066002 (2009) doi:10.1103/PhysRevD.79.066002 [arXiv:0809.4870 [hep-th]].

[97] P. Calabrese, J. Cardy and E. Tonni, Phys. Rev. Lett. **109**, 130502 (2012) doi:10.1103/PhysRevLett.109.130502 [arXiv:1206.3092 [cond-mat.stat-mech]].

[98] P. Calabrese, J. Cardy and E. Tonni, J. Phys. A **48**, no. 1, 015006 (2015) doi:10.1088/1751-8113/48/1/015006 [arXiv:1408.3043 [cond-mat.stat-mech]].